Removal of Cardiopulmonary Resuscitation Artifacts in the Human Electrocardiogram

by

Joar Eilevstjønn

Submitted in partial fulfillment
of the requirements for the degree of
DOKTOR INGENIØR

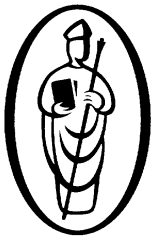

Department of Electrical and Computer Engineering
Stavanger University College
Norway

2004

Abstract

Death from heart diseases is the most common type of mortality in western countries and the survival rate of cardiac arrest is dismally low. The focus of this thesis is signal processing applications to improve the survival rate of out-of-hospital cardiac arrest.

In the treatment of cardiac arrest, two therapeutic methods are most important: (1) Cardiopulmonary resuscitation (CPR) providing life preserving artificial circulation and respiration through chest compressions and ventilations. (2) Defibrillation defined as the termination of the lethal cardiac arrest rhythms ventricular fibrillation (VF) or pulseless ventricular tachycardia (VT) by delivery of an electrical shock to the patient's chest passing current through the heart hoping to restart the normal heart rhythm.

An automated external defibrillator (AED) is commonly used for such shocks, and records and performs signal analysis on the electrocardiogram (ECG) in order to advice when to shock the patient. However, the mechanical activity from chest compressions and ventilations during CPR introduces artifact components in the ECG. For AEDs to perform reliable ECG signal analysis, CPR is therefore discontinued for a substantial time before the potential delivery of a shock. So in connection with analyses and shocks, a large part of the valuable therapy time is wasted by stopping the CPR, thus generating no flow time (NFT) with no cerebral or myocardial blood flow, lowering the chance of return of spontaneous circulation (ROSC). If the need for this hands-off time could be reduced or eliminated by removing these artifacts, it should significantly improve the ROSC rate.

We propose a method for removing CPR artifacts using a novel multichannel adaptive filter, the MultiChannel Recursive Adaptive Matching Pursuit (MC-RAMP) filter. MC-RAMP is a computationally efficient and numerically robust general purpose adaptive filter, but in our setting uses reference channels providing information correlated with the CPR artifacts in the ECG. In one of our experiments we test and find MC-RAMP to perform on par with

the theoretically optimal time-varying Wiener filter, but being more computationally efficient and numerically robust.

Using the most realistic data set to date, human out-of-hospital cardiac arrest data of both shockable and non-shockable rhythms, we test CPR artifact filtering by MC-RAMP and evaluate the feasibility of ECG analysis during CPR. In our experiments we use a shock advice algorithm (ECG rhythm analysis) and individual ECG signal features to reach the conclusion that after CPR artifact filtering, ECG rhythm analysis during ongoing CPR is feasible.

Finally, we analyze and quantify the no flow times (NFTs) during external automatic defibrillation in cardiac arrest patients and show that these patients were not perfused (did not have any natural or artificial blood flow) around half of the time. We propose methods using CPR artifact filtering by MC-RAMP to reduce NFT in connection with analyses and shocks, and show their significant and promising potential for reducing the NFT. By introducing the proposed methods into an AED, the NFT would be significantly reduced, hopefully increasing the survival.

Preface

This dissertation is submitted in partial fulfilment of the requirements for the degree of *doktor ingeniør* at the Norwegian University of Science and Technology (NTNU), Trondheim, Norway. Associate professor Trygve Eftestøl of Stavanger University College (Høgskolen i Stavanger, HiS), Stavanger, Norway, has been my supervisor.

The work, including compulsory courses corresponding to one year full time studies, has taken place in the period of May 2001 to July 2004 and was carried out at the Department of Electrical and Computer Engineering of HiS.

The work has been or is in the progress of being published in international journals [55, 33, 37, 38], international conference proceedings [35], and as abstracts from national or international conference presentations [36, 39].

Acknowledgments

First of all, I would like to thank my supervisor, Associate Professor Trygve Eftestøl, for his inspiration, insight and invaluable support providing helpful guidance and feedback on the work of this thesis.

My colleagues at Høgskolen i Stavanger have all contributed to a highly appreciated job atmosphere. Particularly I would like to thank Professors John Håkon Husøy and Sven Ole Aase for sharing ideas and giving constructive criticism. An additional thank must go to Professor Husøy for making me think about taking a doctorate degree in the first place.

I would like to thank Helge Myklebust and Mette Stavland at the Research and Development Department at Laerdal Medical for involving me in their project and providing valuable data, useful ideas and last, but not least a possible usage of this work. I am also grateful for the cooperation and guidance on medical issues provided by Professor Petter Andreas Steen at Ullevål University Hospital. Also thanks to my father-in-law Odd Skjæveland for constructive comments and questions.

Thanks to my parents Anne Kari and Otto for support and encouragement all my life. Last but not least, I would like to thank my wife Laila for love and support.

Contents

List of Abbreviations

AED	Automated external defibrillator
ALS	Advanced life support
AMSA	Amplitude spectrum analysis (signal feature)
BLS	Basic life support
BMP	Basic matching pursuit
BPM	Beats per minute (signal feature)
CF	Centroid frequency (signal feature)
COMPL	Complexity measure (signal feature)
CPR	Cardiopulmonary resuscitation
DC	Direct current, frequency of 0 Hz
ECC	Emergency cardiovascular care
ECG	Electrocardiogram
EMS	Emergency medical services
ENRG	Frequency band-limited energy (signal feature)
FIR	Finite impulse response
FSMN	First spectral moment (signal feature)
IIR	Infinite impulse response
IRM	Irregularity measure (signal feature)
LMS	Least mean squares (adaptive filter)
MC-RAMP	Multichannel recursive adaptive matching pursuit
MP	Matching pursuit
MPA	Mean peak amplitude (signal feature)
MPPA	Mean peak to peak amplitude (signal feature)
NFT	No flow time
PAD	Public access defibrillation
PEA	Pulseless electrical activity
PF	Peak frequency (signal feature)
PPF	Peak power frequency (signal feature)
PR	Pulse-giving rhythm

RLS	Recursive least squares (adaptive filter)
ROSC	Return of spontaneous circulation
RRTE	Ratio of residual to total energy (signal feature)
SFM	Spectral flatness measure (signal feature)
SNR	Signal to noise ratio
VF	Ventricular fibrillation
VT	Ventricular tachycardia
bpm	Beats per minute
dB	Decibel
s	Second
aka.	Also known as
i.a.	Among other (inter alia)
i.e.	That is (id est)
e.g.	For instance (exempli gratis)
et al.	And others (et alia)

Chapter 1

Introduction

Death from heart diseases is the most common type of mortality in western countries. In the USA alone, it is estimated that each year between 400000 and 460000 people die of sudden cardiac arrest (heart stop) in an emergency department or before reaching a hospital, which accounts for over 60% of all cardiac deaths [10, 110]. There is an estimated event rate of 1–2 sudden cardiac arrests per 1000-person years [10,111] with a survival rate of less than 10% [14]. Similar dismal numbers are reported in other countries in the world. In Norway (1998), more than 6000 persons die suddenly and unexpectedly out of hospitals each year. About 80 percent of these deaths are expected to be caused by cardiac diseases [79].

An incident of cardiac arrest may be witnessed by a bystander which then calls for emergency medical services (EMS). A crucial factor for survival is whether this bystander, the lay rescuer, knows *basic life support* (BLS). Artificial respiration (e.g. mouth-to-mouth ventilation) and circulation (chest compressions) are key elements of BLS. From the late 1950's they have been recognized as parts of a whole and combined to create *cardiopulmonary resuscitation* (CPR) as we know it today [81]. The lay rescuer continues CPR until the arrival of an ambulance with a professional rescue team. They provide *advanced life support* (ALS) by clearing the airways and providing CPR, drug therapy, and *defibrillation* of the heart using a high-energy electrical pulse from a *defibrillator*. Finally, the patient is brought to the intensive care unit of a nearby hospital. If the outcome is successful, the patient has obtained return of spontaneous circulation (ROSC), is admitted to the hospital alive, and finally discharged with normal life functioning.

With the introduction of *automated external defibrillators* (AEDs) during the mid-1980s, providing automatic signal analysis and shock advice, a broader

group of defibrillator operators was reached. Through development of AEDs, defibrillation therapy has become easy to use for lay persons with minimal training. Public access defibrillation (PAD) programs necessitates the use of AEDs by the lay public during BLS, and as a result defibrillation therapy is available to a greater proportion of patients early in cardiac arrest.

In the remaining part of this introductory chapter, we first introduce in Section 1.1 the key problem discussed in this thesis as well as earlier research on this problem. Then the scope and contributions of this work are presented in Section 1.2, before we finally give an outline of the thesis in Section 1.3.

1.1 Key problem and earlier research

There are many varying factors in cardiac arrest resuscitation complicating the scene described above: previous heart disease, presence of witnesses, quality of bystander BLS, response time of the ambulance system, the quality of ALS etc. All in all, the survival rate (to hospital discharge) of cardiac arrest is generally low, typically less than 20% in Europe [52].

As stated in [14], it is thought that "successful treatment depends more on *when* treatment is done than on *what* is done". Early defibrillation has therefore been a high priority goal. Recently, it has been recognized that a period of CPR before defibrillation is beneficial, at least if the patient has been in cardiac arrest for some minutes [23, 103]. The condition of the heart deteriorates fast when no artificial (CPR) or natural circulation is present. Pauses in chest compressions halts artificial circulation and introduces detrimental *no flow time* (NFT), and is thought that only a few tens of seconds significantly reduces the chance of successful defibrillation and ROSC [17, 32, 66, 88, 108].

For AEDs to analyze if the patient can be defibrillated, i.e. has a heart rhythm susceptible to an electrical shock, the electrocardiogram (ECG) is recorded and analyzed. The ECG represents the electrical activity of the heart and plays an important role in assessing the patient's status during the therapy of cardiac arrest. However, the mechanical activity from chest compressions and ventilations during CPR introduces artifact components acting as noise in the ECG. For AEDs to perform reliable ECG signal analysis, CPR is therefore discontinued for a substantial time before the potential delivery of an electric shock. If the need for this hands-off time could be reduced or eliminated by removing these artifacts, thus enabling analysis during CPR, it should significantly reduce the NFT and improve the defibrillation success rate. The primary aim of this work is therefore to develop a method for removing CPR artifacts in ECG to enable reliable signal analysis in ECG *during* CPR.

The work previously done on removal of CPR artifacts, has been done mostly using animal ECG, or an artificial mix of human and animal ECG. Artifact removal has been done successfully on animal ECG applying high-pass digital filters with fixed coefficients [78, 91]. In human ECG, however, the frequency components of the artifacts overlap with the frequency components of the heart activity, which makes separation by such filters infeasible and this limits further analysis. This was indicated by Strohmenger et al. [92] and shown in Langhelle et al. [69] which also suggested the use of adaptive filters instead of fixed coefficients filters. In a mix of pig CPR artifacts and human ECG, Aase et al. used an adaptive filter, the multichannel time-varying Wiener filter, for filtering of CPR artifacts [1]. However, prior to the work in this thesis, no studies have been performed on real human out-of-hospital cardiac arrest ECG of both shockable and non-shockable heart rhythms.

1.2 The scope and contributions of this work

The main motivation factors for removing the CPR artifacts in ECG are:

- To enable reliable signal analysis also during CPR in AEDs, not "wasting" time that could have been used for maintaining a blood flow to the tissues (through chest compressions).
- To visually improve the ECG in settings where the users manually assesses the ECG.

The development and usage of a CPR artifact remover is the main focus of this dissertation, and we might contribute to increased cardiac arrest survival rates if we can:

- Develop an efficient filter for CPR artifact removal revealing the true underlying ECG heart rhythm.
- Evaluate if such a filter makes ECG signal analysis during CPR possible in the out-of-hospital cardiac arrest setting.
- Suggest methods using the CPR artifact filter to reduce the NFT during cardiac arrest resuscitation using AEDs.

We will develop a new multichannel adaptive filter for CPR artifact removal, test this filter using real out-of-hospital cardiac arrest ECG and propose a scheme for using the filter in AEDs. Briefly described, the major contributions of this work are as follows:

- Development of a new multichannel adaptive filter, the MultiChannel Recursive Adaptive Matching Pursuit (MC-RAMP) filter, in general, and for CPR artifact removal usage.

- Selection of existing, and development of some new ECG signal features for possible use in an algorithm for rhythm analysis.

- Comparison of the performance of the theoretically optimal time-varying Wiener filter versus MC-RAMP in the setting of CPR artifact removal in a mix of human and animal ECG.

- Evaluation of the feasibility of performing ECG signal analysis during CPR through tests using an existing AED shock advice algorithm and through investigations of the influence of CPR artifacts on common individual features used in ECG analyses. Tests are done using ECG collected from episodes of out-of-hospital human cardiac arrest.

- Development of additional methods to improve the performance of CPR artifact removal.

- Proposal of a scheme to reduce NFT in AEDs using among other factors artifact filtering. The potential of the proposed scheme is shown by comparing NFT in incidences of actual out-of-hospital cardiac arrest treatment using an AED versus the proposed scheme.

Much of the work presented in this thesis has been or is in the progress of being published in international journals [55, 33, 37, 38], international conference proceedings [35], and as abstracts from national or international conference presentations [36, 39].

1.3 Thesis outline

The following chapters constitute the thesis:

Introductory part

Chapter 1 is this introductory chapter introducing the work in this thesis.

Chapter 2 presents the necessary medical background material to motivate and explain the potential clinical significance of this work. The key problems of current therapy of cardiac arrest are discussed, and the problems focused upon in this dissertation are further discussed along with a short review of previous work.

Materials and methods

Chapter 3 describes the data used in this work, which includes ECG, related information, and auxiliary data channels. The data includes both human and pig cardiac arrest ECG.

Chapter 4 describes the development of a new multichannel adaptive filter, the MC-RAMP filter, which we will use later in the thesis for removal of CPR artifacts in ECG. Modifications to the basic MC-RAMP algorithm improving its performance are also presented.

Chapter 5 presents some features and algorithms to be used to evaluate the CPR artifact removal performance of the MC-RAMP filter. This includes a proprietary AED shock advice algorithm, some features published in the literature, and some features developed by us in this thesis.

Experiments: Removal of CPR artifacts and reduction of NFT

Chapter 6 evaluates the MC-RAMP performance in terms of signal-to-noise ratio (SNR) improvements in filtering of artifacts in a mix of animal CPR artifacts and human cardiac arrest ECG. The performance is compared with the theoretically optimal multichannel time-varying Wiener filter.

Chapter 7 uses a shock advice algorithm to further test the performance of CPR artifact filtering using MC-RAMP. Using ECG segments with and without CPR artifacts close in time and with the supposed same underlying heart rhythm, we filter CPR artifacts from human ECG to see if a shock advice algorithm will advice the same.

Chapter 8 presents methods to improve the results of Chapter 7. The methods include adding a short verification analysis in clean ECG and/or postponing analysis in segments with too difficult noise.

Chapter 9 uses various cardiac arrest rhythms from human ECG to examine the influence of CPR artifacts on individual features used in signal analysis of ECG, and if artifact filtering can reduce this influence.

Chapter 10 analyzes and quantifies the detrimental no flow times (NFTs) in our human ECG collected during external automatic defibrillation. We will propose methods to reduce the NFT and see how much time could have been saved.

Conclusive part

Chapter 11 summarizes the major contributions and conclusions from this work, and finally suggests some directions for further research.

In addition there are two appendices:

Appendix A presents a quantitative complexity analysis of the basic MC-RAMP algorithm.

Appendix B lists the available patient episodes from a human cardiac arrest database used in this work, and for what studies they were used.

Chapter 2

Background

In this chapter we will first present the necessary medical background material to motivate and explain the potential clinical significance of our work. This includes some physiology of the heart, definition of cardiac arrest, ECG and cardiac arrest rhythms, as well as current therapy of cardiac arrest. We will further outline the key problems of current therapy, including the problem with no flow time which is the core problem to be studied in this thesis. Successful filtering of CPR artifacts is essential to solving this problem, and will be discussed, along with a short review of previous work and the outline of directions to be followed.

Some of the material in this chapter is adapted from [33].

2.1 The heart and its conduction system [11, 43, 99]

The heart and its conduction system is shown in Figure 2.1. The heart is a hollow muscular organ (the myocardium – the cardiac muscle) about the size of a clenched fist. It serves as a four-chambered blood pump for the circulatory system. The two main chambers, *the ventricles*, supplies the main pumping function, while the two antechambers, *the atria*, primarily store blood during the time the ventricles are pumping. The heart cycle has two phases; the resting or filling phase (the diastole) and the contractile or pumping phase (the systole).

For the heart to adequately pump blood through the body, the heart must contract in a highly synchronized fashion. First both atria contract, then both ventricles contract. The contractions are coordinated by an elaborate conduction system spreading an electric impulse, the cardiac impulse, throughout

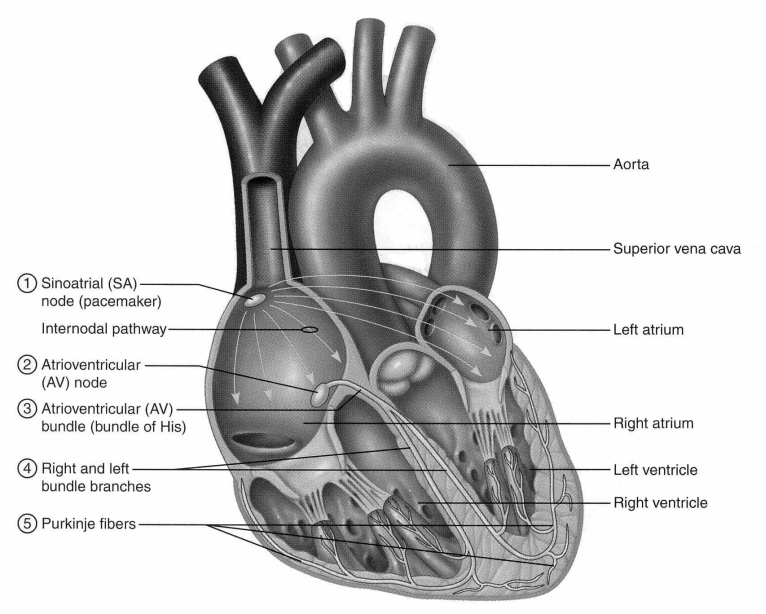

Figure 2.1: The conduction system of the heart (frontal view). The illustration is taken from *Principles of Human Physiology* [43], © 2002 Pearson Education.

the heart. This determines the sequence of excitation (activation) of cardiac muscle cells.

In a healthy heart, the sinus node (sinoatrial node) in the right atrium serves as a pacemaker and initiates the cardiac impulse[1], causing the atria to contract. The impulse is spread through the atria reaching the atrioventricular (AV) node, which leads the impulse into the AV bundle (bundle of His) and its branches (left and right bundle branches and the Purkinje fibers) causing the ventricles to contract. This is repeated for each heartbeat, with the heart rate set by the sinus node (normally about 70 beats per minute (bpm)).

2.2 Cardiac arrest

In cardiac arrest, the normal pumping operation of the heart described above has stopped. Cardiac arrest is defined in the Utstein II international consensus workshop (1991) as the "cessation of cardiac mechanical activity, confirmed

[1] As a backup, if the sinus node fails to function, the AV node or even certain cells in the Purkinje fibers will serve as the heart's pacemaker, although at a lower heart rate.

by the absence of a detectable pulse, unresponsiveness, and apnea[2] or agonal, gasping respiration" [27]. Sudden cardiac death is the term usually used for unexpected death of cardiac causes occurring immediately or within 1 hour of onset of first symptoms [14].

As mentioned in Chapter 1, sudden cardiac arrest claims many lives, several hundred thousand each year in the USA alone. The survival rate of sudden cardiac arrest is dismally low. The chance of having a cardiac arrest increases with age, and men seem to be more prone to cardiac arrest than women [53, 110]. In a study from Seattle, Washington, in 1999-2000, 64.9% of the cardiac arrest patients were men and the mean age was 69.9 years [24].

There are many causes of cardiac arrest, both cardiac and non-cardiac causes[3]. Of the cardiac causes, coronary artery disease is the most common cause. Other possible cardiac causes include cardiac arrhythmias, acute myocardial infarction, valvular heart disease, cardiomyopathy or myocarditis, prolonged QT interval, congenital heart disease, intracardiac tumor, Wolff-Parkinson-White syndrome, and pericardial tamponade [4]. Some non-cardiac causes of cardiac arrest include pulmonary embolism, choking and asphyxia, drug ingestion, substance abuse, stroke, hypoxia, hypoglycemia, alcoholism, allergic reactions, and electrical shock [4].

2.2.1 ECG and cardiac arrest rhythms

The ECG is a recording of the bioelectrical activity of the heart and plays an important role in assessing the patient's status during the therapy of cardiac arrest. The normal heart rhythm is called the sinus rhythm, with electrical impulses originating in the sinus node producing various waves on the ECG as they spread throughout the heart. A typical sinus rhythm is shown in Figure 2.2 characterized by regular P waves, QRS complexes, and T waves representing each heartbeat.

During cardiac arrest, the mechanical pumping of the heart stops and the normal sinus rhythm in the ECG changes to some cardiac arrest rhythm, an *arrhythmia*. The most common groups of rhythms found during cardiac arrest are listed below:

[2] An absence of spontaneous circulation [11].

[3] Since they are not important to us later in the thesis, we only mention the causes without explaining them. We just want to give an impression of the variability of causes. For more information, we refer to a medical dictionary, such as [11], or other medical literature.

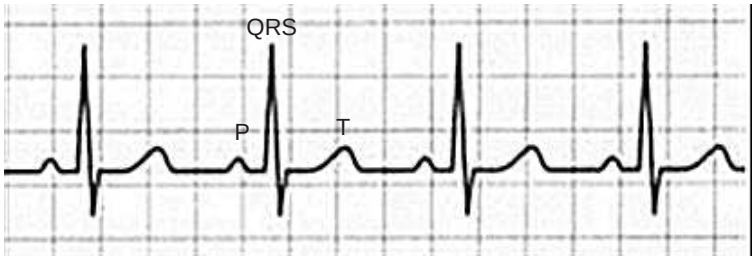

Figure 2.2: ECG of a normal sinus rhythm with its characterizing waves and complexes: The P wave originates from the sequential activation (depolarization) of the right and left atria, the QRS complex is due to right and left ventricular depolarization (normally the ventricles are activated simultaneously) and the T wave is due to the ventricular repolarization.

- **Ventricular fibrillation (VF)** is a seemingly chaotic rhythm that originates in the ventricles. The ventricles quiver and, as a result, there is no useful contraction and no pulse. The fibrillation is maintained by the presence of multiple activation waves moving randomly through the myocardium around areas of refractory tissue [97]. The resulting ECG rhythm is irregular with chaotic deflections that vary in shape and amplitude. Figure 2.3(a) and (b) show two VF examples, both "coarse" VF (high amplitude waves) and "fine" VF (low amplitude waves). VF is considered shockable and should be treated with a defibrillatory electroshock. Left untreated, the VF amplitude seems to decay, and the rhythm converts to asystole (see below) over time. In a study of out-of-hospital cardiac arrest patients in Sweden between 1990 and 1995, initial VF rhythm was estimated in 80–85% of the patients [53], making VF the most common initial cardiac arrest rhythm. For more information on the mechanisms of VF, see [56].

- **Ventricular tachycardia (VT)** is a rapid ventricular arrythmia with rate over 100 beats per minute (bpm). VT consists of three or more premature ventricular complexes[4] (PVCs) occurring in immediate succession. VT may occur with or without pulse, and could have essentially regular waves (monomorphic) or be more irregular and varying in shape (polymorphic). Normally, the P wave is absent and the QRS complex is wide (greater than 120 ms) [5]. In the cardiac arrest context, nonperfusing (pulseless) VT with rate over 150 bpm is considered shockable.

[4] An arrhythmic heartbeat characterized by ventricular depolarization occurring earlier than expected. Appearing on the ECG as an early wide QRS complex without a preceding related P wave. [11]

Figure 2.3(c) shows an example of VT.

- **Asystole** is total absence of ventricular activity, with no ventricular rate or pulse. Some atrial electrical activity may be present [5]. Asystole is not considered shockable, but is often treated with chest compressions, ventilations and medications (hoping to induce VF which is shockable). Figure 2.3(d) shows an example of asystole.

- **Pulseless electrical activity (PEA)** is a clinical situation, not a specific arrythmia, and was previously known as electromechanical dissociation (EMD). PEA exists when organized activity (other than VT) is observed in the ECG, but no pulse is palpable [5]. PEA waveforms can differ greatly in shape and amplitude, with narrow or wide QRS complexes, but are generally regular and organized. Narrow complex PEA is often associated with higher likelihood of successful resuscitation than wide complex PEA [12], and is often difficult to separate from pulse-giving rhythms in ECG. PEA can sometimes be a transitory rhythm after a shock, or have other causes which may be specifically treated. PEA is not considered shockable, but is often treated with chest compressions, ventilations and medications. Figure 2.3(e) and (f) show two examples of PEA.

2.3 Treatment of out-of-hospital cardiac arrest

During cardiac arrest, the heart stops its normal pumping of blood to the body, resulting in death in a matter of minutes. There are at present only two factors thought to reverse this process and make the heart start pumping again [9]:

1. *Cardiopulmonary resuscitation (CPR)* defined as external cardiac massage (chest compressions) and artificial respiration (ventilation) [11]. This is the basic life support (BLS) providing some circulation of the blood counteracting death or brain damage due to lack of oxygen. *Chest compressions* compresses the heart between the breastbone (lower sternum) and spine (thoracic vertebral column) forcing blood through the body. Both hands of the rescuer with the fingers interlocked are placed on the patient's chest and the breastbone is depressed 3.8–5.1 cm [9]. This is repeated at a rate of 100 compressions per minute. *Ventilation* of the patient is done through mouth-to-mouth breathing in BLS or a

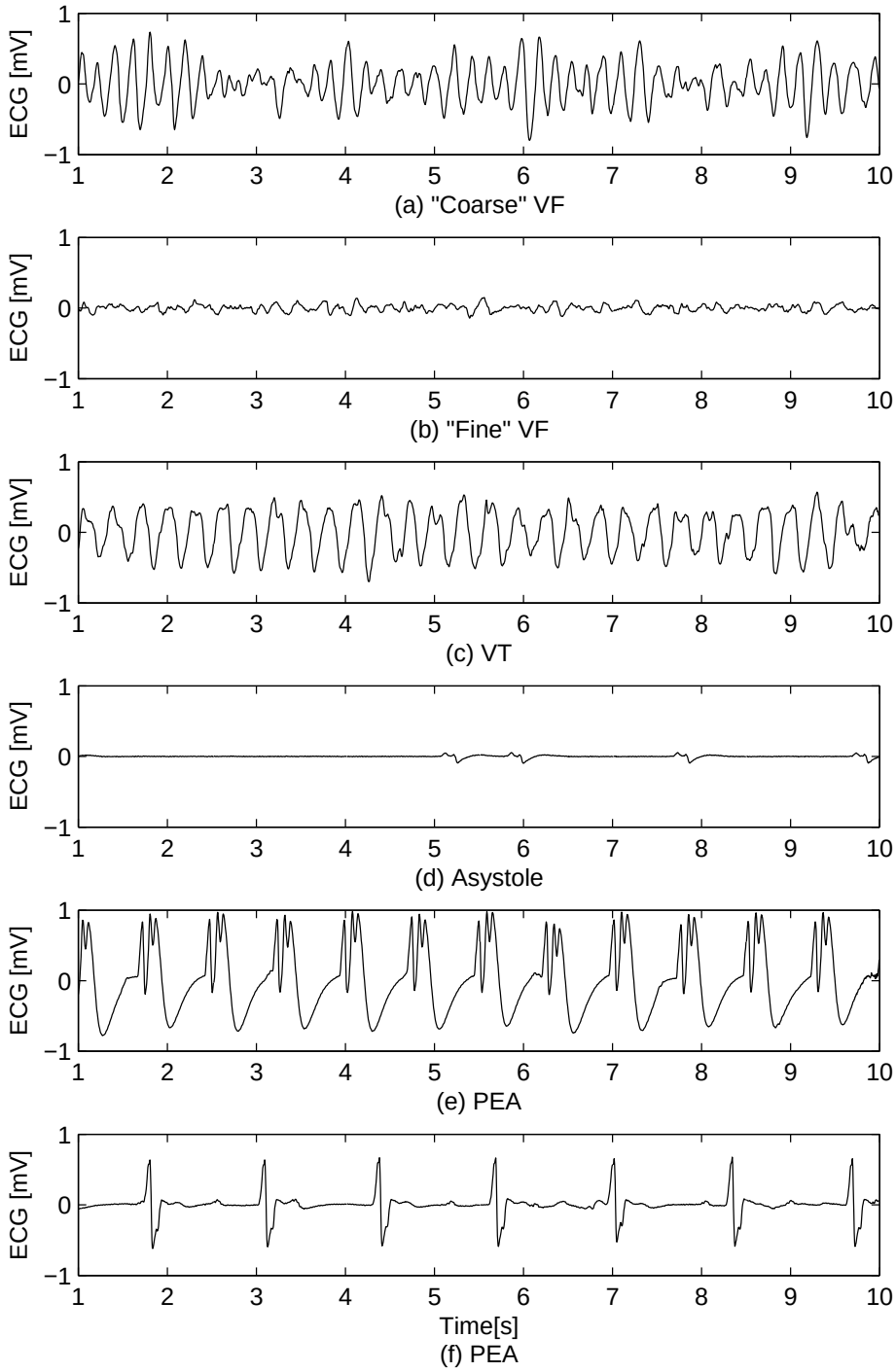

Figure 2.3: Some examples of ECG tracings of cardiac arrest rhythms.

mechanical form of ventilation, often after intubation[5], in advanced life support (ALS). During BLS with mouth-to-mouth breathing, the cycle of 15 compressions before 2 full breaths are repeated. After intubation, ventilations may be provided without stopping the compressions so the patient may be compressed continuously. Note that even well executed CPR can only provide 25%–35% of the normal blood flow [11].

2. *Defibrillation* defined as the termination of VF or pulseless VT by delivery of an electrical shock to the patient's chest [11]. The purpose of the shock is to pass current through the heart, hoping to knock out the chaotic electrical activity of the heart during VF or VT, anticipating that the regular rhythm-generating system in the heart again can take over and generate a pulse. The machine delivering these shocks is called a defibrillator.

The current recommended treatment of cardiac arrest is described in international guidelines, with the latest from 2000 [9], and can be summarized as follows: The AED records ECG, and uses a software algorithm analyzing the ECG waveforms to determine whether the rhythm is shockable (VF or VT) or not. Based on the analysis results, a voice prompt recommends defibrillation or not. The current CPR guidelines recommend immediate defibrillation if the first recognized rhythm is shockable. If this first shock is unsuccessful in terminating the VF or VT, up to two more shocks are recommended before CPR is started. Thereafter series of defibrillation attempts and CPR periods are repeated until return of spontaneous circulation (ROSC) is achieved or the whole resuscitation attempt is discontinued. For non-VF/VT rhythms, CPR is continued until a shockable rhythm is achieved, or the whole resuscitation attempt is discontinued.

Although drugs are also being used during ALS, no drugs have been shown to improve the outcome clinically [9]. Without the use of a defibrillator very few patients with VF obtain ROSC. With the use of a defibrillator approximately 40–60% of the VF/VT patients might achieve ROSC [24, 50, 94, 103], with a survival rate to hospital discharge varying usually between 5 and 30% [24, 40, 50, 52, 94, 103]. For other cardiac rhythms, the prognosis is dismal, usually with a survival rate of 1–5% [24, 40], and most of the survivors have gone through a stage with VF and successful defibrillation before achieving ROSC.

Current international guidelines state that early defibrillation within 5 minutes of call-receipt by the EMS is a high priority goal [9]. To achieve this, non-medical personnel must be enabled to defibrillate in so-called public access

[5] Insertion of a breathing tube through the mouth or nose into the trachea to ensure an open airway [11].

defibrillation (PAD) programs using automated external defibrillators (AEDs, see Section 2.3.1). Therefore, the current focus has turned onto development of more defibrillation efficient, lightweight, and easy-to use defibrillators. For a review on the role of the automated defibrillator in improving survival from sudden cardiac death, see [72].

The most important factors influencing the survival rates of out-of-hospital cardiac arrest patients are:

- Time elapsed from collapse until the first defibrillation attempt [50, 70, 103].
- Whether CPR has been provided or not [26].
- The quality of both CPR and ALS [98, 100].

The interplay of these factors is decisive for the final outcome. Recent studies strongly indicate that it is time-dependent whether defibrillation should be attempted as soon as a defibrillator is available, if good-quality CPR has not been provided in the meantime. If more than a few minutes have passed from the time of arrest until the defibrillator arrives (more than 4–5 minutes response time), a 1.5–3 minute period of CPR should precede the defibrillation attempt [23, 103]. This is probably the result of a deterioration of the myocardium due to lack of myocardial circulation resulting in an inability of the regular rhythm-generating system in the heart to take over after a defibrillation attempt.

2.3.1 The automated external defibrillator (AED)

The AED is a machine capable of delivering electrical shocks to terminate VF/VT rhythms. A capacitor is charged and the energy stored in it is discharged through a pair of electrodes connected to the chest of the patient, normally one electrode at the upper right portion of the chest[6] and one at the left side of the chest below the armpit[7]. The strength (energy) of the electrical shock is expressed in joules (J). The current can be delivered through different waveforms. The two most common groups are *monophasic* and *biphasic* waveforms. The newer biphasic waveforms are shown to be more effective in terminating VF/VT rhythms using a lower energy setting (typically 150 J)

[6] Placed to the right of the upper sternum below the clavicle [11].
[7] Placed to the midaxillary line of the left lower rib cage [11].

than monophasic waveforms (typically 200–360 J) [44, 45, 74]. This is beneficial since the electrical shock in itself can be harmful to the heart, increasingly so for higher energies [107].

An AED records the ECG which is shown for monitoring purposes. More importantly, an AED can analyze the ECG to determine if a shockable rhythm is present. AEDs may be fully automated or semi-automated. If a shockable rhythm is present, a fully automated AED will, after press of an "analyze" button, automatically charge its capacitor and deliver the shock without further input of the operator. In *semi-automatic mode*, also called shock advisory mode, the AED will analyze and indicate if a shock is advised, automatically charge the capacitors, but wait for the operator to press a "shock" button to deliver the shock. Note that the AEDs in semi-automatic and automatic mode advice the operators when to pause and resume treatment (e.g. CPR). For instance, when the machine is analyzing, the operators are told to pause the treatment. Such pauses are detrimental to the patient as will be further discussed in the next section. Some AEDs can also be operated in *manual mode*, that is, with no machine ECG rhythm analysis, and manual start of capacitor charging and delivery of shock.

2.4 Key problems in cardiac resuscitation today

There are many factors complicating and contributing to the outcome of the cardiac resuscitation, and unfortunately the survival rate of cardiac arrest is generally low, typically less than 20% in Europe [52]. The key problems in cardiac resuscitation today are:

- Much time without blood flow being generated, i.e. no flow time
- A large number of unsuccessful shocks
- Quality of compressions and ventilations delivered might be poor

This section will discuss these factors weakening the treatment of cardiac arrest.

2.4.1 Aspects of no flow time

Many shocks given to a patient today is unsuccessful, i.e. no ROSC occurs or even the shock fails to terminate the VF. It is important to consider that

each such defibrillation attempt requires a time period for rhythm analysis, capacitor charging, shock delivery and new postshock rhythm analysis where no CPR can be given, as the rhythm analysis software requires that the patient lies completely still to avoid any ECG artifacts being created. In one study, the median time from initiation of rhythm analysis until shock was given, was 20 seconds [94]. In a follow-up study of the same material, it was shown that the myocardial condition deteriorated substantially during that same period [32]. In a study using swines [108], an increase of the hands-off time (time from CPR end to shock) from 3 to 15 seconds decreased the portion of successfully resuscitated animals (ROSC restored) in each group from 100% to 40%. In the group with 20 seconds hands-off time, no animal survived. Other studies also indicate the same [17, 66, 88].

Hands-off time is often used as the time from CPR end to shock delivery. More generally, we define *no flow time* (NFT) as time with no natural or artificial myocardial and cerebral (brain) blood flow, which occurs in several situations, both as a consequence of the current guidelines [9], the defibrillators, and for other reasons. Some reasons for NFT periods include delivery of shocks, rhythm evaluation (automatic or manual), charging of the capacitor, checking for pulse, ventilations in unintubated patients (which is done in between compression series), intubating, and starting intravenous lines. Normally, more NFT has been associated with AED use compared to manual defibrillation [17]. Overall, a study investigating 184 patients treated with AEDs showed that CPR was performed only 45% of the connected time [7].

Reducing the NFT is the main objective in this thesis, and we will later investigate the means to do so.

2.4.2 The large number of unsuccessful shocks

Many studies report very high defibrillation success rates, 95–99%. Yet the ROSC-rate is frequently less than 50%, and many patients achieving ROSC require many defibrillation attempts [50, 94]. This might be somewhat confusing, and is due to the definition of defibrillation success. As mentioned above, the immediate purpose of using the defibrillator is to terminate the VF or VT, hoping that this will give room for a pulse-generating rhythm (ROSC). Thus defibrillation success is frequently defined as the absence of VF or VT for at least the first 5 seconds after the shock [45]. Clinically, we are interested in ROSC which as suggested above does not only depend on the quality of the defibrillator and defibrillation attempt, but also on the condition of the myocardium, which again depends on the duration of the cardiac arrest and the

CPR provided [103]. A clinical definition of a successful defibrillation attempt could therefore be ROSC, stable or not [94]. In these terms, only 10% of 883 shocks were successful in the study by Sunde et al [94].

It has been shown that a defibrillation attempt in itself is harmful to the myocardium [107]. Therefore, it would be a great potential advantage if defibrillation attempts not resulting in ROSC could be predicted and avoided.

2.4.3 Poor quality of compressions and ventilations

In general one might say that the chance for ROSC is at its highest level immediately after the arrest, when the heart muscle still has a high supply of energy resources and oxygen. As time passes, these resources are drained. The rate of this drainage can at least be reduced by properly performed CPR, which as mentioned above, probably can even improve the myocardial situation if there has been a period without properly executed CPR before the defibrillator is available. However, the quality of CPR given by both lay persons and rescue personnel may be poor (e.g. too shallow chest compressions [104]). The skills involved in the performance of chest compressions and ventilations may be poorly acquired and poorly retained [19,63,106]. To improve this, voice advisory systems have been introduced with good results in training [101,102] and for actual CPR feedback in AEDs [49,112].

2.5 Medical decision support system

The last 15 years has seen advances in research addressing the problems stated in Section 2.4, investigating methods that have a potential for improving the survival rates from cardiac arrest. In essence, the rescuer should be guided by information at least partly gathered on-line and processed in real-time, in her/his decision making on which therapeutic component to use. Such methods are parts of a decision support system. A decision support system might be considered as representing the knowledge of former therapy. A framework for medical decision support system in AEDs was proposed by Eftestøl [30]. The modules in such a system are illustrated in Figure 2.4. In the following, we will discuss the components of the decision support system. This includes the *CPR artifact remover* component, the main contribution of this work. Its primary function is to remove CPR artifacts in the ECG to enable analyses during CPR. The clinical value of this is reduced NFT related to analyses and shocks, since CPR can be continued for a longer period of time.

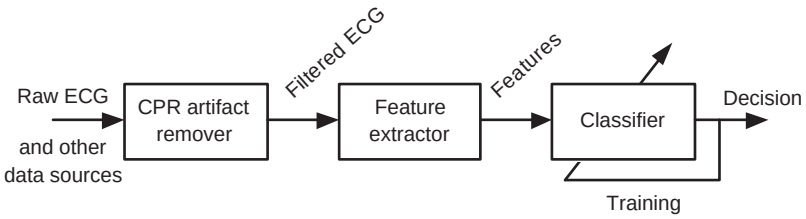

Figure 2.4: The modules in a medical decision support system for cardiac arrest resuscitation.

2.5.1 The raw ECG and other data sources

The integration and availability of multiple information sources are crucial for the other parts of the decision support system and the technical improvements in cardiac arrest resuscitation.

For clinical use in a decision support system we only have the information provided by the defibrillator, i.e. the time series recordings of ECG, an event report (with information on internal statuses and operations), and in some cases other related data channels such as impedance and accelerometer measurements.

For further retrospective analyses the therapy of cardiac arrest is documented in report sheets carrying information about patient demographics and important therapy. Both defibrillator event records and report data are synchronized to the time series data. Based on the integration of this information, components in a visualization of the time series data with events and report details shown, the medical experts are able to interpret and annotate the data. Such structured information can be used to train the decision support system.

2.5.2 The CPR artifact remover

The feature extractor and classifier in the decision support system rely on clean data for reliable analyses. Because of this, CPR must be stopped during analyses in current AEDs. This is because the mechanical activity from chest compressions and ventilations during CPR introduces artifact components in the ECG, affecting and disturbing the analyses. The role of the CPR artifact remover is to remove these artifacts, providing clean data to the feature extractor. As a consequence, NFT around analysis and shocks can be reduced. As discussed in Section 2.4.1, NFT is detrimental in cardiac arrest resuscitation, with more NFT currently being associated with AED use compared to manual defibrillation. Functionality for removing CPR artifacts is not currently

implemented in AEDs, and it is currently not certain if such functionality can enable reliable analyses during CPR.

Developing an efficient CPR artifact remover, evaluating the feasibility of analyses during CPR, and ultimately how to reduce the NFT in AEDs are the main problems we will investigate in later chapters. We discuss these problems further in Section 2.6.

2.5.3 The feature extractor and classifier

In general, a feature extractor measures certain properties or characteristics, termed *features*, in a signal. For a given purpose, this enables the signal to instead be represented by these features – which are most often of lower dimension or size. A *classifier* uses features to discriminate between different signal classes and may calculate the probability of a certain signal belonging to a certain class. The classifier contains prior knowledge about the classes and features, and is often trained using a *training set*, a particular set of signals where their true class belongings are known. For more information, see pattern classification books such as [28, 96].

This section will discuss several uses of a feature extractor and classifier that are, or proposed to be, used in an AED during cardiac resuscitation. In the testing of our CPR artifact remover, we will use a proprietary feature extractor and classifier for rhythm analysis, as well as individual features. See Chapter 5 for a description of these.

Shock advice – rhythm analysis

Rhythm analysis is used to distinguish between shockable rhythms such as VF and VT with rate over 150 bpm, and non-shockable rhythms such as asystole, PEA, and various pulse rhythms. This is used to make a shock advice; a shock/no-shock decision.

A rhythm analysis is implemented in all AEDs, often termed the shock advice algorithm. Most of these algorithms are proprietary and their internal operations are not publicly available. However, through publicly available application notes, some properties of the algorithms can be deduced. The shock/no-shock decision can be based upon features such as the average amplitude, the isoelectric baseline content, QRS detection, waveform organization/regularity and rate [83]. Other features are also tested experimentally and described in the literature [68, 13, 87, 86, 20, 109, 58, 59, 60]. Some of these, as well as a few developed for this thesis, are described in Chapter 5.

Predicting shock outcome – VF analysis

VF analysis is the analysis of VF and VT rhythms to predict the success of defibrillation (shock outcome prediction) in order to avoid wasting time on unsuccessful and potentially harmful defibrillation attempts.

Work aiming at predicting the shock outcome goes back almost 20 years with several research groups having been involved as reviewed by Amann et al [8]. However, no AED available has this kind of functionality. It has only been used for retrospective analysis. The ability to predict the outcome of defibrillation is a key issue in improving resuscitability. The idea is that one or several predictors of defibrillation outcome can be measured from the ECG waveform. There are now quite a few studies showing that the VF waveform contains such information [29,78,84,89,93]. Thus, if the predictors (features), have good discriminative power, we will be able to avoid unsuccessful defibrillation attempts (no ROSC) and shock only when we know that the chance for success (ROSC) is high. Such a decision should be based on a compound analysis of several features, and the predictor's (classifier's) output could be a hard decision SHOCK/DO NOT SHOCK or a soft decision producing a continuous outcome variable, for instance the probability of ROSC, P_{ROSC} [31]. Possible features considered for shock outcome predictors include amplitude features such as mean VF voltage, frequency features such as median frequency, nonlinear dynamics features such as correlation dimension and scaling exponent, bispectral energy, amplitude spectrum analysis (AMSA), wavelets, and $N(\alpha)$ histograms [8].

Measuring the effects of therapy – online monitoring

In addition to shock outcome prediction, features could be used to measure the effects of therapy [32], such as performance feedback during CPR. This could be used to optimize the sequence and quality of the various components of ALS and BLS. Not only the ECG waveform is used for extracting useful features. A recent animal study implies the application of transthoracic impedance signals for breath- and pulse-check [82]. This offers the opportunity to shorten therapy-decision-time following a defibrillation. Also the Zoll AED PLUS defibrillator offers accelerometer based measurements of compression depth. Further processing of these measurements facilitates automated feedback on chest compression performance in order to increase CPR quality [112].

2.6 Problem formulations

We have given some clinical background on cardiac arrests and the key problems in the treatment of cardiac arrest today. The medical decision support system described in Section 2.5 includes a CPR artifact remover component. The main motivation factors for removing the CPR artifacts in ECG are:

- To enable reliable signal analysis also during CPR in AEDs, not "wasting" time that could have been used for maintaining a blood flow to the tissues.
- To visually improve the ECG for decision support in manual mode defibrillation where users manually assesses the ECG.

The development and usage of a CPR artifact remover is the main focus of this dissertation, and we might contribute to increased cardiac arrest survival rates if we can:

- Develop an efficient filter for CPR artifact removal.
- Evaluate if such a filter makes ECG signal analysis during CPR possible in the out-of-hospital cardiac arrest setting.
- Suggest and evaluate methods using the artifact filter to reduce the NFT during cardiac arrest resuscitation using AEDs.

These tasks, to be investigated in later chapters, are further discussed in this section. We also provide a short overview of earlier work in these areas.

2.6.1 Enabling ECG analyses during CPR – filtering CPR artifacts

The mechanical activity from chest compressions and ventilations during CPR introduces artifact components in the ECG. These artifacts will often fool algorithms for ECG signal analysis. For AEDs to perform reliable ECG signal analysis, CPR is therefore discontinued for a substantial time before the potential delivery of an electric shock. If the need for this hands-off time could be reduced or eliminated by removing these artifacts, enabling signal analysis *during* CPR, it should significantly improve the defibrillation success rate as discussed in Section 2.4.1.

In the remainder of this section, we will discuss CPR artifacts, earlier work, and our own work on reducing these artifacts in ECG.

CPR artifacts

The CPR artifacts vary a great deal in shape and amplitude, and may be more or less prominent in the ECG – from apparently not disturbing the heart's own activity at all to being completely dominant with amplitudes exceeding several mV. Artifacts from chest compressions are the dominating artifacts, with ventilation artifacts normally appearing in ECG only as a small baseline drift. Some examples of ECG with CPR artifacts are shown for VF, asystole, and PEA/PR segments in Figures 2.5, 2.6, and 2.7, respectively. The first 10 seconds of each example are with CPR artifacts (mainly chest compression artifacts), whereas the last 10 seconds are without (or with small ventilation artifacts as seen as small baseline "jumps").

The CPR artifacts can have several origins. A CPR artifact model was suggested by Langhelle et al. [69], where the artifacts are composed by the sum of four individual artifact generators:

1. Artifact components originating from the heart due to mechanical stimulation.
2. Artifact components generated by mechanical stimulation of thorax muscles.
3. Artifact components originating from the electrode-skin interface due to mechanical deformation (electrode drag or tap).
4. Artifact components caused by static electricity and the following charge equalizing currents between measurement equipment and patient.

The mechanical activity from both chest compressions and ventilations will generate artifact components from the first three generators, whereas the last more depends on the conditions for static electricity during CPR. The knowledge of these generators can contribute to the identification of physical measurements reflecting the artifacts in some way. These measurements can then be used in a system to remove the artifacts. This is the idea behind the artifact remover we develop and test in later chapters.

Earlier work on CPR artifact filtering

Artifact removal has been done successfully on animal ECG applying high-pass digital filters with fixed coefficients [78,91]. In human ECG, however, the frequency components of the artifacts overlap with the frequency components

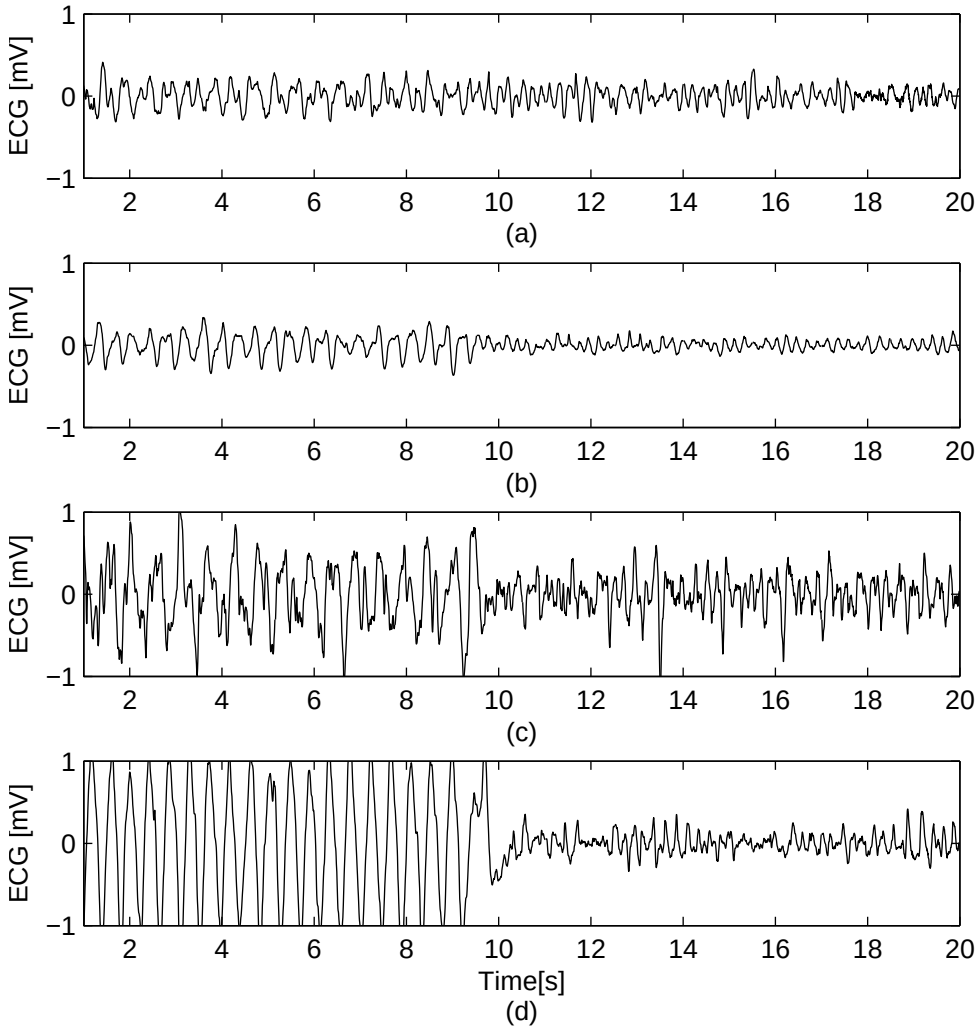

Figure 2.5: Four examples of VF segments with CPR artifacts of varying shape and amplitude. First 10 seconds of each example are with CPR artifacts, last 10 without.

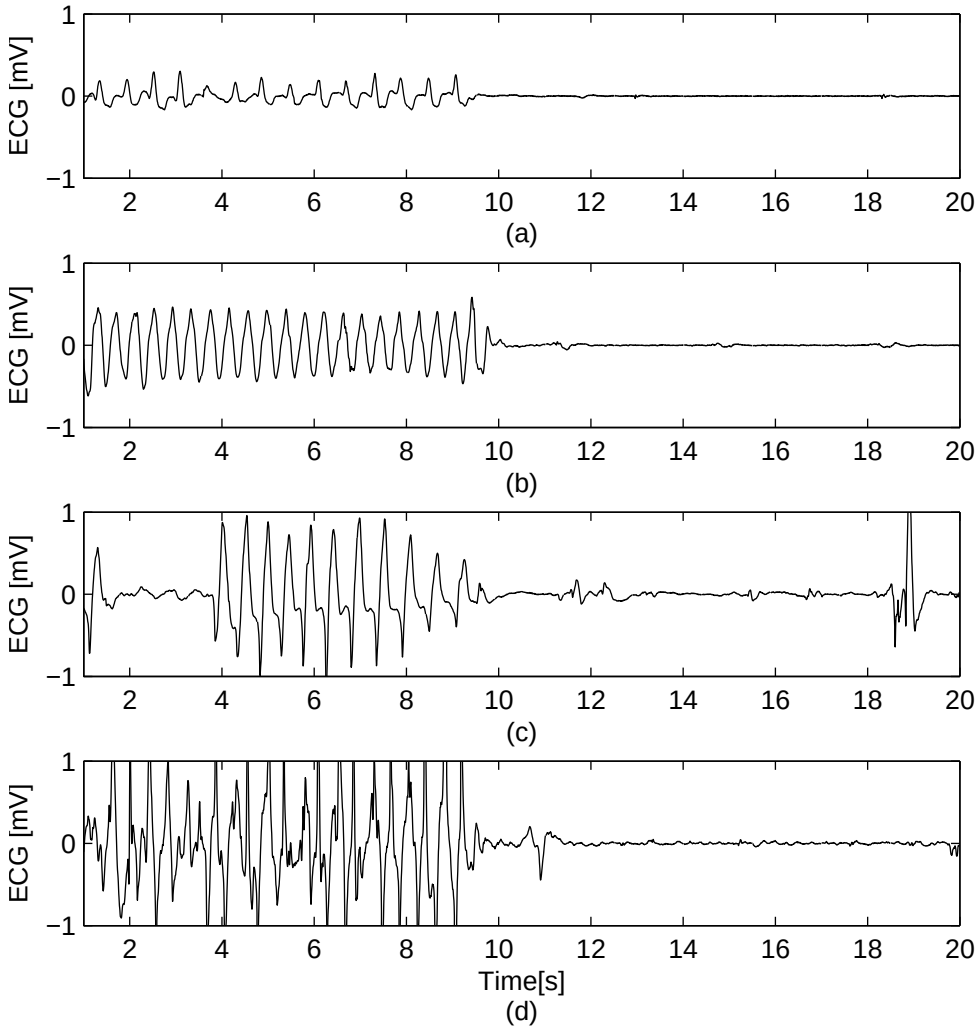

Figure 2.6: Four examples of asystole segments with CPR artifacts of varying shape and amplitude. First 10 seconds of each example are with CPR artifacts, last 10 without.

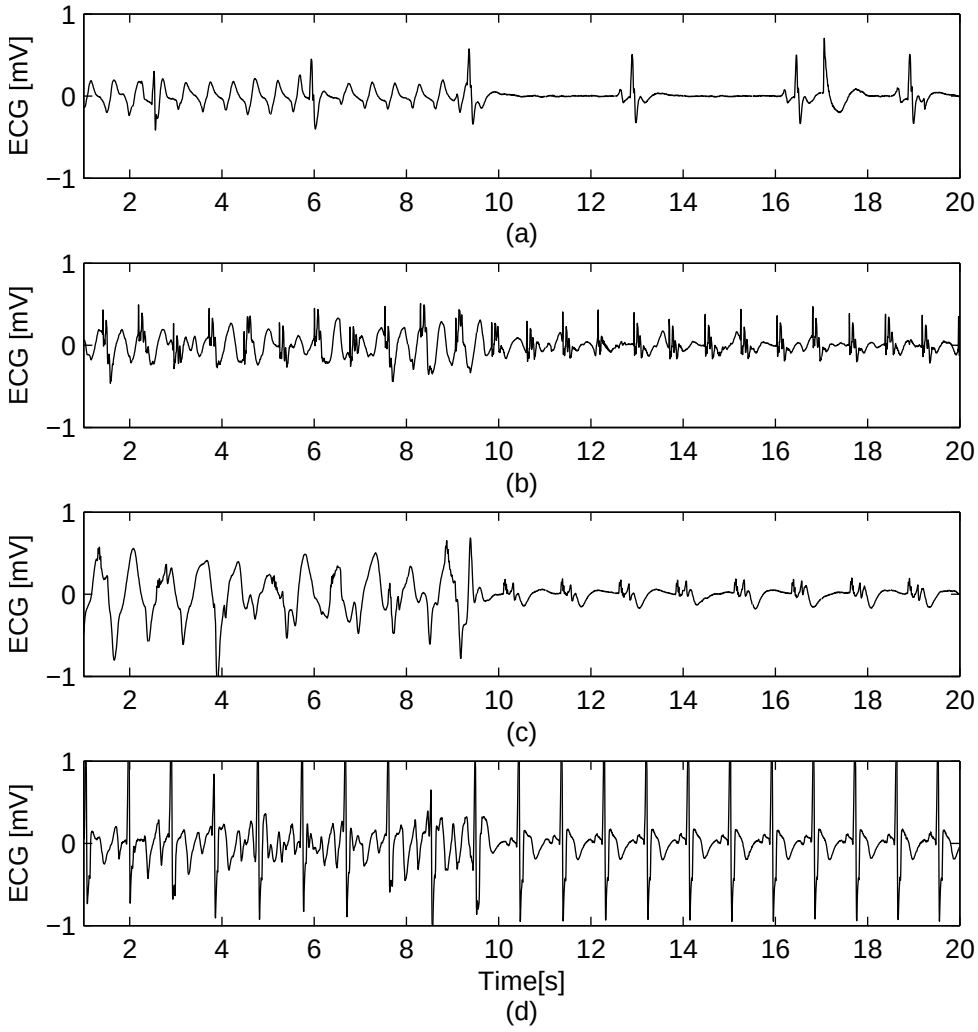

Figure 2.7: Four examples of PEA segments with CPR artifacts of varying shape and amplitude. First 10 seconds of each example are with CPR artifacts, last 10 without.

of the heart activity (e.g. VF), which makes separation by such filters infeasible [69]. In studies by Strohmenger et al. investigating frequency features in VF, the mean dominant frequency in pigs was 9.0 Hz [91] and 3.0 Hz in humans [92]. The rate of chest compressions normally ranges between 80–120 compressions per minute. This corresponds to artifacts with fundamental frequencies in the range 1.33–2 Hz as well as one to three distinct harmonic frequencies. The difference in pigs and humans is illustrated in Figure 2.8 with spectrograms[8] of both pig and human VF with CPR artifacts. The distinct horizontal lines in the spectrograms in the first 10 seconds are the chest compression artifacts (pig: 1–4 Hz, human: 1–7 Hz), which can be seen to *not* overlap with the pig VF (7–16 Hz) in Figure 2.8(a), but do overlap with the human, more low-frequency (1–4 Hz), VF in Figure 2.8(b). Similar results were also shown by Langhelle et al. [69] which instead of fixed coefficients filters suggested the use of adaptive filters[9] for CPR artifact removal.

There have been few studies using real human out-of-hospital cardiac arrest ECG for CPR artifact removal. The only one we know of is a study by Strohmenger et al. [92] showing that the effect CPR has on amplitude and frequency signal parameters in VF is removed by limiting the frequency range to 4.3–30 Hz. However, this frequency range also significantly alters the true values of the parameters (without CPR artifacts) compared to the reference 0.3–30 Hz frequency range. This deteriorated the predictive value (in terms of shock outcome prediction) of the frequency parameters examined.

In a mix of pig CPR artifacts and human VF/VT, Aase et al. used a multichannel time-varying Wiener filter for filtering of CPR artifacts [1]. This theoretically optimal adaptive filter calculates the optimal Wiener solution for every sample [85]. The filter assumes that the CPR artifacts are a sum of several sources and models the artifacts as a sum of contributions from so called reference channel signals. Reference channels are signals that correlate with/resemble the different artifact sources and are recorded simultaneously with the ECG. In the case of [1], *compression depth* and *thorax impedance* was used. Using this filter, the CPR artifacts were successfully reduced [1]. However, the solution relies on the inversion of an estimated multichannel autocorrelation matrix for every sample, a computationally expensive solution. Furthermore, given that reference signals encountered in practice, from time to time, give rise to ill-conditioned autocorrelation matrices further complicates the situation (will suffer numerical problems).

[8] A spectrogram is a time-frequency plot where each vertical line can be said to be the power spectrum density for a given time instant – showing the frequency content of a signal with respect to time. Lighter shades of gray indicate higher content.

[9] An adaptive filter is a filter with time-varying filter coefficients.

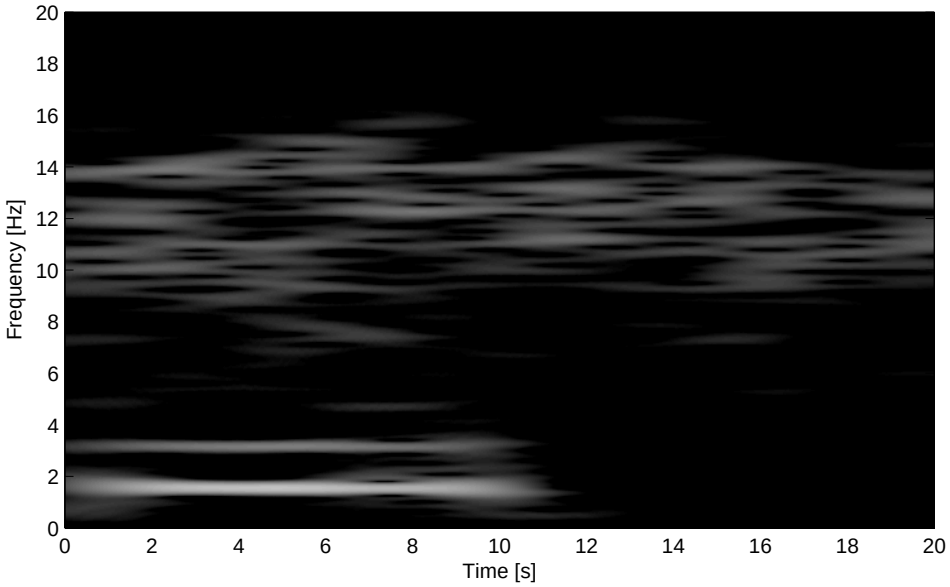

(a) Spectrogram of CPR in pig showing non-overlapping frequency components of pig VF and CPR, making such a signal trivial to filter using standard frequency-selective filters.

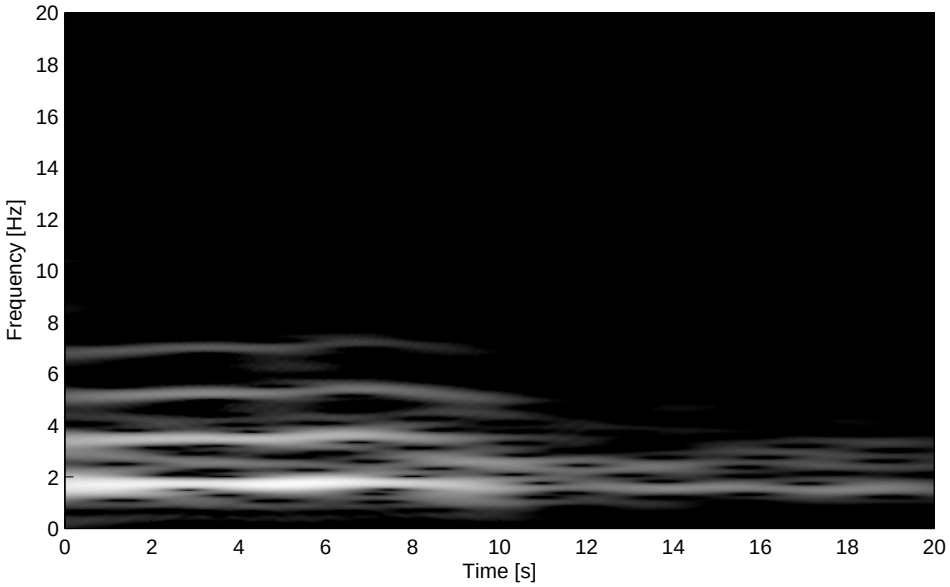

(b) Spectrogram of CPR in human showing overlapping frequency components of human VF and CPR, making the filtering non-trivial.

Figure 2.8: Spectrograms of ECG with pig and human VF with CPR artifacts in the first 10 seconds. Lighter shades of gray indicate higher energies.

Our work on CPR artifact filtering

The previous work on CPR artifact filtering has only used VF or VT rhythms, not including any non-shockable rhythms which are also commonly encountered during cardiac arrests. These also need to be addressed, as the CPR artifacts can often resemble VF/VT confusing the analyses in AEDs. For these broad group of rhythms, the CPR artifact filtering face new and different challenges.

Following the lines of [1] using multichannel adaptive filtering, we develop in Chapter 4, a new algorithm, the multichannel recursive adaptive matching pursuit (MC-RAMP) algorithm, more robust and suitable for filtering CPR artifacts. This algorithm is then further tested and used in later chapters, mostly using real human ECG of both shockable and non-shockable rhythms. The feasibility of ECG analysis during CPR is also discussed, primarily in terms of rhythm analysis, but also VF analysis.

Both the multichannel time-varying Wiener filter and MC-RAMP use reference signals that correlate with/resemble different artifact types, although we will use additional reference channels compared to [1]. Using these signals, the CPR artifacts are modeled in the filter and subtracted from the ECG, revealing the underlying heart rhythm.

2.6.2 Reducing NFT related to analyses and shocks in AEDs

There has recently been an increased attention to the importance of reducing the NFT during CPR [17, 32, 66, 88, 108]. However, aspects of NFT have not been an issue in the current CPR guidelines [9] and thus not especially considered in most AEDs.

There seem to be little work published on reducing NFT in automatic external defibrillation, although some studies address and quantify the problem [7, 15, 17, 94, 104].

NFT occurs for several reasons, caused by both human and machine. If CPR artifact filtering enables signal analysis of ECG during CPR, NFT in connection with analyses and shocks could be reduced. This and other means of reducing NFT are addressed in Chapter 10.

2.7 Summary

This chapter has presented some background on cardiac arrest, ECG, CPR, and some of the crucial problems in cardiac arrest resuscitation: the large number of unsuccessful shocks, poor quality of compressions and ventilations, and too much NFT without any therapeutic treatment.

The problem of filtering CPR artifacts in ECG, thus enabling machine signal analysis of ECG during CPR and reducing NFT in AEDs, has been motivated. Finding a useful method for filtering CPR artifacts and using this in an AED policy minimizing NFT are the main problems addressed in later chapters.

A short overview has been given on earlier work in CPR artifact filtering and NFT reduction. Earlier work in CPR artifact filtering are usually limited to animal, or animal/human mix studies, although indicating that CPR artifact filtering is possible in such cases. There have been no studies using real human out-of-hospital cardiac arrest ECG including both shockable and non-shockable rhythm types.

Chapter 3

Human and animal data

This chapter describes the data used in this work, which include ECG and auxiliary data channels. Human data from a project termed the Laerdal Sister project is our primary source for data in the CPR artifact filtering and NFT reduction experiments. Animal data from a pig experiment as well as human ECG from a Laerdal AED rhythm library are used for creating a controlled mix of human ECG and animal CPR artifacts for the initial tests of CPR artifact filtering.

3.1 Human data

The human data described in this section includes ECGs of VF and VT episodes from a Laerdal AED rhythm data, VF segments from an EMS database from Oslo, and finally ECG and reference channels of out-of-hospital cardiac arrests recorded in the Laerdal Sister project containing a larger selection of rhythms and from multiple cities.

3.1.1 The Laerdal AED rhythm library

The AED rhythm library (proprietary of Laerdal Medical AS, Stavanger, Norway) consists of 481 ECG episodes. These episodes were recorded with various models of Heartstart defibrillators (Laerdal Medical AS) during out-of-hospital cardiac arrests. Each episode is of 15 seconds duration sampled at 100 Hz with 8 bit resolution and annotated by cardiologists. The episodes have no CPR artifacts.

The human VF/VT records were highpass filtered in order to reduce baseline drift appearing in some of the VF/VT records.

Relevance

The database provides 200 episodes of VF and 71 episodes of VT that we used to mix with animal CPR artifacts in the CPR artifact removal experiments in Chapter 6. This mix is used for evaluating our method for removing artifacts using a new adaptive filter in terms of SNR improvements and comparing this filter with the theoretically optimal, but less useful in practice, time-varying Wiener filter.

3.1.2 Human data in prediction of defibrillation outcome

The human ECG is taken from the EMS database described in [94]. The database consists of ECGs, annotations and demographics from out-of-hospital cardiac arrested patients collected over a two-year period (1996–1998) in Oslo. The last 7.5 seconds before each defibrillation shock were extracted from the ECG records. The ECG records are sampled at 100 Hz and consist mainly of VF segments without CPR artifacts. For our purpose the extracted preshock segments are divided into two classes, shocks giving ROSC and shocks not giving ROSC, consisting of 87 and 781 segments, respectively.

Relevance

The database is used in a mix with animal CPR artifacts in an experiment to examine what influence CPR artifacts have on a shock outcome predictor by Eftestøl et al. [29]. The experiment is described in Chapter 9.

3.1.3 The Sister data

The Sister project is an ongoing project (2004) initiated by Laerdal Medical AS in Stavanger, Norway. The goal of the project is to increase the survival rate of sudden cardiac arrest. This is to be done by efforts in several areas:

- Better quality of CPR.
- Reduction of the no flow time in which the patient is not perfused.
- Reduction of the number of unsuccessful shocks.
- Individualization of the treatment – choose treatment according to the patient's state and response to the treatment.

- More precise determination of the patient's circulatory state – when can the CPR cease.

Data in the Sister project are collected using Laerdal HeartStart 4000SP defibrillators. These are HeartStart 4000 defibrillators modified to digitally collect the ECG as well as several reference channels containing additional information for research use, some of which are mentioned in the following. Data have been collected both during in-hospital and out-of-hospital resuscitation attempts of cardiac arrest patients. The use was approved by the regional ethics committee, and CPR was performed by paramedics according to the guidelines 2000 for CPR and ECC (Emergency Cardiovascular Care) [9].

The data used in this thesis were extracted from the first part[1] of the Sister project and were collected from out-of-hospital cardiac arrest patients in Akershus (Norway), Stockholm (Sweden), and London (UK) between March 2002 and October 2003. Several patients from a total of 106 patients from Akershus (manual mode defibrillation), 64 from London (AED mode), and 77 from Stockholm (AED mode), have been excluded for use in the studies in this work due to unavailability at the time of a particular study (not recorded and/or annotated), missing data/files, instrumentation failure etc. Complete annotated data are available from 70 patients from Akershus, 54 from London, and 53 from Stockholm.

Collected signals

All collected signals were sampled at 500 Hz with 16 bits resolution. The ECG (differential) signal had a resolution of 1.031 μV per least significant bit and a bandwidth of 0.9 – 50 Hz.

To remove CPR artifacts using an adaptive filter as described in Chapter 4, signals correlated with the CPR artifacts are needed. In addition to the ECG, the HeartStart HS4000SP defibrillators collect several such signals. Among these are four which we will use as possible reference channels in the adaptive filter for CPR artifact removal:

1. *Thorax impedance* (transthoracic impedance) is the impedance measured between the defibrillator electrodes (pads) and is a factor determining how much electrical current that traverses the heart during a defibrillation shock (lower impedance means higher current). The impedance

[1] Prior to implementation of CPR feedback in the defibrillators used in the Sister project.

is measured using a 32 kHz current giving an approximation of the resistance as seen between the electrodes at high-voltage shock discharges through the chest. The average transthoracic impedance of the adult human is 70 to 80 ohms, but is altered by several factors such as distance between the electrodes, electrode size and couplant with the chest, phase of respiration, electrode-chest wall contact pressure, selected shock energy and number of shocks previously given [64]. However, the average DC value of the impedance is not of interest to us, but rather the variations around this value. During CPR, these variations will reflect ventilation and chest compressions.

Thorax impedance is therefore used as a reference signal for ventilation and compression induced artifact components. The collected signal has bandwidth of 0 – 80 Hz.

2. The *ECG common mode voltage* is related to the ECG differential amplifier in the defibrillator and denotes the voltage common to both electrodes with respect to ground. It is normally the unwanted part of the voltage between each input (of the differential amplifier) and ground that is added to the voltage of both input signal.

   However, the common mode voltage will reflect external noise influences on the ECG, and serves as a possible reference signal for removal of static electricity type artifact components. The collected signal has bandwidth of 0 – 50 Hz.

3. Using the HS4000SP, a pad is placed between the resuscitator's hands and the patient's chest during CPR. This pad contains an accelerometer and a pressure sensor which provides the signals compression acceleration and pad pressure.

   Compression acceleration is used for deriving compression depth, but observations of this signal also indicate it may be correlated with the compression artifacts itself. It is therefore used as a possible reference channel. The collected signal has bandwidth of 0 – 50 Hz.

4. In addition to the pad accelerometer, another accelerometer is placed in the HS4000SP defibrillator itself, termed board acceleration, providing the reference system acceleration.

   Compression depth is estimated through the recorded pad pressure, board acceleration, and compression acceleration. In principle, by a double integration of the difference between the compression acceleration and the

board acceleration signal[2]. This is similar to the method described in [2], but with the pad pressure used instead of a logic signal indicating the beginning of each chest compression. Compression depth is used as a reference signal primarily for compression induced artifacts.

Relevance

Data from the Sister project is used for the studies in Chapters 7–10. In Chapter 7 we filter CPR artifacts from the human ECG from the Sister project to see if a shock advice algorithm will result in the same recommendation when we look at ECG segments close in time with the supposed same underlying heart rhythm, but with and without CPR artifacts. Although improved by CPR artifact filtering, the results still show some degradation in performance. By adding a short verification analysis in clean ECG and/or postponing analysis in segments with too difficult noise, we try to improve these results in Chapter 8. In Chapter 9 we use VF, PEA, and asystole rhythms from the Sister project data to examine the influence of CPR artifacts on individual features used in signal analysis of ECG, and if artifact filtering can reduce this influence. Finally, in Chapter 10 we use the Sister project data to analyze and quantify the no flow times (NFTs) during external automatic defibrillation. We will propose methods to reduce the NFT and see how much time could have been saved.

The studies use data from different sets of patients according to availability at the time of the study, defibrillation mode, specific events in the ECG etc. Appendix B includes a list of the available patient episodes, some demographics, and for what chapters in this dissertation they were used. More about the patient demographics in the Sister data can be found in a study by Wik et al. investigating CPR quality in the Sister data [104].

3.2 Animal data

An animal experiment was conducted in May 2001 to verify the measurement system of the HeartStart 4000 SP defibrillators used in the Sister project. This animal experiment was also used to collect artifacts and reference signals for filtering of CPR artifacts in ECG. The animal artifact signals were mixed with clean human ECG to create realistic examples of artifact corrupted human ECG signals.

The details of the animal experimental protocol, as well as reference channels and preprocessing, are described in the remainder of this section.

[2]To remove external acceleration components.

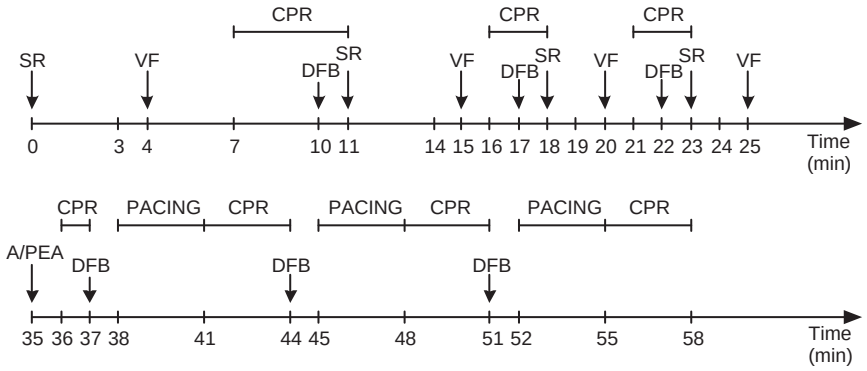

Figure 3.1: Protocol timeline indicating sequence of actions and events during animal experiments. These annotations are used: CPR, cardiopulmonary resuscitation; PACING, pacing; DFB, defibrillation; VF, inducing ventricular fibrillation (including 1 minute preparation); SR, sinus rhythm; A/PEA, asystole or pulseless electrical activity.

Experimental protocol

The study was approved by the Norwegian Council for Animal Research using a well-established model described in [69], and conducted in two healthy anaesthetized pigs (Sus scropha domestica, 22 and 25 kg). The sequence of events of the experimental protocol reported below is, for clarity of presentation, also visualized in the time-event diagram of Figure 3.1.

After preparation, baseline measurements were obtained for three minutes. All measurements were continuously recorded throughout the experiment. The ventilator and anaesthesia were discontinued and VF was introduced by a transthoracic current (90 V AC) for three seconds through separate electrodes and confirmed by characteristic ECG changes.

After three minutes of VF, manual chest compressions (120 min^{-1}) and bag-valve-tube ventilation with 100% oxygen was started (CPR). After three minutes of CPR, defibrillation shocks were given with interspersed CPR and epinephrine 0.5 mg doses intravenously if needed following the guidelines 2000 for CPR and ECC [9] until return of spontaneous circulation (ROSC). The pig was thereafter allowed to stay in sinus rhythm with controlled bag-valve-tube ventilation.

The whole sequence was repeated twice more, but now with only one-minute intervals. Initiation of VF, one minute of untreated VF, CPR for one minute, defibrillation attempts with interspersed CPR and epinephrine if needed until ROSC, followed by one minute of sinus rhythm and controlled ventilation.

VF was thereafter again induced, ventilations were discontinued, and the animals allowed to spontaneously develop asystole or pulseless electrical activity (PEA). After one minute of asystole or PEA, CPR was given for one minute, followed by three shocks given in rapid sequence of 50 J, 100 J, and 150 J. With the animals in continuous asystole and no CPR, external pacing through the chest electrodes was initiated at 180 min^{-1} for three minutes. The pacemaker was discontinued and CPR again given for three minutes followed by two more loops with shocks, pacing and CPR, all with three-minute intervals, before the animal was killed by discontinuing CPR.

Pacing is not commonly used during resuscitation, but was included here to generate high DC offset values on the electrodes, which makes the electrode-skin interface artifact component more prominent.

The resuscitation attempt from VF in pig 1 lasted for 26 minutes and included the delivery of 4 shocks and two doses of epinephrine. In the same animal, the resuscitation episode starting from asystole lasted 16 minutes and required 6 shocks and 2 doses of epinephrine. In pig 2 the corresponding numbers were 30 minutes with 21 shocks and 5 doses of epinephrine, and 15 minutes with 6 shocks and 2 doses of epinephrine respectively.

Collected signals

A prototype of the Laerdal Heartstart 4000SP defibrillators used in the Sister project was used to digitally collect the ECG and reference channels, all sampled at 500 Hz with 16 bit dynamic range. The ECG (differential) signal had a resolution of 1.031 μV per least significant bit and bandwidth 0.9 – 50 Hz.

To get additional information about the CPR artifacts, reference signals correlated with the CPR artifacts were recorded. Four such signals are later used when developing an adaptive filter for removing CPR artifacts in ECG:

- *Thorax impedance* (transthoracic impedance) with variations due to ventilation and chest compressions, bandwidth of 0 – 80 Hz. Used as reference signal for ventilation (and compression) induced artifact components.
- *ECG common mode*, bandwidth of 0 – 50 Hz. Possible use as reference signal for removal of static electricity type artifact components.
- *Compression acceleration* primarily due to chest compressions, bandwidth of 0 – 50 Hz. Compression acceleration is used for deriving compression depth, but observation of this channel also indicate it may be correlated with the compression artifacts itself. Thus, it is a possible reference signal.

- Logic signal indicating the beginning of each chest compression, made available from a switch placed beside the chest accelerometer. Compression acceleration and the switch signal form the basis for an estimated *compression depth* signal as described in [2], which in turn is used as a reference signal primarily for compression induced artifacts.

The animal ECG and reference channels were originally sampled at 500 Hz and preprocessed before being downsampled to 100 Hz to match the sampling rate of the human ECG available.

The animal ECG was filtered with an analog bandpass filter (0.9 – 50 Hz) before it was sampled. Since this analog filter did not have linear phase in the passband, the reference channels were filtered with a digital equivalent of the analog bandpass filter in order to "match the phase" of the ECG channel. This is done to make the reference signals as equal to the correlated components in the artifacts as possible. This bandpass filter is equivalent to the analog bandpass filter used for the animal ECG.

Relevance

In Chapter 6 we use episodes of asystole with CPR artifacts from the animal data in a mix with human ECG to create realistic ECG with CPR artifacts. This mix is used for evaluating our artifact removal filter in terms of SNR improvements and comparing this filter with the theoretically optimal time-varying Wiener filter.

In Chapter 9 a similar mix is used in an experiment to examine what influence CPR artifacts have on a shock outcome predictor by Eftestøl et al. [29].

Chapter 4

Adaptive filter for CPR artifact removal

The main focus of this work is to develop a method for removing CPR artifacts in ECG, enabling signal analysis during CPR, and thus reducing the adverse intervals of no patient blood flow termed NFT.

In this chapter we start by placing the CPR artifact remover in the context of a decision support system for AEDs. Then in Section 4.2 we develop a new multichannel adaptive filter to be used later in this dissertation for removal of CPR artifacts in ECG.

4.1 The decision support system and the role of the artifact remover

The CPR artifact remover is part of a medical decision support system as shown in Figure 2.4 and discussed in Section 2.5. In current AEDs, however, the CPR artifact remover component is absent requiring clean ECG, with no motion or CPR artifacts, for the subsequent signal analysis. CPR must therefore be discontinued for reliable signal analysis. The lack of myocardial and cerebral blood flow during these periods is harmful to the tissues as discussed in Section 2.4.1. The role of the CPR artifact remover is then to be able to present filtered clean ECG so that the subsequent signal analysis can be performed reliably not needing to pause CPR.

The decision support system also contains a feature extractor and a classifier. As discussed in Section 2.5, rhythm analysis (shock advice) and VF analysis

(shock outcome prediction) are two applications of a feature extractor and classifier. Currently, VF analysis is not incorporated into AEDs, only the rhythm analysis. The two types of analyses may require different features. Some features are good for distinguishing classes of rhythms, others for characterizing the variations within one class. So, when a VF analysis system is ready to be incorporated into an AED, we will need the rhythm analysis to first find the VF/VT rhythms that will be presented to the VF analysis to predict the shock outcome. A modified decision support framework to reflect this is shown in Figure 4.1.

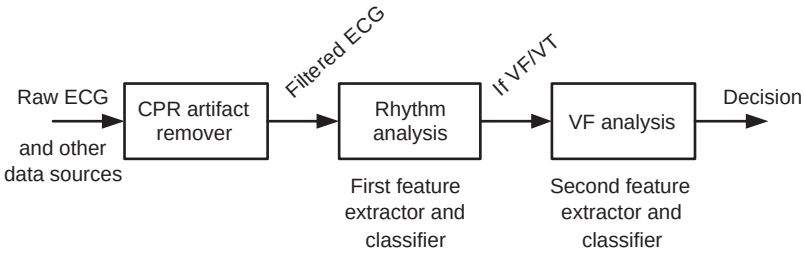

Figure 4.1: The modules in a medical decision support system for both rhythm and VF analysis.

4.2 Multichannel Recursive Adaptive Matching Pursuit (MC-RAMP)

In this section we develop a new multichannel adaptive filter which will be used in this thesis for removal of CPR artifacts in ECG. An adaptive filter is a filter with time-varying filter coefficients. Such a filter is used when the characteristics of what we want to filter are unknown and/or varying with time. It adapts, automatically, to changes in the properties of its input signals. The adaptive filter we will develop, the *MultiChannel Recursive Adaptive Matching Pursuit* (MC-RAMP) filter, is an extension of a new adaptive filter algorithm first presented in [54]. This section is adapted from [55] and [37].

Figure 4.2 shows the structure of our multichannel adaptive filter for CPR artifact removal. In the figure $d(n)$ denotes the artifact corrupted ECG signal, $e(n)$ the restored signal, while $x^{(0)}(n), x^{(1)}(n), \ldots, x^{(K-1)}(n)$ are the K artifact correlated reference signals. As introduced in Chapter 3, we will use four possible artifact correlated reference signals, namely *ECG common mode*, *Thorax Impedance*, *Compression Depth*, and *Compression Acceleration*. In the

following two sections we derive our multichannel adaptive algorithm in a general context, before, primarily in chapters 6 and 7, we test its practical use for CPR artifact removal. The last section of this chapter introduce some modifications of MC-RAMP for increased performance and robustness.

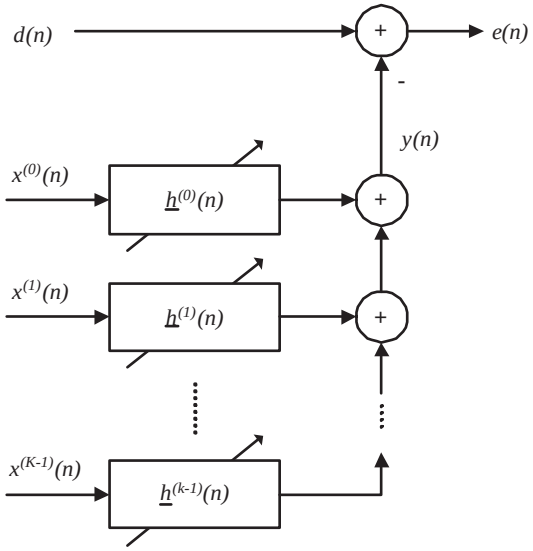

Figure 4.2: Structure of multichannel adaptive filter used in CPR artifact removal. $x^{(0)}(n), x^{(1)}(n), \ldots, x^{(K-1)}(n)$ are the K artifact correlated reference signals, $d(n)$ is the artifact-corrupted ECG signal, while $e(n)$ is the restored ECG signal.

4.2.1 Notation and problem formulation

Again, looking at Figure 4.2, our objective is to find $y(n)$ as the best possible estimate of the artifact part of $d(n)$ so that it can be removed through subtraction of $y(n)$ from $d(n)$. This is a classical problem in adaptive filtering and is commonly solved through finding filter coefficients $\underline{h}^{(k)}(n)$, $k = 0, 1 \ldots, K-1$, for each time instant n that approaches the minimum of the objective function:

$$J(n) = \sum_{i=n-L_2}^{n+L_1} [d(i) - y(i)]^2 \tag{4.1}$$

over some rectangular window of size determined through the selection of L_1 and L_2. Note that other windows, such as the Hamming window or exponentially weighted windows could also be used. For the present purposes, however, rectangular windows with appropriately chosen sizes work well while requiring

less computation than other window selections. We note that selecting $L_1 = 0$ corresponds to using data up to and including time n in finding the filter vectors, $\underline{h}^{(k)}(n)$ to be used at time n. This corresponds to a causal solution to the problem at hand, whereas selecting $L_1 > 0$ implies a non-causal solution using future signal samples in computing the filter coefficients to be used at time n. To avoid confusion, we point out here that the filter to be used at time n is always applied causally to the signal. As we shall see later, selecting $L_1 > 0$ proves beneficial, and the attendant delay imposed by this is acceptable in the present application. In deriving the MC-RAMP algorithm, we shall treat the generic adaptive filtering problem. In the setting of CPR artifact filtering $d(n)$ denotes the artifact corrupted ECG signal and $e(n)$ the restored signal. However, to be consistent with established terminology in the generic adaptive filter context, we will here refer to $e(n)$ as the *error signal* and $d(n)$ as the *desired signal*. Also, for notational convenience and consistency with the literature on adaptive filtering, we shall assume, with no loss of generality, that $L_1 = 0$ and that $L_2 = L - 1$.

Numerous adaptive filters for the generic problem described above have been proposed, the least mean squares (LMS) and recursive least squares (RLS) adaptive filters being prominent examples. None of these are well suited to the present application. The main reasons for this are related to slow convergence (LMS type of algorithms) and temporarily ill-conditioned autocorrelation matrix estimates (RLS) [51]. In the following we present the *MultiChannel Recursive Adaptive Matching Pursuit* (MC-RAMP) which is computationally efficient, has good convergence behavior, and deals nicely with signals that would give rise to ill-conditioned autocorrelation matrix estimates. The idea underpinning the algorithm is the *Matching Pursuit* (MP) technique first to receive prominence in the signal processing community following the 1993 publication of [71].

Before presenting the MC-RAMP algorithm we pause to emphasize that, in general, the motivation for applying an adaptive filter, such as the LMS or RLS algorithms, is to find or track the Wiener solution to the problem at hand as accurately as possible, while *the computational complexity is kept as low as possible.* Thus, all adaptive filter applications involve an explicit complexity/performance tradeoff. A remarkable property of the MC-RAMP algorithm in the present application is the fact that we obtain a performance *quality* on par with the time-varying Wiener filter of [1], while fully realizing the computational benefits of an adaptive filter.

Looking again at Figure 4.2, the error signal can be expressed as:

$$e(n) = d(n) - \sum_{k=0}^{K-1} \sum_{m=0}^{M_k-1} h_m^{(k)}(n) x^{(k)}(n-m), \tag{4.2}$$

where K is the number of channels and M_k is the number of filter coefficients for the filter in channel no. k. Note also that $h_m^{(k)}(n)$ denotes filter coefficient no. m of channel k at time n. In deriving adaptive filter algorithms it has proven useful to define vector and matrix quantities corresponding to the signals and filter unit pulse responses involved [51]. In the following we introduce such suitable definitions for the multichannel adaptive filter in complete analogy with standard practice used in single channel adaptive filter theory [51]. Thus, $\underline{h}^{(k)}(n) = [h_0^{(k)}(n), h_1^{(k)}(n), \ldots, h_{M_k-1}^{(k)}(n)]^T$ is the vector of filter coefficients for channel k at time n. Defining

$$\underline{d}(n) = [d(n), d(n-1), \ldots, d(n-L+1)]^T, \tag{4.3}$$

and $\underline{e}(n)$ similarly, the channel data matrix for channel no. k as

$$\mathbf{X}^{(k)}(n) = [\underline{x}_0^{(k)}(n), \underline{x}_1^{(k)}(n), \ldots, \underline{x}_{M_k-1}^{(k)}(n)], \tag{4.4}$$

where the columns are given by

$$\underline{x}_j^{(k)}(n) = [x^{(k)}(n-j), x^{(k)}(n-j-1), \ldots, x^{(k)}(n-j-L+1)]^T, \tag{4.5}$$

and finally the complete multichannel data matrix and the corresponding multichannel filter vector as

$$\mathbf{X}(n) = [\mathbf{X}^{(0)}(n) \mid \mathbf{X}^{(1)}(n) \mid \ldots \mid \mathbf{X}^{(K-1)}(n)], \tag{4.6}$$

and

$$\underline{h}(n) = \begin{bmatrix} \underline{h}^{(0)}(n) \\ \underline{h}^{(1)}(n) \\ \vdots \\ \underline{h}^{(K-1)}(n) \end{bmatrix}, \tag{4.7}$$

respectively, a little thought reveals that Equation 4.2, for time indices in the range $n-L+1$ to n and when we *assume that the filter for time n is used throughout this range*, can be written as

$$\underline{e}(n) = \underline{d}(n) - \mathbf{X}(n)\underline{h}(n). \tag{4.8}$$

Our desire is now to iteratively improve the current $\underline{h}(n)$ such that the norm of $\underline{e}(n)$ is made successively smaller. For this purpose we shall use a computational procedure known as *basic matching pursuit* (BMP). BMP was presented

in [25] as a possible procedure for finding a sparse representation of a given vector using a linear combination of vectors selected from a dictionary with more elements than the dimension of the space it spans. While our objective is not the same as that of [25], the computational steps to be described below are the same as those of the BMP.

In the sequel it will be convenient to number the columns of $\mathbf{X}(n)$ sequentially, i.e. denote them as $\underline{x}_l(n)$ with $l = 0, 1, \ldots, \sum_{k=0}^{K-1} M_k - 1$. Thus, when we define M as $M = \sum_{k=0}^{K-1} M_k$, $\mathbf{X}(n)\underline{h}(n)$ can be written as

$$\mathbf{X}(n)\underline{h}(n) = \sum_{l=0}^{M-1} h_l(n)\underline{x}_l(n), \tag{4.9}$$

where we note that the $h_l(n)$'s are the filter coefficients numbered sequentially with no reference to channel number. The connection back to channel numbers can be found by writing the index l as

$$l = \nu_q + \sum_{k=0}^{q-1} M_k \tag{4.10}$$

for $\nu_q = 0, 1, \ldots, M_q - 1$ and $q = 0, 1, \ldots, K - 1$. Interpreting l this way, we can also say that $\underline{x}_l(n)$ is column no. ν_q of the data matrix for channel no. q, i.e. the vector we would denote $\underline{x}_{\nu_q}^{(q)}(n)$.

4.2.2 Algorithm development

Using the notation introduced in the previous section, we can explain the algorithm as if we were treating a single channel adaptive filtering problem. Following this explanation we indicate the computational complexity of the algorithm, and show how it can be efficiently used in situations where the estimate of the multichannel autocorrelation matrix, $\mathbf{X}^T(n)\mathbf{X}(n)$ may be ill conditioned. Details of the algorithm as well as a complexity analysis are presented in Appendix A.

Examining once more Equation 4.8, what we really want is to find elements of $\underline{h}(n)$ so that $\mathbf{X}(n)\underline{h}(n)$ is as good an approximation to $\underline{d}(n)$ as possible. If we started with an initial value of $\underline{h}(n)$ equal to zero and are allowed to update only one element of $\underline{h}(n)$, we would select the one term of the expansion in Equation 4.9 that gives us the best approximation to $\underline{d}(n)$. Denoting this term $h_{j_0(n)}(n)\underline{x}_{j_0(n)}(n)$, we realize that we have to find the index, $j_0(n)$, of a column in $\mathbf{X}(n)$ along with its weighting factor $h_{j_0(n)}(n)$. The best we can do in this

situation is to select the $j_0(n)$th column of $\mathbf{X}(n)$ *if this column is the one that is best aligned with* $\underline{d}(n)$. Given this column selection, it would be optimal to find the coefficient, $h_{j_0(n)}(n)$, by projecting $\underline{d}(n)$ onto the normalized selected column. This process of vector selection and coefficient computation is called a *matching pursuit iteration* or an MP-iteration for short. If we were to improve the approximation we could repeat the same procedure as outlined above, but now starting with the new approximation error, i.e. $\underline{d}(n) - h_{j_0(n)}(n)\underline{x}_{j_0(n)}(n)$, rather than with $\underline{d}(n)$. This could be repeated a given number of times, say P times, and each time with a new improved error vector resulting from the previous iteration, for each time instant n. At the next time instant, $n+1$, we would continue with P new MP-iterations starting with the error vector being a consequence of the newly arrived signal samples and the filter coefficient vector of the previous time instant, i.e. $\underline{d}(n+1) - \mathbf{X}(n+1)\underline{h}(n)$.

When a vector that has been selected before is re-selected, the corresponding element of the filter coefficient vector is updated in the same way as the initial value of the filter coefficient was updated from a zero value as described above.

Formalizing the above line of thought somewhat, we derive the *Recursive Adaptive Matching Pursuit* algorithm as follows: Assume that we have an approximation to $\underline{d}(n-1)$ at time $n-1$ given by $\mathbf{X}(n-1)\underline{h}(n-1)$, the *a priori* approximation error at time n is

$$\underline{e}_0(n) = \underline{d}(n) - \mathbf{X}(n)\underline{h}(n-1). \tag{4.11}$$

In building a better approximation through the update of *only one coefficient in* $\underline{h}(n-1)$, we would write the new error as

$$\underline{e}_1(n) = \underline{e}_0(n) - \mathbf{X}(n)h^{update}_{j_0(n)}(n)\underline{u}_{j_0(n)}. \tag{4.12}$$

Note that $j_0(n)$ is the index of the coefficient to be updated in the zero'th MP-iteration at time n, and $\underline{u}_j$ is the M-vector with 1 in position j and 0 in all other positions. Selecting $j_0(n)$ as the index of that column of $\mathbf{X}(n)$ that is best aligned with the a priori approximation error of Equation 4.11 is the best we can do. Thus, $j_0(n)$ is found as the index of the column of $\mathbf{X}(n)$ onto which $\underline{e}_0(n)$ has its maximum projection, or in other words:

$$j_0(n) = \arg\max_j \frac{|< \underline{e}_0(n), \underline{x}_j(n) >|}{\|\underline{x}_j(n)\|}, \tag{4.13}$$

where $< .,. >$ denotes an inner product between the two vector arguments. Given the index $j_0(n)$, the update equation of the corresponding filter coefficient is

$$h_{j_0(n)}(n) = h_{j_0(n)}(n-1) + h^{update}_{j_0(n)}(n), \tag{4.14}$$

where $h_{j_0(n)}^{update}(n)$ is the value of the projection of $\underline{e}_0(n)$ onto the unit vector with direction given by $\underline{x}_{j_0(n)}(n)$, i.e.:

$$h_{j_0(n)}^{update}(n) = \frac{< \underline{e}_0(n), \underline{x}_{j_0(n)}(n) >}{\|\underline{x}_{j_0(n)}(n)\|^2}. \tag{4.15}$$

Thus, the zero'th MP-iteration updates the filter vector as follows:

$$\underline{h}(n) = \underline{h}(n-1) + h_{j_0(n)}^{update}(n)\underline{u}_{j_0(n)}. \tag{4.16}$$

Given this, the updated error expression of Equation 4.12 can be written as:

$$\underline{e}_1(n) = \underline{d}(n) - \mathbf{X}(n)\underline{h}(n). \tag{4.17}$$

If we want to do more than one MP-iteration at time n, the procedure described above starting with finding the maximum projection of $\underline{e}_0(n)$ onto a column of $\mathbf{X}(n)$ can be repeated with $\underline{e}_1(n)$ taking the role of $\underline{e}_0(n)$. This can be repeated as many times as desired, say P times[1].

The main steps of the adaptive algorithm is summarized in a flowchart, see Figure 4.3. Note that in the flowchart we have simplified the notation somewhat.

In Appendix A it is shown that the algorithm is characterized by a computational complexity given by $(7+K)M - \frac{K(K-1)}{2}$ multiplications, $M+1$ divisions and $M-1$ comparisons. This is valid if we do one MP-iteration for each time instant n. It is also shown in the appendix that each possible subsequent MP-iteration at time n, requires M multiplications, 1 division, and $M-1$ comparisons. Thus, relative to the zero'th MP-iteration at time n, the subsequent MP-iterations are cheap. Finally, we point out that the complexity is linear in the total number of filter coefficients for a given number of channels and MP-iterations.

4.2.3 Modifications to the basic MC-RAMP algorithm

For improved filter performance and robustness, some modifications to the basic MC-RAMP algorithm described above are introduced for the experiments using MC-RAMP in later chapters. The modifications will of course introduce additional computational complexity, but it is tolerable in the present application.

[1] Note that if $P > 2$ it is entirely possible that one particular coefficient is updated more than once at a given time n.

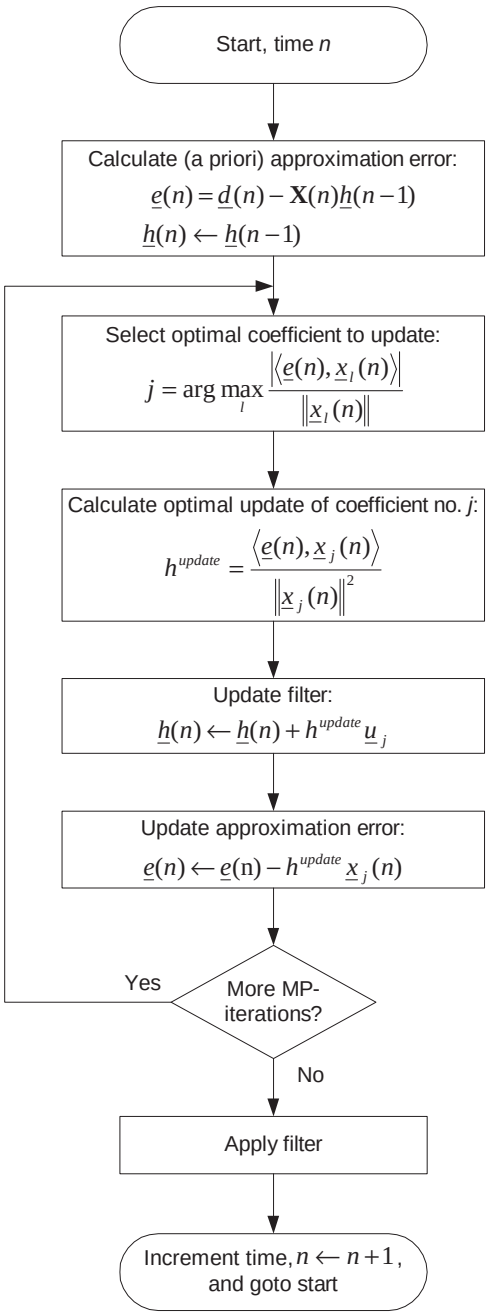

Figure 4.3: Flowchart indicating the computational steps of the MC-RAMP algorithm.

Dealing with rank deficiency

In the present application, it will happen from time to time, that some of the reference signals have very low power levels. This is for example the case when the *Depth* reference signal disappears as a consequence of a pause in the administration of chest compressions. If we based our CPR artifact removal system on estimated autocorrelation matrices, we would experience rank deficiency leading to numerical problems. Such problems were indeed experienced in earlier work [1]. While such problems, in the context of [1], could be solved through monitoring of the condition number of the matrix or by computing pseudo-inverses through the use of the singular value decomposition (SVD) [75], these are all computationally demanding solutions. In the proposed MC-RAMP algorithm all we need to do is to monitor the norm of the columns of $\mathbf{X}(n)$, i.e. $\|\underline{x}_j(n)\|$ for $j = 0, 1, \ldots, M-1$. The norm value will reflect the local energy, or average power, of the reference channel. Since these quantities are already computed as part of the algorithm, no additional computational effort is involved in this step. To avoid instability in MC-RAMP we simply prevent columns of $\mathbf{X}(n)$ having a norm below a certain threshold in participating in the vector selection process of the MP-iterations. It is evident from the detailed algorithm presentation in Appendix A that this is easily accomplished.

Note that this threshold may vary for each reference channel as a consequence of the reference channels not being normalized in any way and thus having different power. When a reference channel goes below the norm (energy) threshold, its contribution to the reconstructed artifact signal may still be non-zero, since its filter coefficients are no longer updated, but not necessarily zero. To avoid the contribution acting as noise, we let filter coefficients of reference channels that are inactive decay exponentially towards zero.

Rank deficiency resulting for other reasons than that mentioned above pose no problem for the present algorithm simply because it is not dependent on estimated inverses of the autocorrelation matrix.

Dealing with low correlated reference signals

Sometimes a reference channel will have very low correlation with the ECG signal. This may indicate that the contribution of that reference channel will be insignificant or even possibly harmful given incidental similarities with the underlying heart rhythm. Therefore, the zero-lag cross-correlation coefficient between the ECG and each reference channel (or actually the columns of $\mathbf{X}(n)$, i.e. $\|\underline{x}_j(n)\|$ for $j = 0, 1, \ldots, M-1$) are calculated for the current window

defining the short-term analysis region and iteratively updated for each time instant. That is, for time instant n, the absolute value of the cross-correlation coefficient at zero lag, $|\rho_j(n)|$, defined as

$$|\rho_j(n)| = \frac{| < \underline{d}(n), \underline{x}_j(n) > |}{\|\underline{d}(n)\|^2 \|\underline{x}_j(n)\|^2}, \tag{4.18}$$

is calculated for $j = 0, 1, \ldots, M-1$. Reference channels having too low correlation with the ECG are set inactive and their filter coefficients are decayed exponentially towards zero.

Adjustable window length

We have the option to adjust the window length, defined by L_1 and L_2, according to the maximum correlation coefficient between the reference channels and the ECG. In practice, higher correlation often indicate large CPR artifacts in the ECG, compared to the underlying heart rhythm, and suggests using smaller window lengths letting MC-RAMP adjust its coefficients more locally. Note that the window length is chosen from only a few choices according to some correlation thresholds found empirically, and only adjusted every 50 samples.

Lowpass filtering the reconstructed artifact signal

Finally, the reconstructed artifact signal $y(n)$ is lowpass filtered with corner frequency f_{LP} before subtracting it from the original ECG $d(n)$. This is to remove high-frequency noise that may be introduced due to the constant change of the MC-RAMP filter coefficients or from noise present in the reference channels.

Chapter 5

Features used for evaluating the CPR artifact removal

In this chapter we present some features and algorithms to be used in the validation of the CPR artifact removal capabilities of the MC-RAMP filter introduced in Chapter 4.

First we briefly describe a proprietary shock advice algorithm found in the HeartStart 4000 defibrillator containing multiple features and a classification system. This algorithm is used in Chapters 7 and 8 for evaluating if rhythm analysis (shock advice) can be performed during CPR by removing the CPR artifacts using MC-RAMP.

Then we describe some features that are used in Chapter 9 to study the effect CPR artifacts have on common types of features encountered in rhythm or VF analysis. We expect that feature values are altered by the presence of CPR artifacts and want to see if CPR artifact filtering can remedy this situation.

5.1 The HeartStart 4000 AED shock advice algorithm

An AED analyzes a patient's ECG and determines if a shock can be advised. It performs feature extraction and rhythm classification to differentiate between shockable rhythms such as VF and VT with rate over 150 bpm, and non-shockable rhythms such as asystole, PEA and various pulse rhythms. For our experiments in Chapters 7 and 8 using an AED shock advice algorithm to

evaluate the performance of CPR artifact filtering, we use an offline PC version of the AED algorithm found in the Laerdal HeartStart 4000 defibrillator[1].

The algorithm is fed with ECG signals sampled at 200 Hz with 16 bits resolution, and uses two or three consecutive 3 second segments for one final shock/no-shock decision. The decision is based upon measurements of the average amplitude, the isoelectric baseline content, waveform organization/regularity and rate. Since the algorithm is part of a commercial product, the details of its internal operations are not known to us. For public available information on this algorithm, see [83].

5.2 Some features found in the literature

Many features have been proposed to characterize rhythms in the ECG for shock advice or shock outcome prediction purposes. The following sections describe a few representative features found in the literature. The features will not be used to design a system for shock advice or shock outcome prediction in this dissertation. We will only investigate the effect CPR artifacts have on these features (Chapter 9). That is, how much will artifact noise affect the feature values, and can the artifact filter described in Chapter 4 reset this influence.

5.2.1 VF-filter (Kuo and Dillman, 1978)

The VF-filter algorithm was originally applied by Kuo and Dillman in 1978 in an ECG monitoring system for detection of VF when no QRS complexes or paced beats could be detected [68]. The VF-filter corresponds to a narrow band-stop filter applied to the signal, assumed to be quasi-sinusoidal, with central frequency equivalent to the mean signal frequency. The output of the filter is the VF-filter leakage and is computed as

$$\text{leakage} = \frac{\sum_{n=1}^{L} |x(n) + x(n - [T/2])|}{\sum_{n=1}^{L} (|x(n)| + |x(n - [T/2])|)}, \tag{5.1}$$

where the mean signal period

$$T = \frac{2\pi \sum_{n=1}^{L} |x(n)|}{\sum_{n=1}^{L} |x(n) - x(n-1)|}, \tag{5.2}$$

[1] aka. Philips HeartStart XLT

with $[\,\cdot\,]$ denoting rounding towards nearest integer, $x(n)$ the signal samples and L the number of samples in the signal segment.

If the VF-filter leakage was below a certain threshold (0.625), VF was detected. The original threshold value is not of interest to us, as we will only consider *leakage* and T as possible features in a classifier for rhythm or VF analysis.

5.2.2 Spectral analysis (Barro et al., 1989)

For a system to detect ventricular arrhythmias in real time, Barro et al. introduced some features based on spectral analysis [13]. The detection of VF is based on VF reportedly consisting of a narrower band of frequencies than rhythms with complexes. Rhythms with complexes, such as sinus rhythm or PEA, often present more distinct and organized (and over a wider frequency range) peaks in the spectrum, corresponding to the heart rate and its harmonics, than VF rhythms [13].

Each segment of ECG is passed through a Hamming window to minimize the effects of segmentation on the spectra. The discrete Fourier transform of a segment is found and the amplitude spectrum is approximated by the absolute value of the complex Fourier coefficients[2]. That is, the components of the amplitude spectrum, a_i, are approximated as

$$a_i = |X(f_i)|, \tag{5.3}$$

where the N-point discrete Fourier transform $X(f_i)$ of a signal $x(n)$ is defined as

$$X(f_i) = \sum_{n=0}^{N-1} x(n) e^{-j2\pi n f_i / f_s} \tag{5.4}$$

for discrete frequencies $f_i = \frac{i}{N} f_s$ for $i = 0, 1, \ldots, \frac{N}{2} - 1$ with f_s denoting the sampling frequency.

After calculating the amplitude spectrum, the frequency of the maximum peak in the range of 0.5–9 Hz is found, denoted F_P. All amplitude spectrum components whose value is less than 5% of this maximum are equated to zero. Thus, insignificant components are not allowed to influence the features subsequently calculated. F_P is used as a feature in itself, named peak frequency (PF). In addition to the peak frequency, four other spectrum features are obtained, termed the normalized first spectral moment (FSMN), A_1, A_2, and A_3:

[2] In the original paper [13], each coefficient in the amplitude spectrum was approximated by the sum of the real and imaginary component of the corresponding fourier transform coefficient. This is a consequence of the high cost of computations in real time implementation 15 years ago.

1. FSMN is defined as

$$\text{FSMN} = \frac{1}{F_P}\frac{\sum a_i f_i}{\sum a_i}, \tag{5.5}$$

   The sum includes spectrum components ranging from 0 to 100 Hz[3].

2. A_1 is the ratio between the area contained within the band 0.5 Hz and $F_P/2$, and the total area between 0.5 Hz and $20F_P$. High values indicate noise.

3. A_2 is the ratio between the area in the range $0.7F_P$ to $1.4F_P$, and the total area between 0.5 Hz and $20F_P$. High values indicate VF.

4. A_3 is the ratio between the sum of areas around the second to eighth harmonic (area around is $\pm 0.3F_P$ around each harmonic frequency[4]), and the total area between 0.5 Hz and $20F_P$. Low values indicate VF.

In the orignal paper [13], VF was identified if FSMN $\leq 1.55, A_1 < 0.19, A_2 \geq 0.45$, and $A_3 \leq 0.09$.

5.2.3 Lempel-Ziv complexity measure (Lempel and Ziv, 1976)

The circulatory system is a complex system with many feedback paths and nonlinear dynamic behavior [6]. Experiments have shown, in response to electrical stimulation, the generating of complex temporal or spatio-temporal patterns in the heart exhibiting typical chaotic or nonlinear system behavior, e.g. spiral waves and rotors in VF [21, 22, 46, 47, 56, 80, 86, 95, 105]. Since different nonlinear physiological processes of the heart have different complexity, this can be used to separate different heart rhythms. For instance, VF appears more chaotic and complex than normal sinus rhythm, and this is reflected in various complexity measures. For instance, the degree of complexity measured by correlation dimension [61] is larger for VF than for sinus rhythm [86]. However, correlation dimension calculations are computationally demanding

[3] In the original paper [13], the range of the sums are limited from 0.5 Hz to the frequency of the 20th harmonic or 100 Hz, whatever comes first. The paper is somewhat confusing as to whether the range is summed using only the multiples of the peak frequency (i.e. the harmonics), or if all points of the calculated amplitude spectrum in the range are included in the sum. Papers by others testing the spectral analysis by Barro, have used the latter of the two variants [20, 59]. As will we. However, both variants of the FSMN feature will for most cases reflect the same.

[4] Note that the papers [20, 59] differ in the calculation of A_3 compared to the original paper [13] (the band centered on each harmonic defined as 0.6 Hz versus $0.6F_P$ in the original paper).

and require long data sequences to be accurate, excluding them for clinical use [109]. Lempel and Ziv introduced a simple-to-compute complexity measure in 1976 which can instead be used to characterize the complexity of a signal.

Zhang et al. used and described the Lempel and Ziv complexity measure for detecting VF and VT [109]. We have implemented the algorithm as it is described in [62].

The Lempel-Ziv complexity measure are obtained from first converting an ECG segment into a string of symbols by binary or tertiary[5] quantification of the samples[6]. Then, the algorithm calculates the complexity of the string in relation to the number of *insert symbol(s)* and *copy a substring* operations needed to reproduce the string. Briefly described, the string sequence of characters is scanned from left to right and the complexity measure $c(n)$ is increased by one unit every time a new subsequence of consecutive characters is encountered in the scanning process. The complexity $c(n)$ for a string of length n is then normalized giving the normalized Lempel-Ziv complexity measure:

$$C(n) = \frac{c(n)}{b(n)}, \tag{5.6}$$

where

$$b(n) = \frac{n}{\log_{base}(n)}, \tag{5.7}$$

with $base = 2$ for binary representation or 3 for tertiary representation. After normalization, the complexity measure reflects the rate of new pattern occurrences with time.

For further details, and a complete development of the algorithm, we refer to [62] or [109].

5.2.4 Irregularity measure (IRM) (Ripley et al., 1989)

Ripley et al. described techniques for recognition of ventricular arrhythmias which included a measure of irregularity based on the intervals between threshold crossings in the ECG signal [87].

[5] Binary representation was used in [62] and [109]. We have tested both binary and tertiary representation. Tertiary representation is useful for letting baseline content and noise with values near zero have its own symbol. Preliminary rhythm analysis results indicate that using tertiary representation, better distinction of classes is achieved.

[6] Binary: $x(n) > 0$ mV $\rightarrow 1$, $x(n) < 0$ mV $\rightarrow 0$. Tertiary: -0.01 mV $< x(n) <$ 0.01 mV $\rightarrow 0$, $x(n) >$ 0.01 mV $\rightarrow 1$, and $x(n) < -0.01$ mV $\rightarrow -1$. $x(n)$ is the sample value.

From an ECG segment, the times of each positive threshold crossing are recorded. The threshold is set to 0.3 mV. To prevent double-counting of multiphasic deflections, a "refractory period" of 100 ms follows each threshold crossing. The mean interval between the threshold crossings are calculated along with the standard deviation from the mean. The irregularity measure IRM is defined as the ratio of the standard deviation to the mean.

5.2.5 Count20

Count20 is a simple feature reflecting the amount of baseline content in an ECG segment. Count20 is defined as the number of signal samples between 0 and 20% of the maximum absolute signal value in the analyzed segment [60], and then normalized to the segment length.

5.2.6 Spectral features: centroid frequency, peak power frequency, energy and spectral flatness measure

For a classifier used to predict outcome of defibrillation in patients with VF, Eftestøl et al. studied four spectral features [29]. The four features thought to contain information predictive of shock outcome were centroid frequency[7], peak power frequency, energy, and spectral flatness.

All four features are computed from the estimated power spectral density (PSD) of an ECG segment. Often, the PSD is estimated by averaged modified periodograms (the Welch method) [85]:

$$\hat{P}(f) = \frac{1}{K}\sum_{m=0}^{K-1}\frac{1}{L}\left|\sum_{n=0}^{L-1} w(n)x_m(n)e^{-j2\pi nf/f_s}\right|^2, \tag{5.8}$$

where f is the physical frequency (from 0 to $f_s/2$, with f_s denoting the sampling frequency) and $x_m(n)$ denotes sample n in a block m of ECG. Each ECG segment is divided into K blocks, each of length L. The blocks are normally overlapping. Each block is weighted by a window function $w(n)$. The window function and averaging of blocks are methods used to produce a smoother estimate of the PSD.

The centroid frequency (CF) is defined as

$$\mathrm{CF} = \frac{\int_{f_l}^{f_u} f\hat{P}(f)df}{\int_{f_l}^{f_u} \hat{P}(f)df}, \tag{5.9}$$

[7] aka. median frequency

where f_l and f_u are the lower and higher frequency band limits. In this work, we use 0 and 25 Hz for lower and upper limits, respectively, as was also used in [29].

The peak power frequency (PPF) is defined as

$$\text{PPF} = \arg\max_f [\hat{P}(f)]. \tag{5.10}$$

The frequency band-limited energy (ENRG) is defined as

$$\text{ENRG} = \int_{f_l}^{f_u} \hat{P}(f)df. \tag{5.11}$$

The spectral flatness measure (SFM) [57] is defined as

$$\text{SFM} = \frac{e^{\int_{f_l}^{f_u} \ln \hat{P}(f)df}}{e^{\int_{f_l}^{f_u} \hat{P}(f)df}}. \tag{5.12}$$

SFM ranges from 0 (peaky spectrum) to 1 (flat spectrum).

5.2.7 Amplitude spectrum analysis (AMSA)

Used as a feature to predict optimal timing of ventricular defibrillation, AMSA was first introduced as *amplitude spectrum area* in a journal article by Marn-Pernat et al. in 2001 [73], but renamed to *amplitude spectrum analysis* in [84].

AMSA is defined as the sum of products of individual frequencies and the corresponding amplitudes of the amplitude spectrum[8] from 4 to 48 Hz:

$$\text{AMSA} = \sum_i a_i f_i, \tag{5.13}$$

where a_i is the amplitude value of the ith sinusoidal component of the spectrum with frequency f_i. The range of the sum is the component indices corresponding to frequencies from 4 to 48 Hz.

[8] In [73] AMSA was termed "the area under the curve that defines the amplitude spectrum" which it is not. However, it might be termed the frequency weighted area (approximation) under the amplitude spectrum curve.

5.3 Additional features developed for this work

There have been many features in the literature that reflect the ECG waveform rate in some way. We developed an algorithm that will find the rate of beats (QRS complexes) in organized rhythms as well as the frequency of the dominant sinusoidal component in VF-like rhythms.

We have also developed some other features partly as by-products of the rate feature. These include two amplitude measures, ratio of residual to total energy, slope count and a complexity measure.

The outlines of our algorithm for finding the features will be presented in the following subsections. Note that details such as logic for exception handling and most threshold values are omitted for clarity of presentation since we have not fully developed a shock advice algorithm, and we will only use these features when investigating the influence of CPR artifacts in the ECG.

5.3.1 Preprocessing

Each ECG segment (typically 3–5 seconds duration) is first checked for maximum absolute amplitude, average power ($P_{AVG} = \frac{1}{L}\sum_{n=1}^{L}|x(n)|^2$, a feature in its own) and the number of signal peaks over a threshold. If these three measures are not above their respective thresholds[9], further processing is futile, and the algorithm returns zero values.

Subsequently the signal is smoothed using a simple 3 tap FIR lowpass filter. However, care is taken to preserve the amplitude of all peaks over 70% of the maximum absolute amplitude. Using the difference signal ($x(n) - x(n-1)$), large noise spikes in the ECG are detected and removed using interpolation between the spike start and end.

5.3.2 Beats per minute (BPM)

The technical criteria interpreting the human use of "rate" depends on the heart rhythm present. For instance, rate of QRS complexes in pulse rhythms and dominant frequency in VF rhythms need different detectors and measurements. Since we normally do not know the heart rhythm in advance, we employ seven different rate calculation alternatives and use the one best suited. We will present the rate as beats per minute (bpm), although we are not always measuring actual heartbeats.

The seven rate alternatives are:

[9] Empirically determined thresholds: maximum absolute amplitude > 0.08 mV, average power $>$ 1.25e-3 $(\text{mV})^2$, number of peaks over ± 0.08 mV > 2

1. Find positive peaks over a (signal dependent) threshold amplitude. Find intervals between peaks. Check for missing peaks, false detections or outliers. Calculate median peak interval and standard deviation.

2. Same as alternative 1, but with negative peaks.

3. Calculate autocorrelation and find the lag at the largest peak besides the peak at zero lag. This lag is the period. The signal is then divided into non-overlapping blocks of one period length and standard deviation is calculated from either positive or negative peaks, or positive or negative flanks, whatever gives the smallest standard deviation.

4. Find positive zero crossings (from negative to positive amplitudes, ignoring small baseline activity). Calculate median period and standard deviation of interval between crossings.

5. Same as alternative 4, but with negative zero crossings.

6. The local maximum and minimum points are found (using sign crossing of the differential signal). Limit "false" and uninteresting peak points by employing different thresholds such as minimum peak to peak amplitude. The intervals between maximum points are found and median and standard deviation of the intervals are calculated.

7. Same as alternative 6, but with the intervals between the minimum points.

Then the period T from the "best" alternative is chosen. "Best" is based on the lowest standard deviation among the alternatives, along with additional logic to discriminate between likely and unlikely alternatives.

The BPM feature is then calculated as

$$\text{BPM} = 60 f_s / T \tag{5.14}$$

where f_s is the sampling frequency in Hz and the period T is given in number of samples. Typically, VF and VT rhythms will have more bpm (> 150) than most PEAs and pulse rhythms.

5.3.3 Ratio of residual to total energy (RRTE)

Using the median period length T found during the calculation of the BPM measure, the ECG segment is divided into K non-overlapping blocks of length

T, and each block is normalized to unit variance. For an organized ECG rhythm, each block then contains one period of the repeating rhythm. The total energy for the segment is now

$$E_{total} = \sum_{k=1}^{K} \sum_{n=1}^{T} x_k^2(n), \tag{5.15}$$

where $x_k(n)$ denotes sample number n in block number k.
The ensemble mean of the signal blocks is found by

$$x_{mean}(n) = \frac{1}{K} \sum_{k=1}^{K} x_k(n), \tag{5.16}$$

representing one typical period or cycle of the present heart rhythm.
This "typical" signal period is then subtracted from each block of ECG and the residual energy is calculated:

$$E_{residual} = \sum_{k=1}^{K} \sum_{n=1}^{T} (x_k(n) - x_{mean}(n))^2, \tag{5.17}$$

As a feature of how repetitive and predictable the heart rhythm is, we calculate the ratio of residual to total energy (RRTE):

$$\text{RRTE} = \frac{E_{residual}}{E_{total}}, \tag{5.18}$$

and use this as a potential feature for a shock advice algorithm. The higher the RRTE is, the less predictable and chaotic the rhythm is. Contrary, low RRTE indicates a highly repetitive rhythm. Typically, VF rhythms will have larger RRTE than PEA and pulse rhythms.

5.3.4 Complexity measure (COMPL)

A variant feature correlated with, but not the same, as RRTE can be calculated from the blocks of ECG as used in the previous section. The ensemble standard deviation of the ECG blocks are calculated:

$$x_{SD}(n) = \sqrt{\frac{1}{K-1} \sum_{k=1}^{K} (x_k(n) - x_{mean}(n))^2} \tag{5.19}$$

The median value of $x_{SD}(n)$ is a number used as the complexity measure feature $COMPL$ reflecting the predictability and complexity of an ECG rhythm. Typically, VF rhythms will have larger values than PEA and pulse rhythms.

5.3.5 Slope count

Slope count is a measure reflecting the ratio of steep to gentle slopes in the ECG segment, and defined as the percentage of signal samples with absolute slope rate below 5% of the maximum absolute slope in the segment. The absolute slope rate for sample number n, $a_{dx}(n)$, is simply defined as

$$a_{dx}(n) = |x(n) - x(n-1)|. \tag{5.20}$$

Typically, segments of pulse rhythms and PEA with narrow QRS complexes will have few, but steep slopes, giving a high slope count value. VF and VT rhythms often have slopes within a narrow slope range giving a low slope count value.

5.3.6 Peak amplitudes

During the calculation of the BPM feature, the position of the peaks and troughs in the ECG segment are found. We can then calculate the mean peak amplitude (MPA) as the mean absolute amplitude value of the peaks and troughs. By matching the corresponding peaks and troughs, the mean peak-to-peak amplitude (MPPA) is also calculated. However, MPA and MPPA are normally highly correlated (with MPPA about twice the value of MPA for sinusoid rhythms) so in the following we will only use MPPA.

5.4 Example calculation of the features

In this chapter, we have presented many features designed for either rhythm or VF analysis in ECG. To illustrate the various features and the unfortunate influence of CPR artifacts on the features, we calculate features values in three examples of ECG with and without CPR artifacts. The examples, consisting of one VF, one asystole, and one PEA rhythm, are shown in Figure 5.1. The ECG tracings are all 20 seconds in length, with CPR artifacts in the first 10 seconds. Values for all the features presented in this chapter are calculated from a 5 second window in artifact corrupted ECG, and from a 5 second window in clean ECG, for all the three examples as indicated by the shaded areas in the figure. The values of the features are presented in Table 5.1. Note that these calculations serve only as an example. More on how CPR artifacts affect different features and if CPR artifact filtering can improve the situation are presented in Chapter 9.

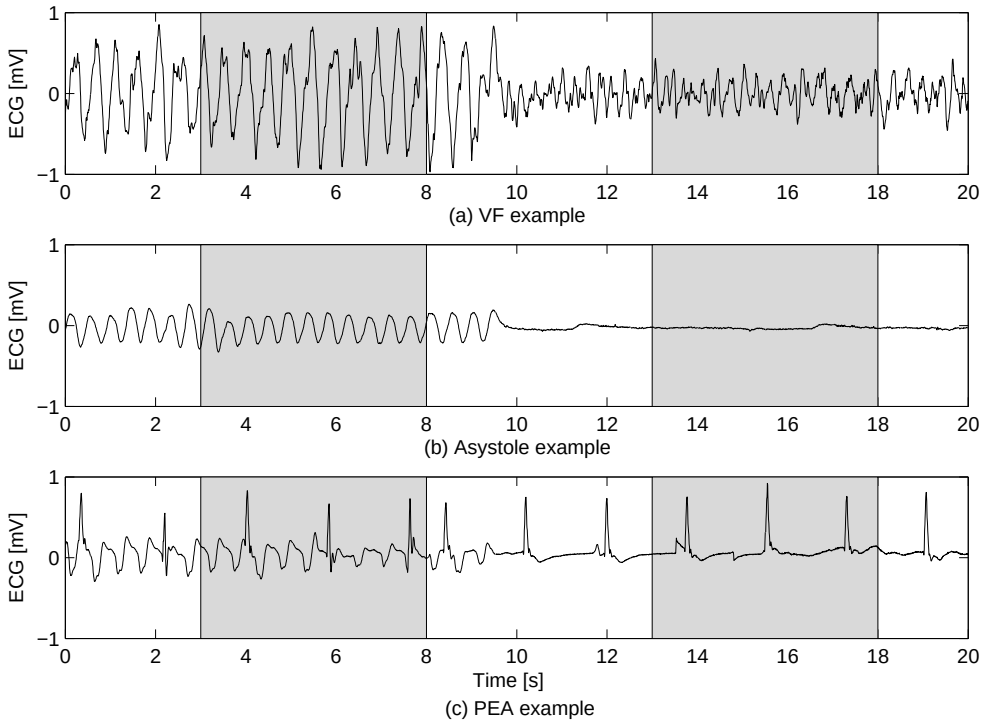

Figure 5.1: Three ECG examples of human cardiac arrest rhythms used for illustrating different signal features. First 10 seconds of each tracing have CPR artifacts. The shaded areas indicate where the features have been calculated. The feature values are shown in Table 5.1

Table 5.1: ECG feature values in examples of one VF, one asystole, and one PEA rhythm. The features are calculated both in clean ECG and ECG with CPR artifacts as indicated in Figure 5.1.

	VF		Asystole		PEA	
Feature name	w/CPR	clean	w/CPR	clean	w/CPR	clean
Leakage	0.44	0.62	0.20	0.90	0.73	0.88
T	71	35	81	17	53	40
FSMN	1.57	1.59	1.13	23.62	3.18	4.94
A1	0.010	0.079	0.000	0.000	0.029	0.008
A2	0.56	0.40	0.89	0.15	0.20	0.10
A3	0.31	0.27	0.11	0.49	0.44	0.37
PF	2.05	3.47	2.25	0.34	1.86	1.12
Lempel-Ziv	0.16	0.32	0.16	0.29	0.20	0.36
IRM	0.15	0.30	0.07	0.98	1.05	0.00
Count20	0.25	0.37	0.26	1.00	0.72	0.94
CF	2.63	4.50	2.38	2.94	3.15	4.35
PPF	2.34	3.52	2.34	0.00	1.76	1.76
ENRG	49.58	3.25	3.13	0.01	2.89	2.68
SFM	0.04	0.26	0.01	0.26	0.12	0.17
AMSA	8.07	7.30	2.53	0.64	5.40	4.69
BPM	124	364	135	0	112	34
RRTE	0.10	0.97	0.06	0.00	0.52	0.07
COMPL	0.31	1.61	0.25	0.00	0.64	0.21
Slope count	0.12	0.17	0.04	1.00	0.62	0.88
MPPA	0.95	0.34	0.37	0.00	0.38	0.48

Chapter 6

Comparing MC-RAMP and the time-varying Wiener filter

The mechanical activity from chest compressions and ventilations during CPR introduces artifact components in the ECG. For AEDs to perform reliable ECG signal analysis, CPR is therefore discontinued for a substantial time before the potential delivery of an electric shock. If the need for this NFT could be reduced or eliminated by removing these artifacts, it should significantly improve the defibrillation success rate [17, 32, 66, 88, 108].
The artifact components from CPR originate from mechanical stimulation of the heart and thorax muscles, and from the electrode-skin interface due to mechanical deformation [69]. Static electricity and the following charge equalizing currents between measurement equipment and patient during CPR also cause artifacts [69]. We will simulate CPR artifacts in human ECG, by manually adding artifacts collected during pig resuscitation to human VF and ventricular tachycardia (VT) rhythms as also done by Langhelle et al. [69] and Aase et al. [1].
To test the MC-RAMP adaptive filter developed in Chapter 4 for removing CPR artifacts in ECG, we will in this chapter filter a mix of animal CPR artifacts and human VF/VT. The performance will be evaluated in terms of signal-to-noise ratio (SNR) improvements, and compared with the theoretically optimal multichannel time-varying Wiener filter from a previous study by Aase et al. [1]. This chapter is adapted from [55].

6.1 Materials and methods

In the study by Aase et al. [1] CPR artifacts were successfully reduced in the recorded ECG signal using a multichannel time-varying Wiener filter, and

this made subsequent successful ECG signal analysis possible. Two reference channels were used: thoracic impedance and compression depth. Here, we will also investigate the use of two additional reference channels: compression acceleration and ECG common mode voltage.

The previous study [1] also showed that CPR artifact removal becomes increasingly more difficult when the compression rate goes from 60 to 90, and to 120 min^{-1} which is the highest rate that should be of clinical interest. This is due to a higher degree of overlap between the artifact and VF signal in the frequency domain. We select the worst-case scenario for our experiments, i.e. a compression rate of 120 min^{-1}.

The filtering experiments performed by Aase et al. focused on artifacts due to chest compressions and ventilation [1]. In the filtering experiments, the Wiener filter used reference signals proportional to the compression depth (measured directly by a mechanical compression device) and the ventilations (represented by the thorax impedance measurement, as seen between the defibrillator electrodes). The experimental setup by both Langhelle [69] and Aase [1] minimized the electrode-skin interface artifacts by collecting ECG from separate monitoring electrodes that were not mechanically affected during CPR as well as the use of a separate ground electrode which minimized the possible influence of static electricity. As discussed by Aase et al., successful filtering was limited by the reference signals having a low sampling rate of 25 Hz, compared to 100 Hz for the ECG. Also, the experimental setup indicated additional artifact components not reflected by the two reference signals used.

In [1] the multichannel Wiener filter required, *for each new signal sample*, the inversion of an estimated multichannel autocorrelation matrix of dimension given by the sum of the number of filter coefficients in all artifact correlated channels. Two artifact correlated reference channels and filters with just a single coefficient resulting in 2×2 autocorrelation matrices were used in [1]. In a more realistic setting, the possibility of adding more artifact correlated reference channels and using longer filters is desirable. For such situations the computational complexity of the matrix inversion of the solution of [1] quickly becomes prohibitive. Furthermore, given that reference signals encountered in practice, from time to time, give rise to ill-conditioned autocorrelation matrices further complicates the situation. To deal with these issues we will use the *MultiChannel Recursive Adaptive Matching Pursuit* (MC-RAMP) filter developed in Chapter 4. Note that the modifications in Section 4.2.3 are not used in this chapter, only MC-RAMP in its basic form.

6.1.1 Simulating CPR artifacts in human ECG

New animal experiments were conducted to collect artifacts and reference signals. To evaluate the feasibility of online CPR artifact removal in a more realistic setting, the data were collected in a setup where the chest compressions were manually performed (rather than by a mechanical device), and all the reference signals had sufficient resolution and bandwidth. The details of the animal experiment are described in Section 3.2.

To simulate CPR artifacts in human ECG, pig asystole ECG with CPR artifacts were added to human VF/VT (described in Section 3.1.1). The signal records used in the experiments are as follows:

- Artifacts: Animal asystole data with CPR artifacts are used to model artifacts in human ECG. 15 second records from two pigs were used, 12 records from each animal making a total of 24 records to mix with the human ECG. Each record was normalized to unit variance.
- Human ECG: The data records are 15 seconds each and of type:

  VF: 200 records.

  VT: 71 records.

In order to simulate a wide range of noise conditions, we added the animal data, now considered artifact noise, to the human VF/VT data using an adjustable scaling factor. Denote by $x_h(n)$ the human VF/VT signal and $a_n(n)$ the normalized artifact signal. Setting

$$a(n) = C \cdot a_n(n) \tag{6.1}$$

where C is a chosen constant, the noisy signal $x(n)$ is modelled as

$$x(n) = x_h(n) + a(n). \tag{6.2}$$

Given a target SNR defined as

$$\mathrm{SNR} = 10 \log_{10} \left(\frac{\sigma_{x_h}^2}{\sigma_a^2} \right). \tag{6.3}$$

with σ^2 denoting variance, the constant C is found as

$$C = \sqrt{\frac{\sigma_{x_h}^2}{10^{\frac{\mathrm{SNR}}{10}}}} \tag{6.4}$$

By individually computing C for the construction of every noisy signal record, a fixed SNR is ensured for the whole ensemble.

6.2 Results

In this section we describe the selection of the MC-RAMP parameters, show two examples of artifact filtering, before we present and discuss the full scale experiment.

6.2.1 Parameter selection

Although VT segments are available, we will select the filter parameters using VF segments only. This is reasonable since VF is more commonly encountered in the out-of-hospital defibrillation scenario [24, 53].

In the proposed filter structure of Figure 4.2, the filter lengths for all reference channels, $M_0, \ldots, M_{K-1}$, must be chosen. The window length, $L_1 + L_2 + 1$, must also be chosen. Note that L_1 and L_2 for a rectangular window, as in our case, need not be equal. That is, the number of future and past samples, respectively, to take into account when calculating the filter coefficients, can be different, making the window non-symmetric. For the MC-RAMP algorithm, the number of MP-iterations, P, for each time instant and the norm threshold, τ, preventing rank deficiency, must be chosen. Experimental evidence suggest a setting of $\tau = 0.2$, which is the value used in the following. In the experiments reported, we have set $P = \lceil M/2 \rceil$, where $M = \sum_{k=0}^{K-1} M_k$. While the results are not very sensitive to the exact value of P, in fact a P of 1 or 2 gives only marginally inferior results, the selected P is indicative of the best possible performance with the proposed algorithm. When computing the results, only the 9 second center part of each 15 second segment is used in order to avoid filtering edge effects. The parameter settings are selected for maximum SNR improvement. In order to limit the search for the best parameter settings, two constraints are introduced:

- The parameter selection experiments are performed on a limited data set (6 animal artifact signals mixed with 20 human VF signals giving 120 mixed signals). The obtained SNRs after restoration are averaged over the 120 signals.

- Only one input SNR (i.e. VF+artifact SNR before filtering) setting is used: 0 dB.

Selecting parameters for the two-channel system

For tuning of the parameters L_1 and L_2, we only use two reference channels, thorax impedance and compression depth. The filter lengths M_1 (for thorax impedance) and M_2 (for compression depth) are also set equal, $M_1 = M_2 = M_c$.

For MC-RAMP, the number of past (L_2) and future (L_1) samples taken into account when calculating the filter coefficients can be adjusted independently. The average restored SNRs obtained for $M_c = 3$ as a function of L_1 and L_2 are shown in Figure 6.1. We observe that the SNR results are fairly symmetrical about the diagonal with respect to L_1 and L_2, indicating that we can set $L_1 = L_2$. Using this additional constraint, the results obtained for filter lengths 1 through 6 are shown in Figure 6.2. Using future samples (i.e. non-causal solution, $L_1 > 0$) will introduce a time delay in a real-time system. Observing that the system performance increases with increased window size, the choice of L_1 must be a compromise between an acceptable time delay and signal restoration performance. From Figure 6.2 a suitable compromise is a window size of 300, i.e. $L_1 = L_2 = 150$, giving a delay of 1.5 s in the present situation. The performance also increases with increased filter length. This is in contrast to the result in [1] where single tap filters gave the best results. The reference channels in [1] were originally sampled at 25 Hz and upsampled to 100 Hz. This low time resolution, along with rank problems, may explain why 1 tap filters worked best in those experiments. Regarding the filter length selection, we furthermore observe from Figure 6.2 that the largest benefit comes from increasing the number of filter coefficients M from 1 to 2. Increasing M further results in improvements, but increasing M beyond a value of 5 or 6 leads only to marginal gains in the artifact reducing capabilities. We conclude for now that 5 tap filters for the thorax impedance and compression depth channels seems to be reasonable choices.

Extending the number of reference channels

As suggested in Section 3.2, the use of additional reference channels may improve the artifact removal performance. The two additional channels of current interest are *ECG common mode* and *compression acceleration* (i.e. chest compression acceleration, from which the compression depth is derived). Test results showing the effect of adding these reference channels in addition to the original two channels are shown in Table 6.1. The tests are done for two cases; when the existing channels, thorax impedance and compression depth, have short (1-tap) filters and longer (5-tap) filters. From the presented table, we

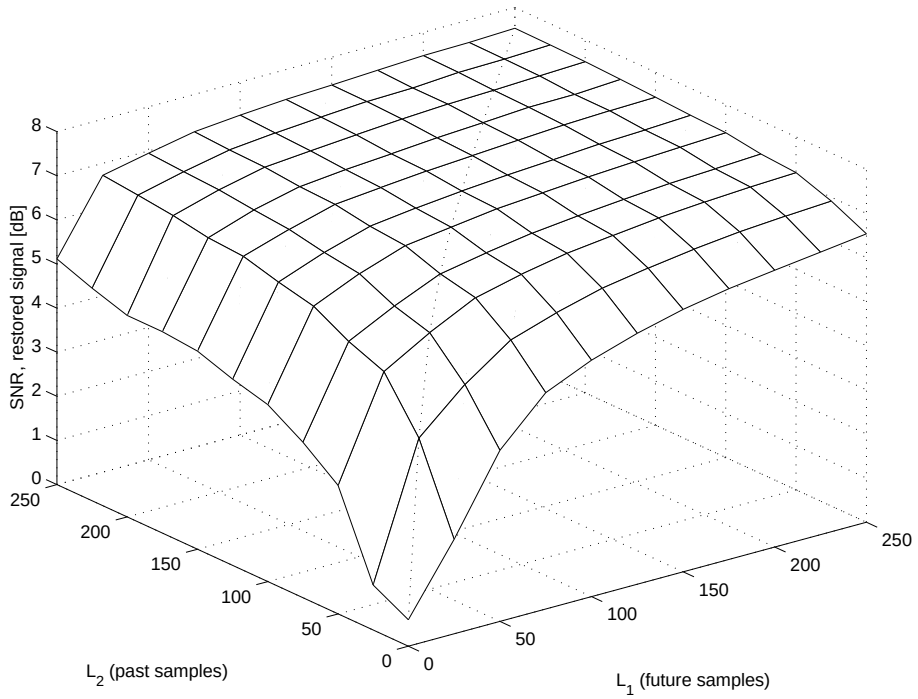

Figure 6.1: Artifact removal performance of MC-RAMP as a function of the number of past (L_2) and future (L_1) samples taken into account when calculating the filter coefficients. Two reference channels, thorax impedance and compression depth, are used, each with a filter length of 3. The input SNR is 0 dB. The dotted line is the diagonal where $L_1 = L_2$.

again observe the significant gains in terms of artifact reducing capabilities when increasing the filter lengths. Furthermore, we observe that the additional channels seem to be most useful when we use short filters for the thorax impedance and compression depth channels. For longer filters, we still observe a slight increase in performance when adding compression acceleration, while ECG common mode seems to have no significant positive effect. In the following experiments, we will not further investigate the use of ECG common mode since it seems to have little (positive) effect on the performance. Compression acceleration however, having some positive effect, will be further investigated in our full scale experiment in Section 6.2.3.

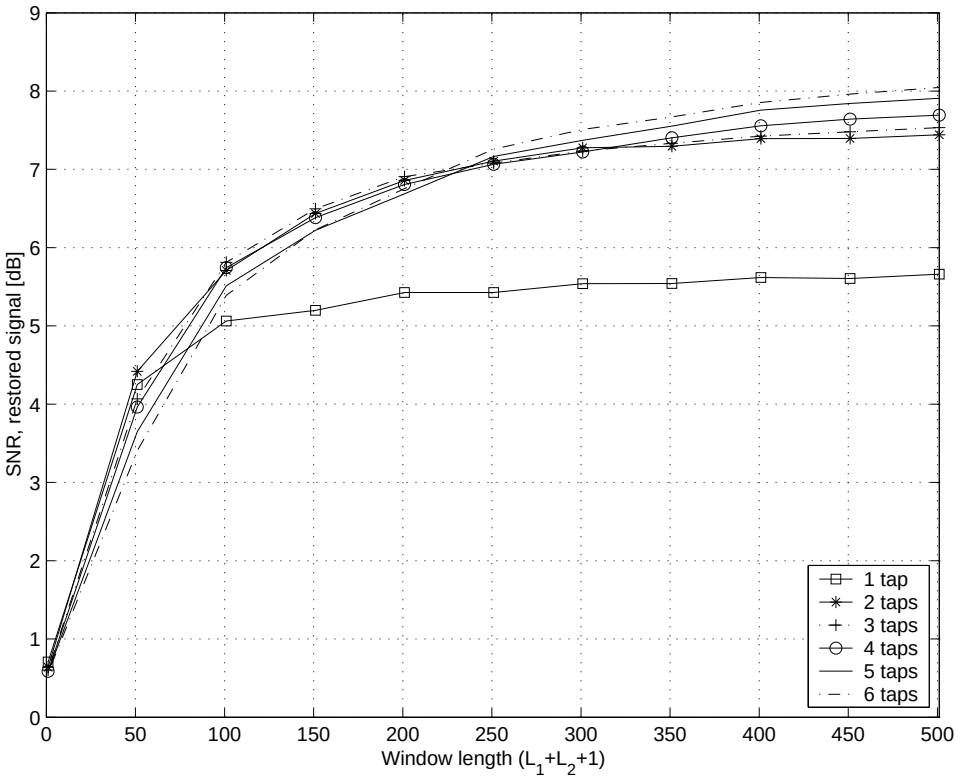

Figure 6.2: Artifact removal performance of MC-RAMP as a function of the window length $L_1 + L_2 + 1$, $(L_1 = L_2)$, and the number of filter taps in each channel. Two reference channels, thorax impedance and compression depth, are used. The input SNR is 0 dB.

6.2.2 Filtering examples

Before presenting the overall results we visualize the effect of the proposed system with two filtering examples. Both examples use two reference channels, thorax impedance and compression depth, each having a 5-tap filter. In the first example, we select a 15 second human VF record, to which an animal artifact is added to give an SNR of -5 dB. Figure 6.3 shows the result. In the second example, a 15 s human VT record is mixed with an animal artifact, SNR is -5 dB. Figure 6.4 shows the resulting waveforms. Both examples show good filtering results with SNR improved by over 9 dB. Some errors are still present in the reconstructed signal, indicating that the artifact exhibits additional, seemingly high-frequency, features not seen in the two reference channels. Some reference error might be due to some remaining spontaneous

Table 6.1: MC-RAMP test results showing the effect of adding extra reference channels in addition to the original two channels (compression depth and thorax impedance) for varying filter taps.

Filter taps				Performance in dB		
Impedance	Depth	ECG common mode	Acceleration	Mean	Median	Std.dev.
1	1	0	0	5.54	5.42	1.41
1	1	1	0	5.73	5.70	1.62
1	1	2	0	5.77	5.62	1.57
1	1	0	1	5.92	6.13	1.61
1	1	0	2	6.42	6.55	1.43
1	1	1	1	5.88	6.00	1.65
1	1	2	2	6.34	6.48	1.45
5	5	0	0	7.37	7.39	1.82
5	5	1	0	7.24	7.22	1.76
5	5	2	0	7.17	7.10	1.75
5	5	0	1	7.59	7.63	1.83
5	5	0	2	7.23	7.38	2.15
5	5	1	1	7.38	7.49	1.78
5	5	1	2	7.07	7.16	1.91

electric activity in the heart of the animal, indicating that ECG due to the animal's heart activity is not completely isoelectric.

6.2.3 Full scale experiment and SNR evaluation

Using all the data, we evaluated two configurations of the proposed artifact removal system in terms of SNR improvement. The first configuration is the two channel system, using thorax impedance and compression depth as reference channels (5-tap filter for each channel) with the MC-RAMP algorithm. The second configuration is the three channel system, using thorax impedance, compression depth (both 5-tap filter) and compression acceleration (1-tap filter) as reference channels. For comparison, these two experiments were also

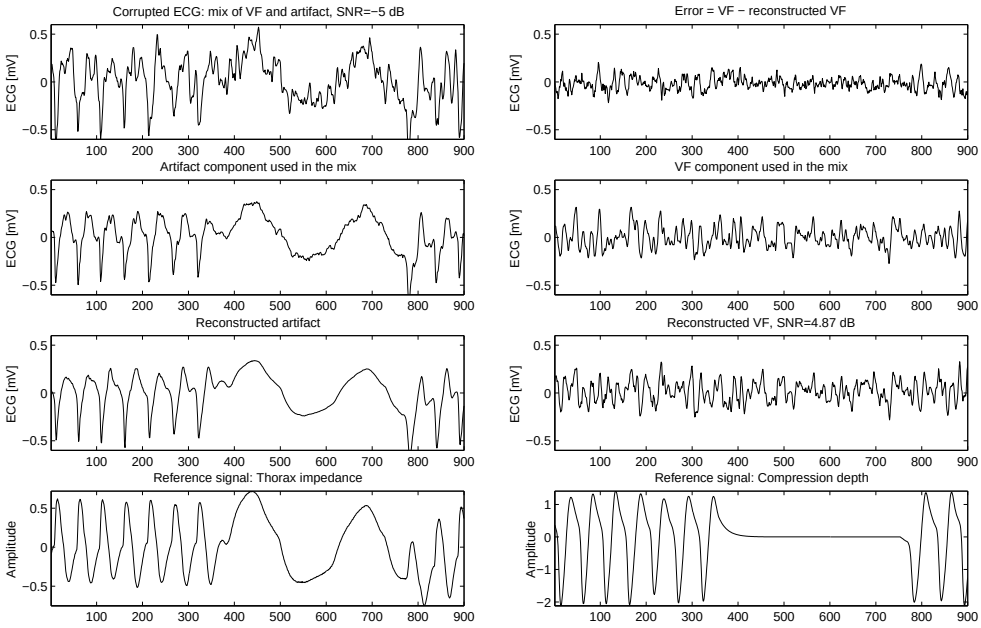

Figure 6.3: VF filtering example using the MC-RAMP two channel filter system. Corrupted ECG SNR is -5 dB. After filtering, the SNR is 4.87 dB.

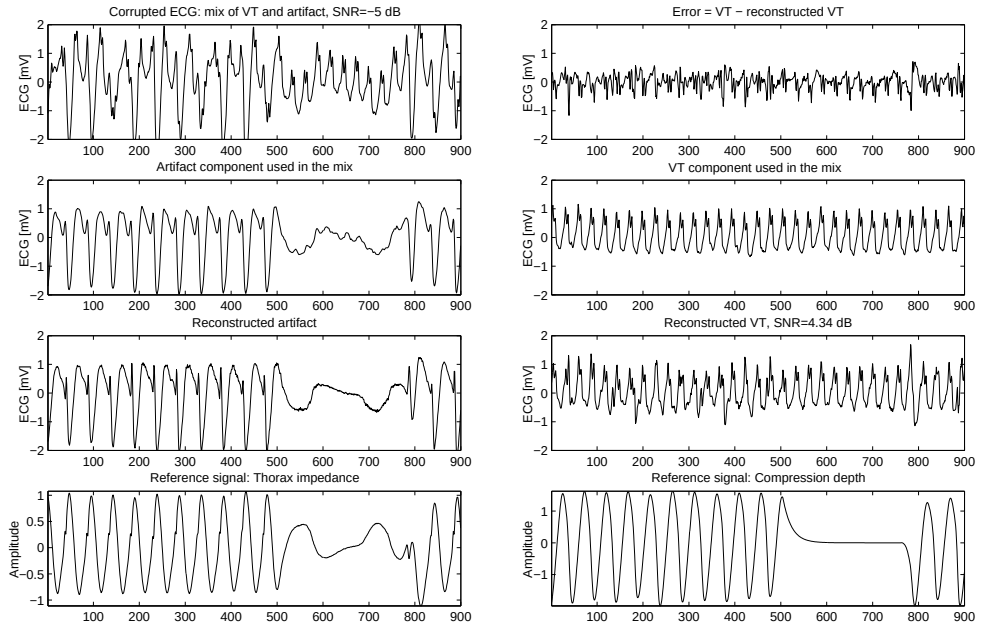

Figure 6.4: VT filtering example using the MC-RAMP two channel filter system. Original SNR is -5 dB. After filtering, the SNR is 4.34 dB.

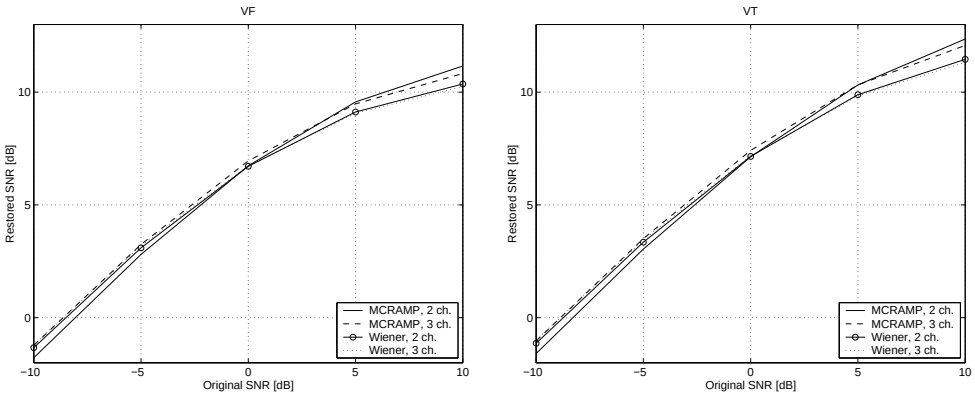

Figure 6.5: Average SNR performance of the artifact removal system for the MC-RAMP and the time-varying Wiener filters. Two (compression depth and thorax impedance) or three (compression acceleration in addition) reference channels are used.

repeated using the time-varying Wiener filter solution [1] with the same window length ($L_1 = L_2 = 150$) and filter lengths as for MC-RAMP. The results are shown in Figure 6.5. We observe that VT performance is slightly better than for VF, but the trends as to channel configuration and filter type are equal. Wiener and MC-RAMP are quite close in performance, although 3 channel MC-RAMP seems to give the best overall results. The difference in performance between 2 and 3 channels are larger for MC-RAMP than for the Wiener filter solution.

6.2.4 Statistical analysis

For the comparison of the restored SNR levels for VF for the two different filter types and the two channel configurations, Wilcoxon rank-sum test is used. Statistical significance is set to the 0.05 level. When comparing 3 versus 2 channels for MC-RAMP, 3 channels are significantly better for SNRs -10 to 0 dB ($P << 0.001$), but significantly worse for SNRs 5 and 10 dB ($P = 0.023$ and $P << 0.001$, respectively).[1] For Wiener filter, 3 channels are significantly better for SNR = -10 dB ($P = 0.0075$), not significantly different for SNRs -5, 0, 5 dB ($P = 0.052$, $P = 0.62$, and $P = 0.11$, respectively), and significantly worse for SNR = 10 dB ($P = 0.0015$).

When comparing Wiener filter versus MC-RAMP for 2 channels, Wiener filter is significantly better for SNRs -10 and -5 dB ($P << 0.001$), not significantly

[1] The performance were only evaluated at SNRs -10, 5, 0, 5, and 10 dB.

different for SNR = 0 dB ($P = 0.53$), and significantly worse for SNRs 5 and 10 dB ($P << 0.001$). For 3 channels, MC-RAMP is not significantly different than Wiener filter for SNRs -10 and -5 dB ($P = 0.57$ and $P = 0.24$, respectively), but significantly better for SNRs 0, 5, and 10 dB ($P << 0.001$). Neither MC-RAMP nor Wiener filter have much positive effect for an input SNR of 10 dB.

6.3 Discussion

The MC-RAMP multichannel adaptive filter was successfully used for removal of CPR artifacts in ECG signals. We found that at a sampling rate of 100 Hz, a two channel filter, each with 5 filter coefficients and using thorax impedance and chest compression depth as reference signals, performed well when the L_1 and L_2 parameters defining the window of samples used in adapting the filter were both set to 150. Some improvement was observed when the number of reference channels was increased from 2 to 3, by including the compression acceleration.

In [1] it was established that automated ECG analysis could be reliably performed when the artifact corrupted ECG signal was processed by the time-varying Wiener filter. This was a direct consequence of the filter's artifact attenuation capability as measured by the SNR improvement. Here we have demonstrated equally good SNR improvements using the proposed algorithm, the MC-RAMP. Given the salient properties of this algorithm in terms of computational complexity and numerical robustness, the prospects of doing reliable real time ECG analysis while CPR is being administered are indeed promising.

6.4 Summary

In this chapter we demonstrated the use of the MC-RAMP adaptive filter described in Chapter 4 in a mix of animal CPR artifacts and human VF/VT. Evaluated in terms of SNR improvements, the CPR artifacts were successfully reduced. We also showed that the computational efficiency of our solution was *not* accompanied by any performance degradations compared to the computationally more expensive time-varying Wiener filter solution of [1]. Also, MC-RAMP is numerically robust, not having the problem of rank deficiency sometimes encountered in the time-varying Wiener filter solution.

Chapter 7

CPR artifact removal in human ECG

In Chapter 6, the performance of the MC-RAMP filter was shown to be on par with the theoretically optimal time-varying Wiener filter, but being less computationally complex for longer filters and more robust when ill-conditioned reference channel signals occur.

We now want to test the MC-RAMP algorithm on human ECG and reference channel data recorded during actual out-of-hospital cardiac arrests; the most realistic data set for this application to date. We want to study how an AED shock advice algorithm performs in ECG episodes with CPR artifacts, before and after artifact removal. A shock advice algorithm performs feature extraction and rhythm classification to differentiate between shockable rhythms such as VF and VT with rate over 150 bpm, and non-shockable rhythms such as asystole, PEA and various pulse rhythms.

Previous studies have only investigated CPR artifact reduction in situations with VF and VT, i.e. shockable rhythms. For these rhythms, the aim is to reduce the CPR artifacts enough to make a shock advice algorithm indicate shock; maintaining a high enough sensitivity. It has not, however, been established that the artifacts are uninfluenced by the underlying cardiac rhythm. It is therefore equally important to investigate filtering during non-shockable rhythms, such as pulseless electrical activity (PEA), asystole, and pulse-generating rhythms. As the artifacts often can resemble VF/VT, this is necessary to ensure that the shock advice algorithm maintains a high enough specificity. These rhythms constitute a new and different problem, and the challenge is now to clean up the rhythms to make the shock advice algorithm indicate no shock. This chapter is adapted from [37].

7.1 Materials and methods

In this section we describe the human ECG data, the data processing, and experimental methods used in this study.

7.1.1 Data collection

The data used in this study were extracted as part of a prospective study of out-of-hospital cardiac arrest patients in Akershus County, Norway (47 patients), Stockholm, Sweden (38 patients) and London, UK (20 patients) between March 2002 and May 2003. The ECG and reference channels for MC-RAMP were recorded as part of the Sister project and are described in Section 3.1.3. For this study, all four reference channels were included: compression depth, compression acceleration, thorax impedance, and ECG common mode.

To enable comparison of the shock advice analysis performance in ECG segments with and without CPR, we extracted continuous segments consisting of 10 seconds with CPR immediately followed by 10 seconds without, padded with one second buffers in the beginning and the end for filter initialization etc. Since shocks will not be given when the patient is being lifted or intubated, segments having large motion artifacts were excluded.

The episodes were annotated and classified into five classes of underlying heart rhythms:

Shockable:

1) Ventricular fibrillation (VF)

2) Non-perfusing ventricular tachycardia (VT) with rate over 150 beats per minute

Non-shockable:

3) Asystole

4) Pulseless electrical activity (PEA)

5) Pulse-giving rhythm (PR)

7.1.2 Data preprocessing

Before applying MC-RAMP, the ECG episodes and reference channels were downsampled to 200 Hz[1], which is the sample rate used by the shock advice algorithm in our experiments (see Section 5.1). 50 Hz 4th order comb filters were applied to the ECG and all reference channels in order to remove the DC and any 50 Hz mains noise, and 20 Hz 40 taps lowpass FIR filters to the thoracic impedance channel and the ECG common mode channel. The latter had an additional 8.9 Hz, 2nd order notch filter applied due to observed noise in the collected data[2].

7.1.3 Experiments

To test the MC-RAMP algorithm, we examined how an AED shock advice algorithm performed in ECG episodes with CPR artifacts, before and after artifact removal. The shock advice algorithm used for the experiments is described in Section 5.1. For filtering of CPR artifacts, the basic MC-RAMP and its modifications as described in Chapter 4 were used.

Each ECG episode consisted of 10 seconds with CPR artifacts[3] and 10 seconds without[4]. See Figure 7.1 for an example episode. It was assumed that the underlying heart rhythm was the same throughout each episode, so that the shock advice in principle should be the same in the subsegments with and without CPR. The performance of the CPR artifact removal algorithm was therefore tested by comparing the results from the first half with CPR to the annotated "reference" second half with clean ECG.

A total of 184 shockable and 348 non-shockable episodes were randomly distributed into a training set and a test set, stratified so that each set had 89 VF, 3 VT, 52 asystole, 114 PEA, and 8 PR episodes. Care was taken to ensure that the episodes from the three geographic locations (Akershus, Stockholm, and London) were distributed evenly into both sets. The training set was used

[1] In the analogue electronics of the defibrillator, the ECG is filtered with a second order bandpass (0.9–50 Hz) filter without linear phase in the passband. The reference channels were therefore filtered with a digital equivalent of this analogue filter in order to make the reference signals as equal to the correlated components in the ECG artifacts as possible.

[2] The 8.9 Hz periodic noise probably originates from an electrical component in the defibrillator, but is only present in the ECG common mode channel and has no effect on the CPR artifact filtering results.

[3] As indicated by compressions registered in the Depth reference channel. A CPR period is allowed up to 3 seconds of break in the midst of the compressions, eg. due to administering of ventilations.

[4] Padded with one second buffers in the beginning and the end for filter initialization etc.

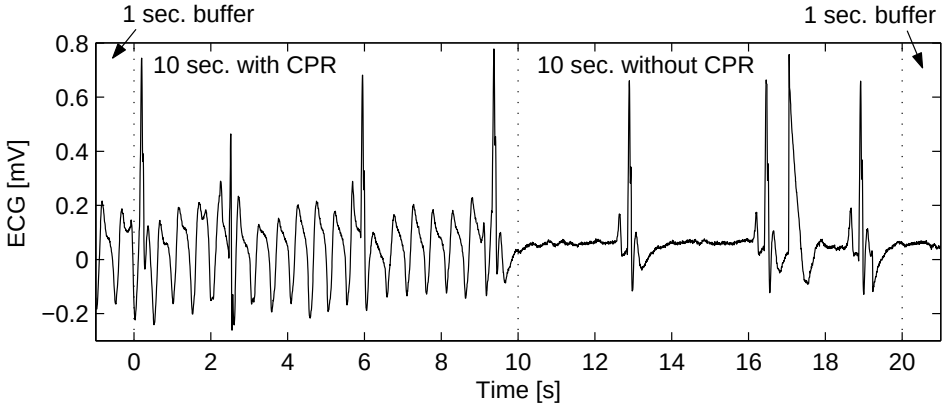

Figure 7.1: Example of an episode. First half is with CPR, second half without. Underlying heart rhythm is PEA throughout the whole episode. A noise spike is present at approximately 17 seconds.

for tuning the MC-RAMP algorithm and the test set for evaluating the CPR artifact removal system.

The performance was evaluated in terms of sensitivity and specificity. Sensitivity is defined as the number of episodes correctly classified as shockable divided by the total number of shockable episodes (class 1 and 2), and specificity as the number of episodes correctly classified as non-shockable divided by the total number of non-shockable episodes (classes 3-5).

7.2 Results

In this section we first tune the MC-RAMP algorithm, before we present the overall experimental results and show some filtering examples.

7.2.1 Tuning the MC-RAMP algorithm

The training set was used for tuning the MC-RAMP algorithm. Our implementation of MC-RAMP has several parameters, the most important listed below:

1. The vector $\underline{M}$ with the number of filter coefficients for each channel.
2. L_1 and L_2, the number of future and past samples, respectively, to take into account when finding the filter coefficients.

3. The -3 dB cut-off frequency, f_{LP} , of the lowpass filter applied on the reconstructed artifact signal before subtracting it from the original ECG signal.

4. P, the number of filter coefficient-updates to compute for each time instant.

5. Energy thresholds for each reference channel. Below this threshold, the filter coefficients of a reference channel are not updated, but slowly faded towards zero.

6. Correlation coefficient thresholds for each reference channel. Filter coefficients of reference channels with correlation with the ECG channel below this threshold are not updated, but slowly faded towards zero.

7. Option to turn on/off the possibility of automatic adjustment of L_1 and L_2 during filtering, as well as the correlation and energy thresholds that decides when and to what values L_1 and L_2 are to change. Also, we may set how often this adjustment is to take place.

An exhaustive search for the best MC-RAMP performance with respect to all these parameters simultaneously will be too computationally expensive and time consuming. Based on preliminary experiments, we chose to fix the parameters of items 4-7 without further testing [5]. The remaining MC-RAMP parameters were selected by running filter tests on the training set. Due to the large number of degrees of freedom in adjusting the parameters, we ran decoupled tests, adjusting only one parameter type at a time.

We begin by adjusting the vector M with the number of filter coefficients for each channel. Test results with the performance for different values of M are shown in Table 7.1. From this table we suggest using 5 filter coefficients for each of the reference channels, i.e. $M = [5 \quad 5 \quad 5 \quad 5]$.

In Chapter 6, best result was achieved by making the observation window symmetrical, i.e. $L = L_1 = L_2$. Table 7.2 lists the performance for different values of L. From this table we suggest using $L = 200$.

Using M =[5 5 5 5], and $L_1 = L_2 = 200$, the cut-off frequency, f_{LP}, of the reconstructed artifact lowpass filter was thereafter adjusted over the range 5–20 Hz, and 11 Hz appeared to give the best balanced result (see Figure 7.2).

[5] The energy thresholds are set to about 20% (30% for the common mode channel) of the mean standard deviation of each reference channel during CPR in the training set. The correlation coefficient threshold is set to 0.35 for all reference channels. L_1 and L_2 are automatically adjusted every 50 samples. P is set to 4 unless otherwise noted.

Table 7.1: MC-RAMP performance in terms of sensitivity and specificity in the training set for different number of filter taps for each reference channel. Both for ECG with and without CPR artifacts. $L_1 = L_2 = 200$, $f_{LP} = 11$ Hz

Filter taps					MC-RAMP performance			
					CPR		no CPR	
Depth	Impedance	ECG common mode	Acceleration	P	Sensitivity [%]	Specificity [%]	Sensitivity [%]	Specificity [%]
1	1	1	1	2	97.8	74.7	98.9	100
2	2	2	2	2	96.7	79.3	100	99.4
3	3	3	3	4	97.9	79.9	100	99.4
4	4	4	4	4	98.9	81.0	100	99.4
5	5	5	5	4	98.9	82.2	100	99.4
6	6	6	6	4	97.8	81.0	100	99.4
5	0	0	0	2	94.6	75.3	100	100
0	5	0	0	2	95.7	73.0	100	100
0	0	5	0	2	92.4	73.6	100	100
0	0	0	5	2	96.7	74.7	100	100
5	5	0	0	3	97.8	75.9	100	100
5	0	5	0	3	96.7	75.3	100	100
5	0	0	5	3	96.7	79.3	100	100
0	5	5	5	3	97.8	76.4	100	100
5	0	5	5	3	96.7	79.9	100	99.4
5	5	0	5	3	98.9	81.6	100	99.4
5	5	5	0	3	98.9	75.9	100	100

From the parameter selection tests, we choose to use M =[5 5 5 5], $L_1 = L_2 = 200$, and $f_{LP} = 11$ Hz for all following tests. We note, however, that generality of these settings may not be assured due to the small size of the training set. The settings have also been adapted to give good results using the current shock advice algorithm, and will likely need to be adjusted for other shock advice algorithms.

During compressions, which create the most prominent artifacts, the compression depth reference channel seems to be the one contributing most (indicating the highest correlation with the artifact components in the ECG). The compression acceleration and thorax impedance follows thereafter. The ECG com-

Table 7.2: MC-RAMP performance in the training set for different values of L reflecting the length of the observation window. M =[5 5 5 5], $f_{LP} = 11$ Hz

L	MC-RAMP performance			
	CPR		no CPR	
	Sensitivity [%]	Specificity [%]	Sensitivity [%]	Specificity [%]
50	92.4	83.3	97.8	100
100	96.7	82.2	98.9	99.4
150	98.9	81.0	100	98.9
200	98.9	82.2	100	99.4
250	97.8	79.3	98.9	100

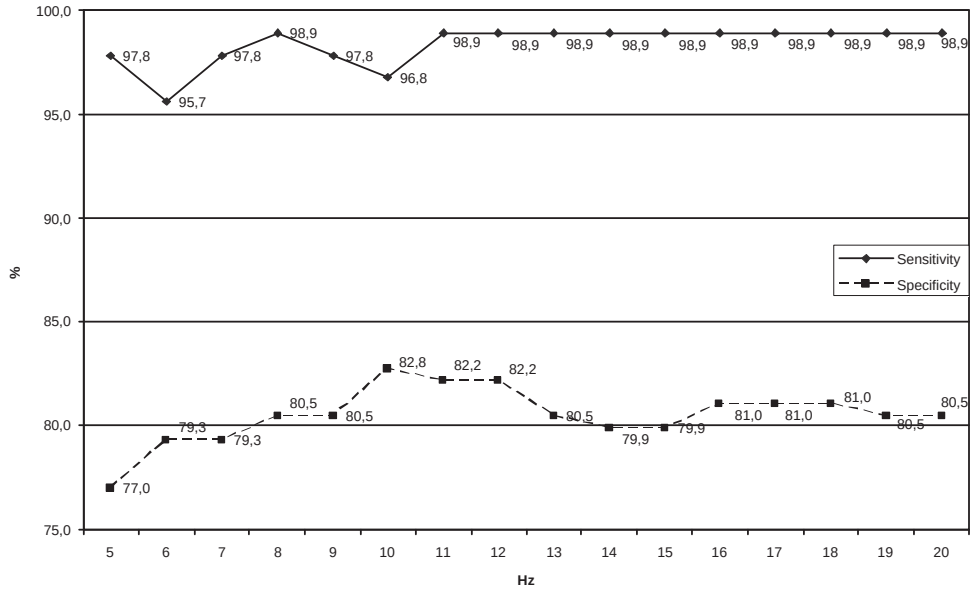

Figure 7.2: Sensitivity and specificity after artifact filtering using MC-RAMP in CPR corrupted ECG from the training set for different cut-off frequencies f_{LP} of the reconstructed artifact lowpass filter. M =[5 5 5 5], $L = 200$

Table 7.3: Sensitivity (sens.) and specificity (spec.) for the training and test set.

		Performance in (%)			
		CPR		no CPR	
		Sens.	Spec.	Sens.	Spec.
Training set	Unfiltered	90.2	76.4	100	100
	w/MC-RAMP	98.9	82.2	100	99.4
	w/4.3 Hz HP filter	73.9	91.4	69.6	98.9
Test set	Unfiltered	81.5	67.2	97.8	98.9
	w/MC-RAMP	96.7	79.9	97.8	98.3
	w/4.3 Hz HP filter	64.1	90.2	53.3	98.3

mon mode channel is mostly used for various non-CPR noise phenomena in the ECG. However, keep in mind that the MC-RAMP filter will automatically choose which and what amount of the reference channels needed for making a model of the CPR artifacts as present in the ECG. In general, over an ECG episode, all four reference channels will normally contribute at some time.

7.2.2 Results of the CPR artifact removal

Using the best parameter setting found in Section 7.2.1, we tested the performance of the shock advice algorithm after filtering the test set using the MC-RAMP filter. For comparison, we also tested the performance after artifact filtering using a fixed coefficient 4.3 Hz highpass (HP) filter (40 taps FIR filter) as tested by Strohmenger et al. for removal of CPR artifacts [92] for VF analysis. The results are shown in Table 7.3. As can be seen from the table, the 4.3 Hz highpass filter is inferior to MC-RAMP, and gives even worse results than using no filter at all.

Only considering MC-RAMP: From the training set a sensitivity of 98.9% and specificity of 82.2% were achieved during CPR, an increase of approximately 8% and 6%, respectively, compared to the unfiltered training set. The test set gave a sensitivity of 96.7% and specificity of 79.9%, an increase of approximately 15% and 13% respectively, compared to no filtering.

Figure 7.3 shows three examples of successful filtering where false classification during CPR is turned into correct classification after filtering. Each plot is an episode of 20 seconds with first 10 seconds with CPR. From the top, the original ECG, filtered ECG, reference channels compression depth, thorax impedance, ECG common mode, and compression acceleration, respectively,

are plotted. The results of the shock advice algorithm are written in the ECG plots for each half of the episodes.

For some episodes, the shock advice algorithm will give correct classification for both unfiltered and filtered ECG. The CPR artifacts may be small or of such a character that the algorithm will not be misled. However, filtering of CPR artifacts will often visually improve the ECG and is of interest for an AED operator. Figure 7.4 shows three such examples.

Unfortunately, sometimes MC-RAMP fails to filter an episode properly. Possible reasons for this are discussed in Section 7.3. Figure 7.5 shows three examples where we (still) get wrong shock advice after filtering.

7.3 Discussion

CPR artifacts have previously been successfully removed from VF/VT segments in animals [78, 91] and in a mix of human VF/VT and animal CPR artifacts [1, 55, 69]. The present study indicates that this is also possible for clinical human data. The 96.7% sensitivity for VF/VT after filtering in the present study (versus 81.5% unfiltered) is close to the 97.8% sensitivity in segments without CPR in the present study, and similar to previously reported sensitivities for semi-automated defibrillators [76,77]. Thus most patients with a shockable rhythm could have been shocked earlier without a hands-off interval for ECG analysis, and thus an increased probability of ROSC [32,88,108].

It is however also important that the defibrillator accurately assesses non-shockable rhythms. It is vital that no shocks are given to patients with a potentially perfusing rhythm, and unnecessary shocks should be avoided in patients with asystole or PEA where they can do no good. Previous studies have not included non-shockable rhythms in the artifact filtering evaluation [1, 55, 69, 78, 91, 92]. In the present study the specificity of only 79.9% for the test set (versus 67.2% unfiltered and 98.3% in the segments without CPR) indicate that artifact filtering of non-shockable segments constitute a more difficult problem than for VF/VT episodes.

A possible reason for this is the great variability in CPR artifact size and character. There were episodes with large and spiky CPR artifacts without similar spikiness in the reference channels, and the filter can only remove artifacts reflected in the reference channels. The residuals after filtering were sometimes relatively large, resembling VF, e.g. in Figure 7.5(b), especially apparent for some asystole episodes. This could be due to insufficient filtering or missing components in the reference channels, but it cannot be excluded

that compressions could induce VF-like activity in the heart which disappears immediately with the cessation of compressions. Thus it cannot be excluded that the underlying heart rhythm was not the same during the ten seconds with and ten seconds without CPR artifacts in some of the analyzed ECG episodes.

We assumed a linear mix of CPR artifacts and underlying heart rhythm in the ECG, but this assumption is probably not true under all conditions. This is particulary seen in episodes with large and spiky CPR artifacts where the spikiness is not found in the reference channels. We might need to use our reference channels in some nonlinear fashion in order to shape the reference channel more to the "nonlinear" CPR artifacts sometimes seen in the ECG. The large and spiky artifacts may also be the result of an instrumentation problem or a particular electrode/skin condition.

Another type of troublesome episodes occurs when the rate of the compressions and underlying heart activity (e.g. PEA complexes) are almost the same. For these, the MC-RAMP algorithm will often remove portions of the underlying heart activity in the ECG signal as well. Components in the ECG correlated with the reference channels are removed, unfortunately also incidental similarities.

The shock advice algorithm used in this study is based on hard decisions, that is, fixed thresholds for various ECG features. There are always borderline cases for shock/no-shock classification, also for ECG segments without CPR artifacts, and we have observed several in our data set. Sometimes a borderline case will be correctly classified on the non-CPR ECG, but incorrectly on the CPR part due to some small residual after filtering. Figure 7.5(c) shows one such example. It is possible that another shock advice algorithm could be developed with features less sensitive to such post-filtering residuals and decision rules based on pattern recognition principles [28].

7.4 Summary

Using the MC-RAMP multichannel adaptive filter, we have filtered human ECG episodes of out-of-hospital cardiac arrest with CPR artifacts, and evaluated the result using a shock advice algorithm. A satisfactory VF/VT sensitivity of 96.7% was achieved. The specificity was only 79.9%, indicating that artifact filtering of non-shockable episodes constitutes a more difficult problem than for VF/VT episodes. Several factors are speculated to have contributed to the relatively low specificity, such as missing artifact components in the reference channels, inadequate shock advice algorithm, and spontaneous underlying heart activity.

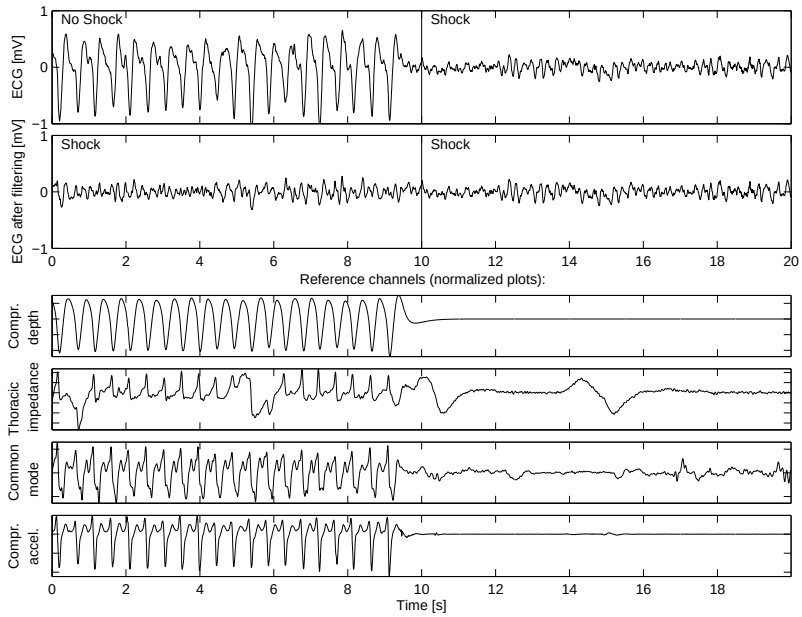

(a) Successful VF episode

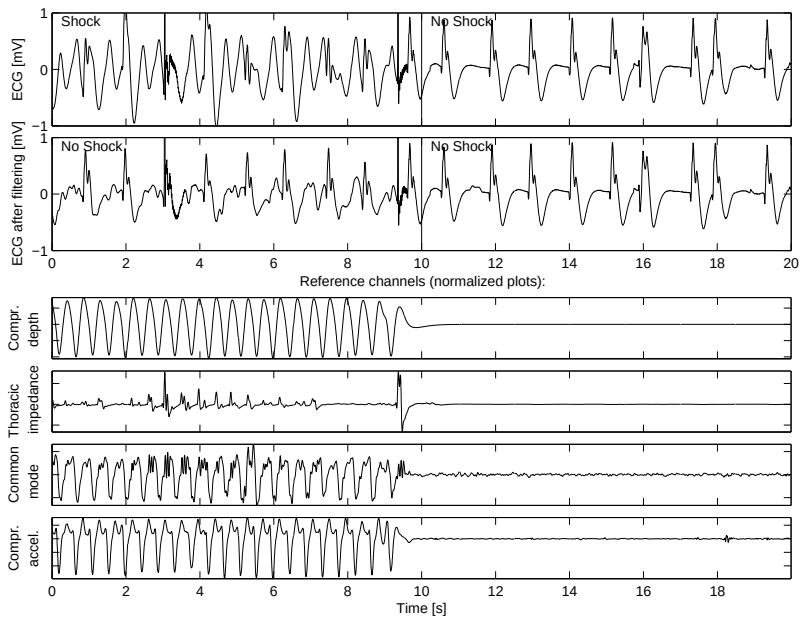

(b) Successful PEA episode

Figure 7.3: Three examples of successful filtering – segments with false classification during CPR, but correct classification after MC-RAMP filtering.

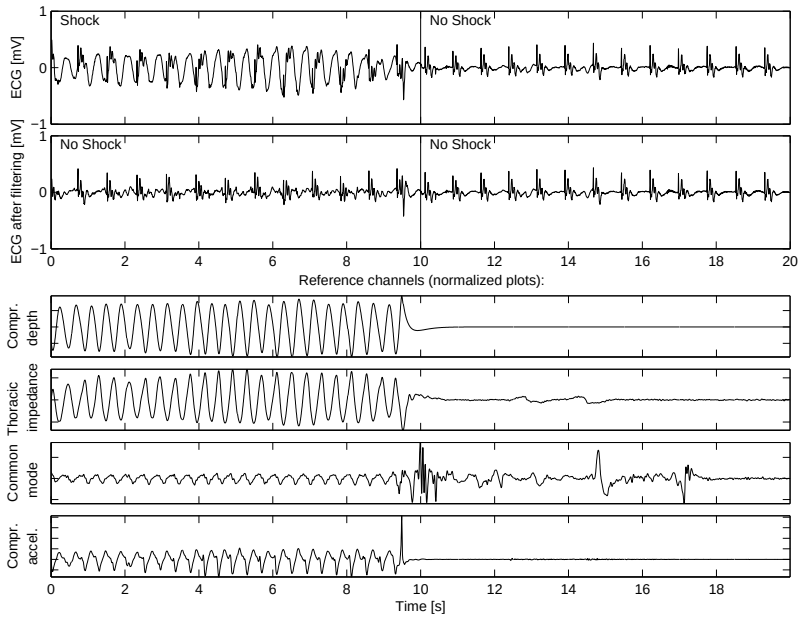

(c) Successful PR episode

Figure 7.3 (continued)

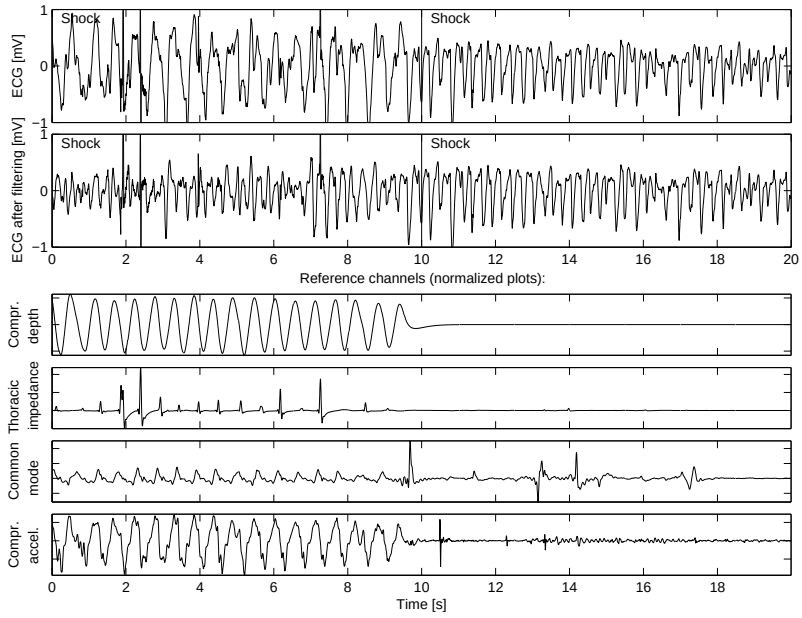

(a) "Indifferent" VF episode

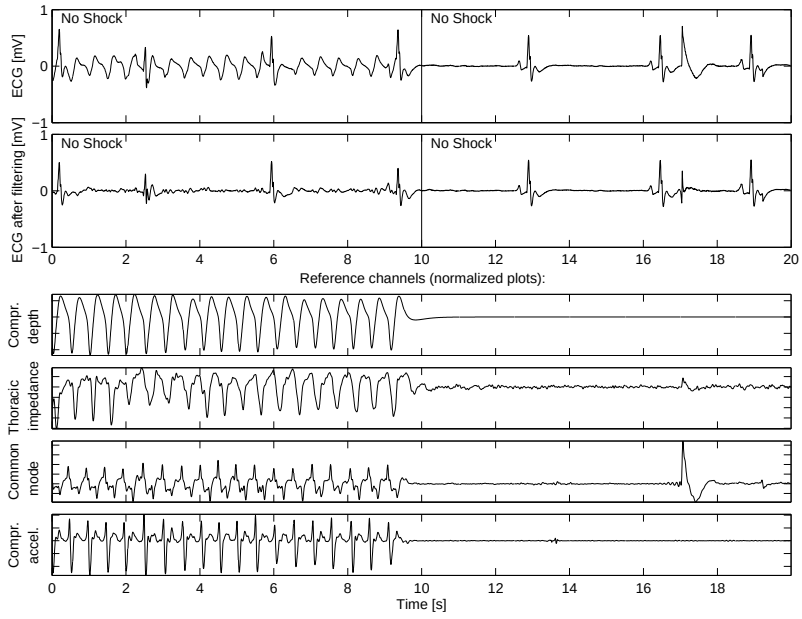

(b) "Indifferent" PEA episode

Figure 7.4: Three examples of "indifferent" filtering – segments with correct classification both during CPR and after MC-RAMP filtering. However, filtering *visually* improves the ECG.

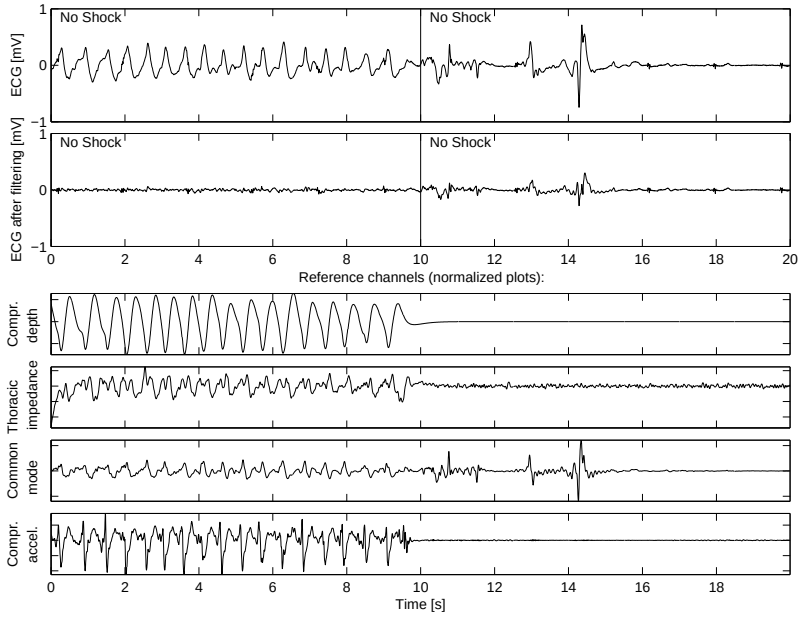

(c) "Indifferent" asystole episode

Figure 7.4: (continued)

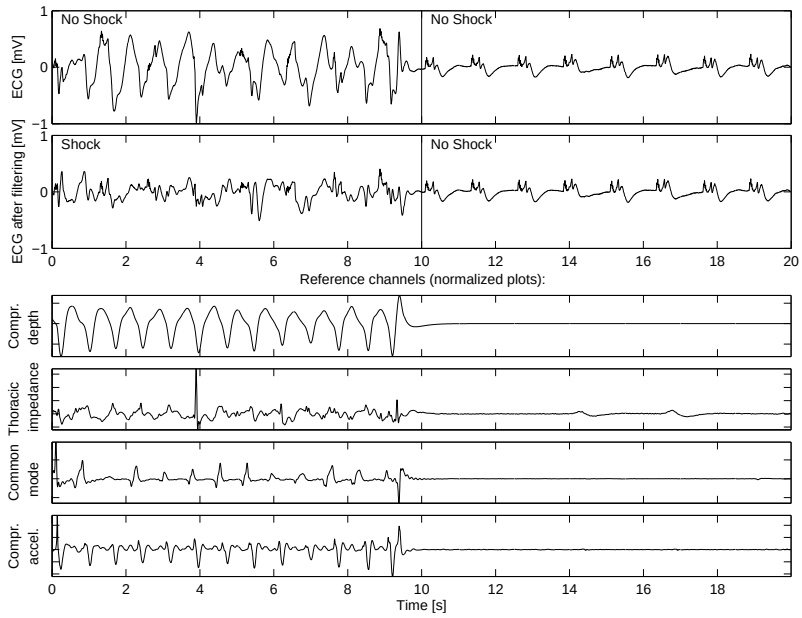

(a) Unsuccessful PEA episode

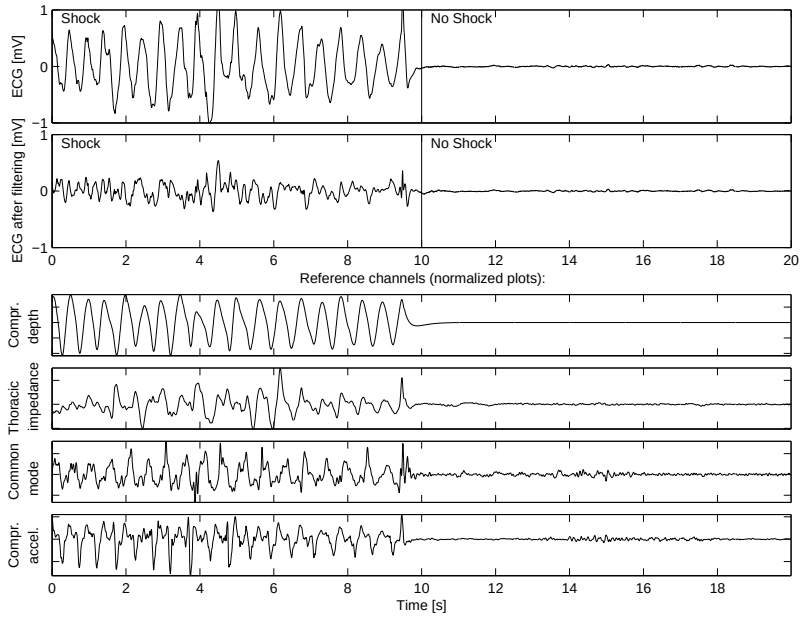

(b) Unsuccessful asystole episode

Figure 7.5: Three examples of unsuccessful filtering – wrong classification after MC-RAMP filtering.

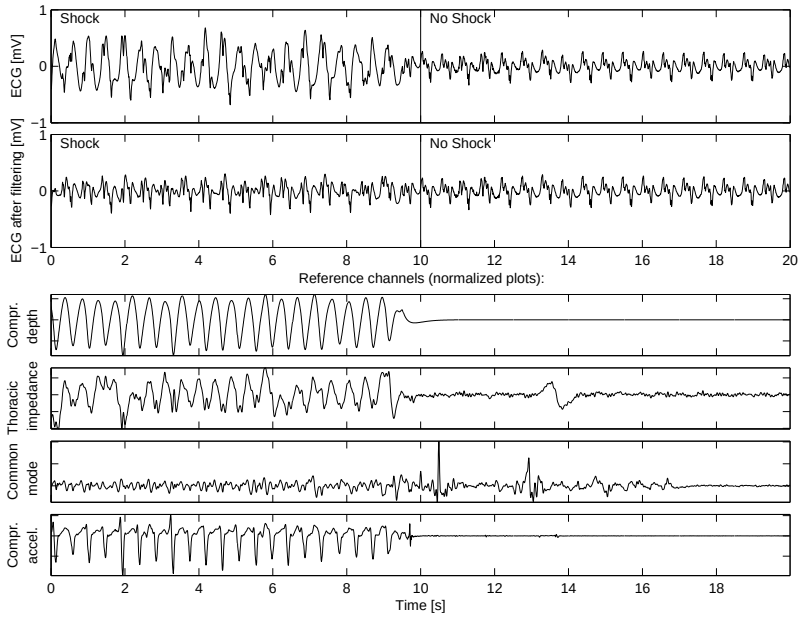

(c) Unsuccessful PEA episode

Figure 7.5: (continued)

Chapter 8

Improving performance: adding verification and noise detection

In Chapter 7 we tested CPR artifact filtering in human ECG and viewed the performance of a shock advice algorithm before and after artifact filtering. Although improvement in performance after filtering, the specificity found, about 80%, is probably too low for clinical use[1] [65]. The sensitivity exceeding 95% is good and satisfactory for clinical use [65].

The reason for having rhythm analysis done during CPR is to reduce the adverse NFT with no blood flow to the tissues. Ideally, having rhythm analysis during CPR should save all NFT currently used for rhythm analysis. However, this may not be feasible if we require very high sensitivity and specificity of the shock advice algorithm. By introducing methods to increase the performance, some NFT may be introduced as well, although less than current practice.

In this chapter, we want to investigate and test such methods for improving the specificity. Low specificity means that too many analyses indicate shock where we actually have a non-shockable rhythm. A straightforward remedy to consider would be to add a short verification analysis after an analysis during CPR that indicated shock. This verification could be after CPR is stopped,

[1] According to the recommendations in [65], AEDs in artifact free ECG should have >99% specificity of normal sinus rhythm, >95% in asystole. Although PEA is not mentioned, for some other non-shockable arrhythmias, giving at least some degree of circulation, >95% specificity is recommended. We also note the >90% and >75% sensitivity recommendations for coarse VF (peak-to-peak amplitude >200μV), and rapid VT, respectively.

in clean and easy to analyze ECG, just prior to delivering a shock. Another method for improving the specificity is to detect when we can not trust the result of the CPR artifact filtering, and rather postpone our decision until CPR is stopped.

8.1 Methods for improving specificity in rhythm analyses during CPR

This section describes two methods for improving specificity in rhythm analyses during CPR. We note that methods for improving specificity may influence sensitivity as well.

8.1.1 Verification before shock

To improve specificity for rhythm analyses during CPR, we propose to add a short verification analysis after CPR is stopped. If an analysis during CPR indicates shock, this justifies a stop of CPR, and a short verification analysis is then run in clean ECG. If the verification analysis also indicates shock, a shock is delivered. If not, the shock is cancelled and CPR resumed.

The time used for a short verification analysis will vary depending on what algorithm used, but should typically be 3–5 seconds. The shock advice algorithm described in Section 5.1 primarily uses majority voting of results from (maximum) three consecutive 3 seconds segments of ECG for one final shock/no-shock decision. As shown in Figure 7.1, the data in our experiments consist of ECG episodes of 10 s with CPR following 10 s without. For verification analysis in this chapter, we will simply use the result of the first 3 s segment of the shock advice algorithm as run on the clean last half of the ECG episode.

In general, during the time allocated to the verification analysis, a VF analysis could also be run. This could be the P_{ROSC} analysis introduced by Eftestøl et al. [31]. The P_{ROSC} analysis is based on four spectral features (see Section 5.2.6). Using principal component analysis and a histogram technique this multidimensional information was expressed in a single variable, P_{ROSC}, reflecting the probability of defibrillation success. Using such a scheme, with both rhythm verification and VF analysis, the total analysis would not only verify if the rhythm is shockable, but if the following shock is likely to give ROSC.

8.1.2 Detecting too difficult noise and artifacts

Sometimes the CPR corrupts the ECG to such a degree that artifact filtering is very difficult, and indeed, will not remove the artifacts satisfactorily. A typical situation occurs when the CPR artifacts in the ECG are very large and spiky, appearing "non-linearly" or poorly correlated with the reference channels. In such instances, the result of the artifact filtering will often be confusing or cluttered up. It would be favorable to be able to detect such ECG, and instead of making a shock/no-shock analysis based on difficult ECG, rather postpone the analysis until the CPR is stopped and the ECG is clean. Three examples of such ECG episodes are shown in Figure 8.1.

We propose a detector of difficult artifacts in an ECG segment primarily based on the detection of one or more of the following traits:

- large noise spikes in the ECG not correlated with the compressions,
- large amplitude of peaks in the ECG corresponding to peaks in the compression depth channel, and
- low relative sharpness of the compression peaks, i.e. compression artifacts in the ECG being very spiky and narrow compared with the compressions in the compression depth channel.

Together with the correlation coefficient between the ECG and compression depth channel, these items will produce features that are thresholded to indicate when we have ECG with too troublesome noise and artifacts.

Correlation between the ECG and compression depth channel

The maximum cross correlation coefficient between the ECG and compression depth channel is found as well as the delay between the two signals. The maximum positive correlation coefficient is used unless the absolute value of the minimum negative correlation coefficient is "much" larger.

Detecting noise spikes

Detecting noise spikes is based on counting the number of times the ECG voltage exceeds a certain noise amplitude threshold. We have used 2 mV for positive peaks and -2 mV for negative peaks. If we have a minimum of two positive or two negative peaks in a segment of ECG, noise spikes are flagged as present.

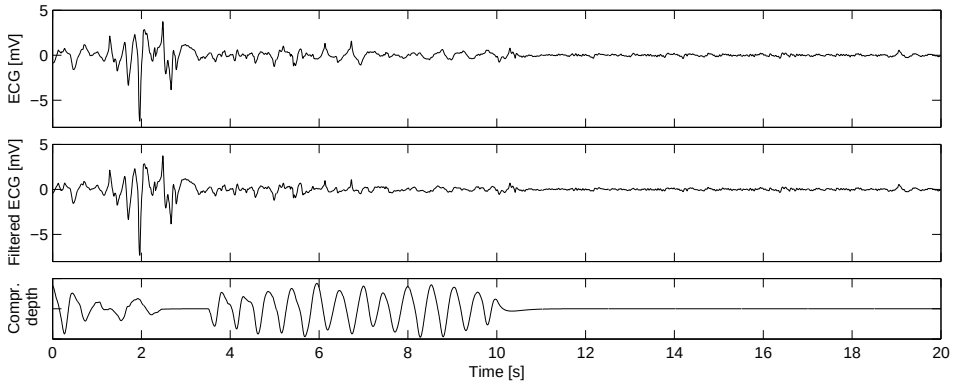

(a) Generally noisy VF episode, with large and spiky CPR and motion artifacts.

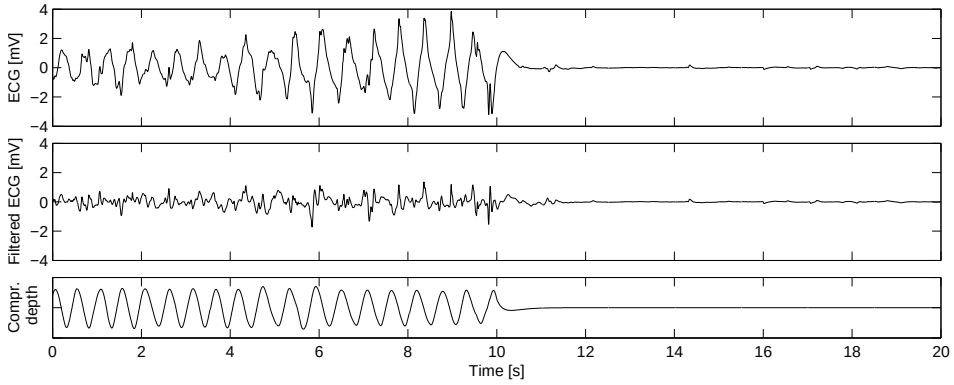

(b) Asystole episode with very large, and somewhat spiky and varying CPR artifacts.

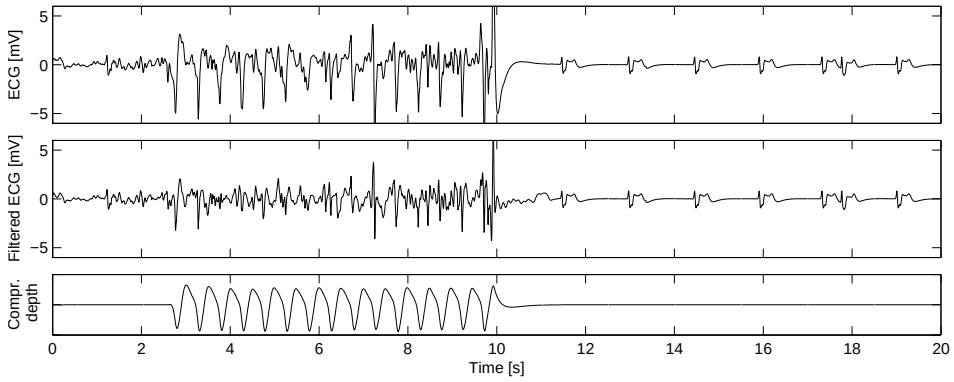

(c) PEA episode with very large and spiky CPR artifacts.

Figure 8.1: Examples of ECG with very high amplitude and/or "non-linearly" artifacts resulting in poor artifact filtering results. It would be better to postpone the shock advice in such cases. Note the values on the amplitude axes.

In some cases, amplitudes exceeding ±2 mV can be valid QRS complexes and not noise. To exclude such instances being classified as noise, we calculate the rate of the ECG using the BPM feature described in Section 5.3.2. The rate of the peaks found are then compared with the ECG rate, and if within 5% of each other, the peaks exceeding ±2 mV are not classified as noise.

Detecting large compression artifacts

First, the local maximum and minimum points in the depth channel are found. Points corresponding to peaks with too low amplitude are removed so that the remaining points correspond to real compressions. Then, we search for positive and negative peaks in the ECG around local neighborhoods where we expect to find peaks corresponding to compressions as found in the depth channel. The maximum/minimum amplitude of the peaks are found and the upper quartile value (75 percentile) of the positive and negative peaks, calculated separately, are recorded as two features. Very high values of these features indicates large compression artifacts that may be difficult to remove completely.

Relative sharpness

With relative sharpness we want to measure and compare the sharpness of the compression artifacts in the ECG to the sharpness of the peaks in the compression depth channel. Low relative sharpness indicates that the artifact peak in the ECG are spiky and more narrow than the corresponding peak in the depth channel.
To calculate relative sharpness, we find how many samples of every peak in the ECG and depth channel that exceeds 75% of the peak's maximum (or minimum) value. For every corresponding pair of peaks, the ratio of the number of samples of the ECG and depth channel are calculated. The median value (50 percentile) of the relative sharpness for the positive and negative peaks are calculated separately and recorded as two features.

Using the features together

Finding more than two peaks exceeding ±2 mV will always flag the ECG segment as noisy. Else, for flagging a segment as potentially troublesome for the artifact filtering, we use a combination of the maximum cross correlation coefficient, peak amplitudes, and relative sharpness. Also, the ECG waveform rate must be below 180 bpm since we seldom experience troublesome and dominating artifacts over this rate. The features are thresholded progressively, i.e. at lower correlation values, we need higher peak amplitudes and lower relative sharpness number to flag it as noisy.

Table 8.1: Sensitivity (sens.) and specificity (spec.) for the training and test set using various methods (verif = added verification analysis (Section 8.1.1), pp = detecting difficult artifacts and postponing the decision (Section 8.1.2))

		Performance in (%)			
		CPR		no CPR	
		Sens.	Spec.	Sens.	Spec.
Training set	Unfiltered	90.2	76.4	100	100
	w/MC-RAMP	98.9	82.2	100	99.4
	w/pp	98.9	83.9	100	99.4
	w/verif	97.8	97.1	100	99.4
	w/pp+verif	97.8	97.7	100	99.4
Test set	Unfiltered	81.5	67.2	97.8	98.9
	w/MC-RAMP	96.7	79.9	97.8	98.3
	w/pp	96.7	82.2	97.8	98.3
	w/verif	92.4	95.4	97.8	98.3
	w/pp+verif	92.4	96.0	97.8	98.3

8.2 Experiments

To test if the methods proposed will improve the specificity, we redo the experiment from Section 7.1.3 using the MC-RAMP filter parameters found in Section 7.2.1, augmenting it with the proposed methods. The data sets are the same as described in Section 7.1.1.

8.2.1 Results

Table 8.1 shows the effects of the added methods on both the training and test set from Chapter 7. For both sets, the specificity is increased significantly to clinically acceptable levels. The short verification analysis seems to contribute the most to the increased performance. Unfortunately, the sensitivity is slightly reduced for both sets when introducing a short verification analysis.

Too difficult conditions for CPR artifact filtering was detected in 6% of the segments (15 and 16 segments in the training and test sets, respectively), thus postponing the analysis until CPR stopped (i.e. the last 10 s without CPR of each ECG segment).

8.3 Discussion

The two proposed methods increases the specificity. However, the results show that the method postponing analysis on very noisy ECG segments yield perhaps surprisingly low performance increase. Only about 2% increase in specificity. This may be because most very noisy segments found are during non-shockable rhythms with very distinct noisy artifacts in the ECG. After filtering, the ECG will often still be so noisy that the shock advice algorithm used will classify it as non-shockable regardless. Nevertheless, for visualization and confidence in the filtering results, the method postponing the analysis under difficult conditions may be useful for an AED user.

The method using a short verification analysis will increase the specificity about 15%. Unfortunately, the sensitivity seems to be reduced (by 1.1% and 4.3% in the training and test sets, respectively). This may be because some of the VF segments in our data sets are borderline cases with small VF amplitudes. The verification analysis checks the first 3 seconds after CPR and sometimes these 3 seconds will contain VF with too low amplitude resulting in a negative verification and no shock advice. The verification analysis used here is rather simple and the drop in sensitivity could be avoided using a better verification analysis. Also, the verification analysis could include a P_{ROSC} analysis [31], in which case the VF segments with low amplitudes most likely would result in too low probability of ROSC and thus no shock is advised anyhow.

Both methods introduced here will cause an increase in NFT, compared to having no methods for increasing specificity. The verification analysis used in this chapter need 3 seconds, whilst if we need to postpone our analysis, the whole analysis time (typically 6–7 seconds) is needed.

Using both methods gave the best results, giving specificity only about 2% lower than the specificity in clean ECG, which should be good enough for clinical use [65]. However, the improved performance by the difficult conditions detector is rather small and further experiments should be conducted to see if the additional computational complexity and cost in NFT are worthwhile.

8.4 Summary

The specificity of a shock advice algorithm after artifact filtering in ECG with CPR artifacts was found too low for clinical use in Chapter 7. This chapter have introduced two methods for increasing the specificity of analyses during

CPR. The methods are introducing a short verification analysis after CPR is stopped, prior to the shock, and adding detection of conditions where we can not trust the results of artifact filter and should rather postpone our analysis until CPR is stopped. Tested on human ECG, the performance was found high enough to be considered for clinical use.

The reason to introduce artifact filtering and shock advice during CPR, is to reduce the NFT. The potentials of our methods in terms of reducing NFT in cardiac arrest resuscitation will be discussed in Chapter 10.

Chapter 9

Robustness of ECG features during CPR

In Chapter 5 we presented several features used to discriminate different rhythms and states of the heart. Studies have shown that CPR over time has a beneficial effect on the arrested heart, and this is reflected in ECG features [3,34]. However, CPR generates artifacts in the ECG which temporarily influence and disturb the features, making ECG analysis during CPR unreliable. This disturbance is instantaneous and temporary and often make the feature values reflect the nature of the CPR artifacts instead of the underlying heart rhythm.

In previous chapters we have investigated CPR artifact reduction using the MC-RAMP filter and primarily evaluated the performance in terms of SNR improvement (Chapter 6) or sensitivity and specificity of a shock advice algorithm (Chapter 7 and 8). In this chapter we will examine in detail the degree of robustness of the individual ECG features. That is, how CPR artifacts affect different features and if CPR artifact filtering can reset this influence. We will study feature trends and illustrate the feature variability for three different rhythm classes: VF, asystole, and PEA. Also, we will examine if the degree of robustness of the features can indicate the feasibility of rhythm classification and VF analysis during CPR.

9.1 Materials and methods

For this study we use all the VF, asystole, and PEA segments from the two data sets used in Chapter 7. That is, we have 178 VF, 104 asystole, and 228

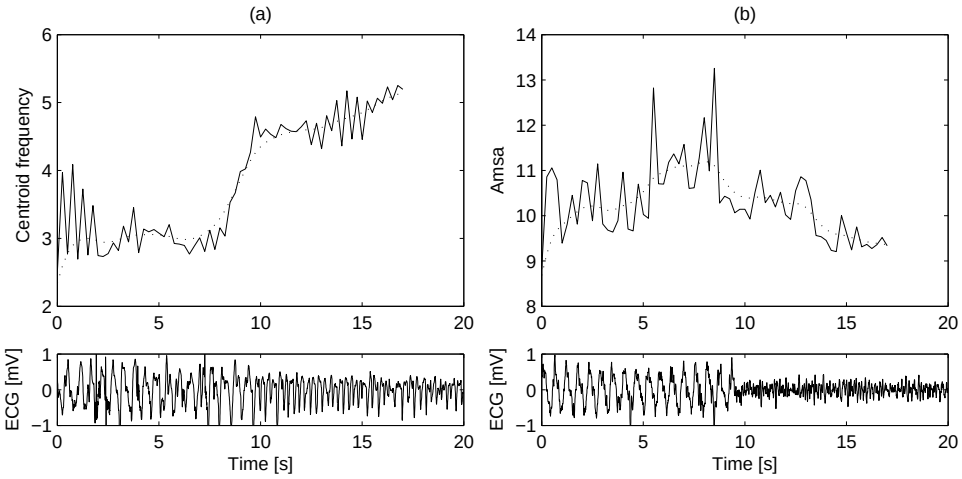

Figure 9.1: Two examples of feature values in VF segments. Solid line is actual calculations. Dotted line is after smoothing using a first order low-pass Butterworth filter.

PEA segments, each of 20 seconds duration, with the first 10 seconds corrupted by CPR artifacts. We will use both unfiltered and MC-RAMP filtered ECG segments. MC-RAMP is applied with the optimal settings found in Chapter 7.

20 features from Sections 5.2 and 5.3 will be used in the experiments: VF-filter leakage, mean signal period (T), BPM, RRTE, slope count, COMPL, MPPA, Lempel-Ziv complexity measure, IRM, AMSA, CF, PPF, ENRG, SFM, count20, FSMN, A1, A2, A3, and PF.

For each ECG segment, we will calculate each feature every 0.25 s in (overlapping) blocks of 3 s length. That means, ECG blocks for calculation start times up to 7 s will contain CPR artifacts, blocks with start times from 7–10 s are transition blocks partly containing artifact corrupted ECG, and blocks with start times from 10 s and above are without CPR artifacts. Figure 9.1 shows two examples of feature values in two VF ECG segments. The feature values will often fluctuate from calculation to calculation as can be seen in these examples. This may be due to high sensibility to measurement noise. As they probably represent little clinical value, these fluctuations are not so important from a clinical point of view, but rather the trend the feature follows. The fluctuations might be reduced using larger block lengths. However, another way of smoothing the feature values to reveal the trend is by applying a low pass filter to the feature values. We will use a first order Butterworth low-pass IIR filter[1] [85].

[1]With cutoff frequency corresponding to 0.2 Hz with the feature sampling rate of 4 Hz.

9.2 Results

In the following we will not study feature values of individual ECG segments, but rather the feature trend and variability (in terms of median and quartile values) of the three rhythm classes (VF, asystole, and PEA), with and without CPR artifacts. Also, in terms of CPR artifact influence on features, the feasibility of rhythm classification and VF analysis during CPR are evaluated.

In order to compare feature values in ECG with and without artifacts, we will assume, as a working hypothesis, that most of the ECG segments will have stable feature values over the time period considered here, i.e. 20 seconds. This should be valid for most of the segments in this study.

9.2.1 Feature trend and variability during CPR

All the calculated values for one feature in one ECG segment constitute the individual trend. The ensemble of all these trends were used to determine the general trend and variability of a feature for the different rhythm classes. To lessen the influence of outliers, the general trends were calculated using the ensemble median of all trends for all features and classes. The variability of a feature was calculated from the ensemble lower and upper quartile values.

The feature trend and variability for the 20 features are shown in Figures 9.2 to 9.5. The figures illustrate the class separating abilities as well as the varying influence of CPR artifacts on the features before and after artifact filtering. Details on the feature values can be found in Table 9.1 (VF), Table 9.2 (asystole), and Table 9.3 (PEA). The tables present values for four situations:

1. Unfiltered right side (URS): Averages of the ensemble median and quartiles of the feature calculations with start from 11 to 17 s, i.e. from ECG with no CPR artifacts. The ECG is not filtered with MC-RAMP. This situation gives the "reference" values for each feature.

2. Filtered right side (FRS): Same portion of the ECG segments as URS, but filtered with MC-RAMP. Deviations from URS should be minimal.

3. Unfiltered left side (ULS): Averages of the ensemble median and quartiles of the feature calculations with start from 1 to 6 s, i.e. from ECG with CPR artifacts. The ECG is not filtered with MC-RAMP. Deviations from URS are expected.

4. Filtered right side (FLS): Same portion of the ECG segments as ULS, but filtered with MC-RAMP. Deviations from URS should lessen (improve) after filtering.

The tables also show the relative deviations of the averaged median values for FRS, ULS, and ULS compared to the URS value.

For most features in unfiltered ECG, the CPR artifacts alter the feature values, both in terms of median and quartile values. After filtering, both median value and variability are generally improved (more alike values for ECG with no artifacts) during CPR for VF segments . For asystole and PEA, the results are more varying.

9.2.2 Feasibility of rhythm analysis during CPR

In Chapter 7 we have seen that the performance of a shock advice algorithm for rhythm analysis was degraded by CPR artifacts, but improved again after filtering using MC-RAMP. In this section we illustrate these findings from a feature space perspective by studying some examples of features in a 2D feature space.

The rhythm analysis use features for discrimination between different rhythm classes, normally shockable rhythms versus non-shockable rhythms. The results from Section 9.2.1 show that features are influenced by CPR artifacts, and that artifact filtering will not always cancel this influence. However, the situation may still be improved and class separation abilities be preserved. Figure 9.6 shows two examples of 2D feature spaces populated by 100 segments each of VF, asystole, and PEA in settings of no artifacts, with artifacts, and after artifact filtering. The four features used, BPM, slope count, RRTE, and count20, are examples of features showing promising class separating abilities in Section 9.2.1.

It can be seen that the original clustering of the shockable and non-shockable rhythms in the feature space is reduced with CPR artifacts present, but improved again after CPR artifact filtering. However, there is still some perturbation of the features present illustrating the problems of reduced shock advice performance encountered in previous chapters.

9.2.3 Feasibility of VF analysis during CPR

VF analysis is used to predict the outcome of a potential shock given shortly after the analysis, hoping to avoid futile defibrillation attempts. To reduce the NFT, it is desirable to do the VF analysis during CPR.

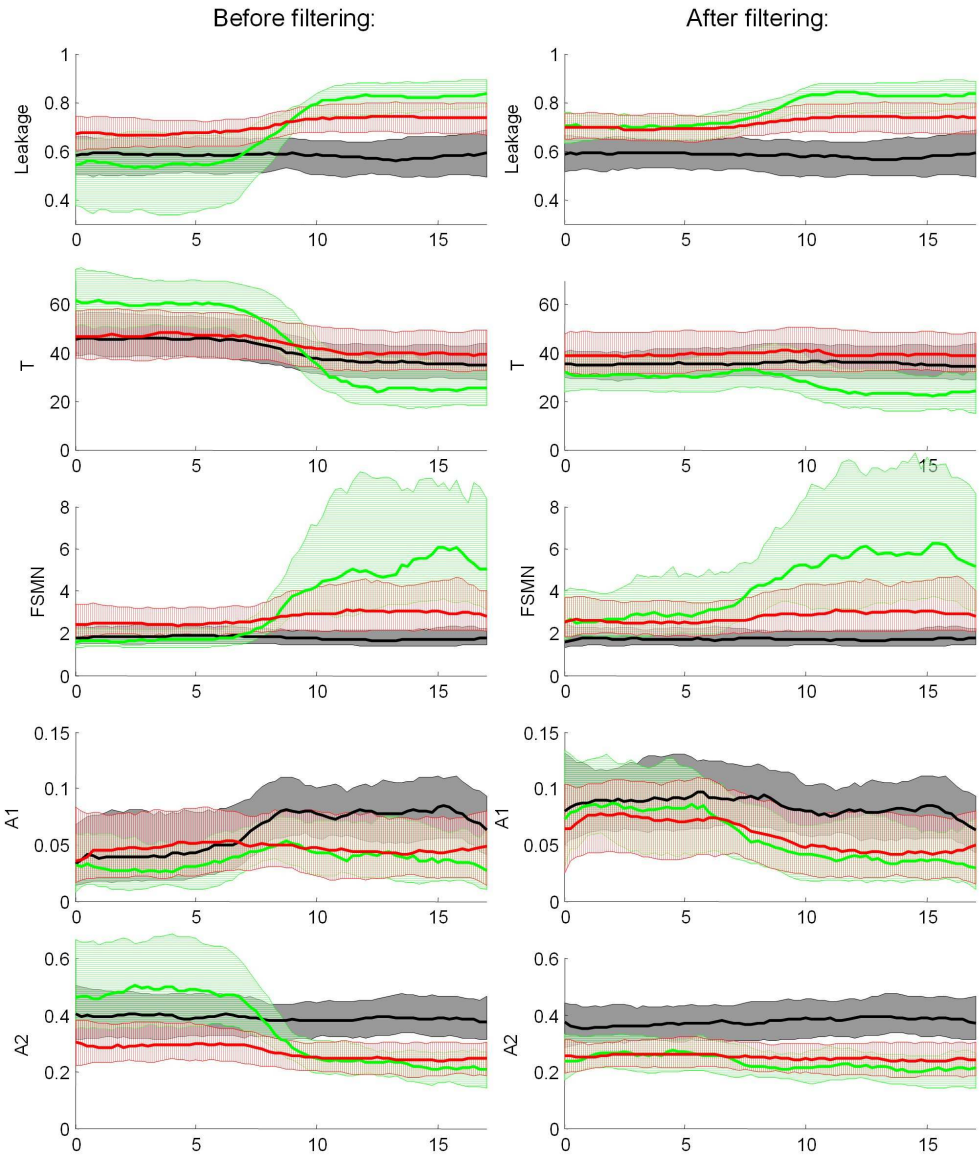

Figure 9.2: For the features Leakage, T, FSMN, A1, and A2: Ensemble median and quartile feature values for different rhythm classes in ECG segments with first half having CPR artifacts. There are two plots for each feature, one before artifact filtering (left) and after (right). Horizontal axis on each plot indicate start of feature calculation in seconds. The solid lines are ensemble median values of different rhythm classes: black line denotes VF, green line denotes asystole, and red line denotes PEA. The area between the lower and upper quartile is also plotted, gray shaded area for VF, green shaded area for asystole, and red shaded area for PEA.

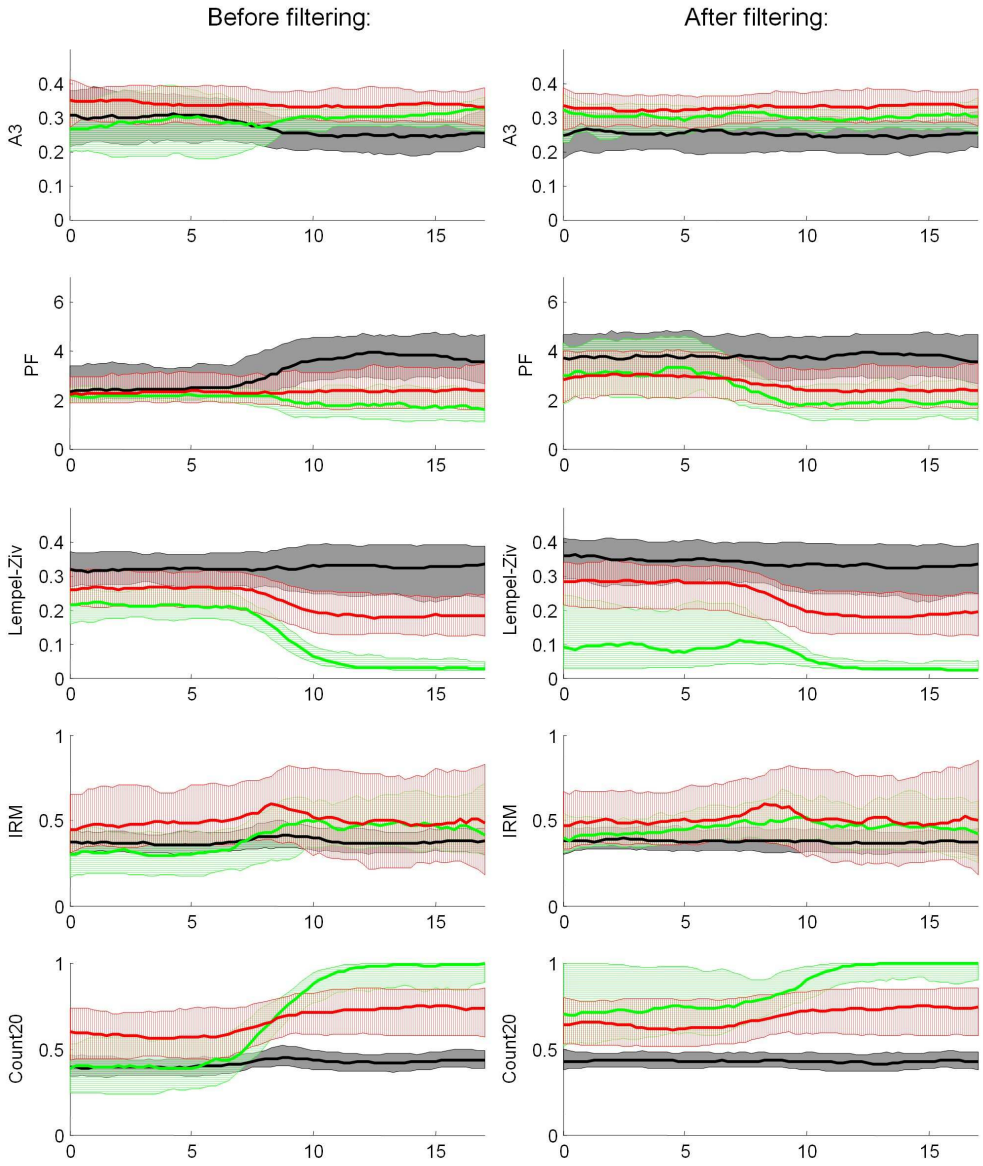

Figure 9.3: For the features A3, PF, Lempel-Ziv complexity measure, IRM, and count20: Ensemble median and quartile feature values for different rhythm classes in ECG segments with first half having CPR artifacts. Layout, symbols and shadings as in Figure 9.2.

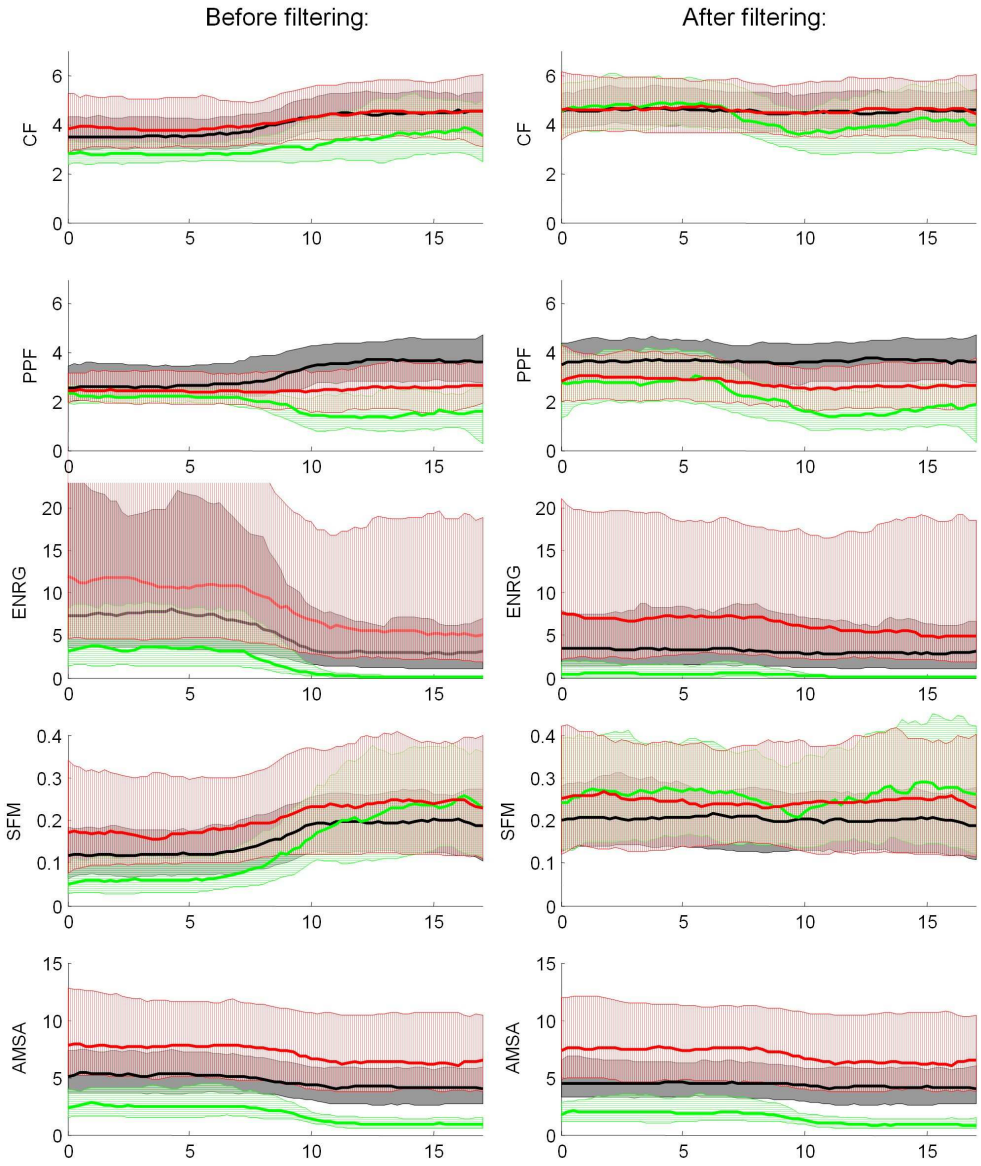

Figure 9.4: For the features CF, PPF, ENRG, SFM, and AMSA: Ensemble median and quartile feature values for different rhythm classes in ECG segments with first half having CPR artifacts. Layout, symbols and shadings as in Figure 9.2.

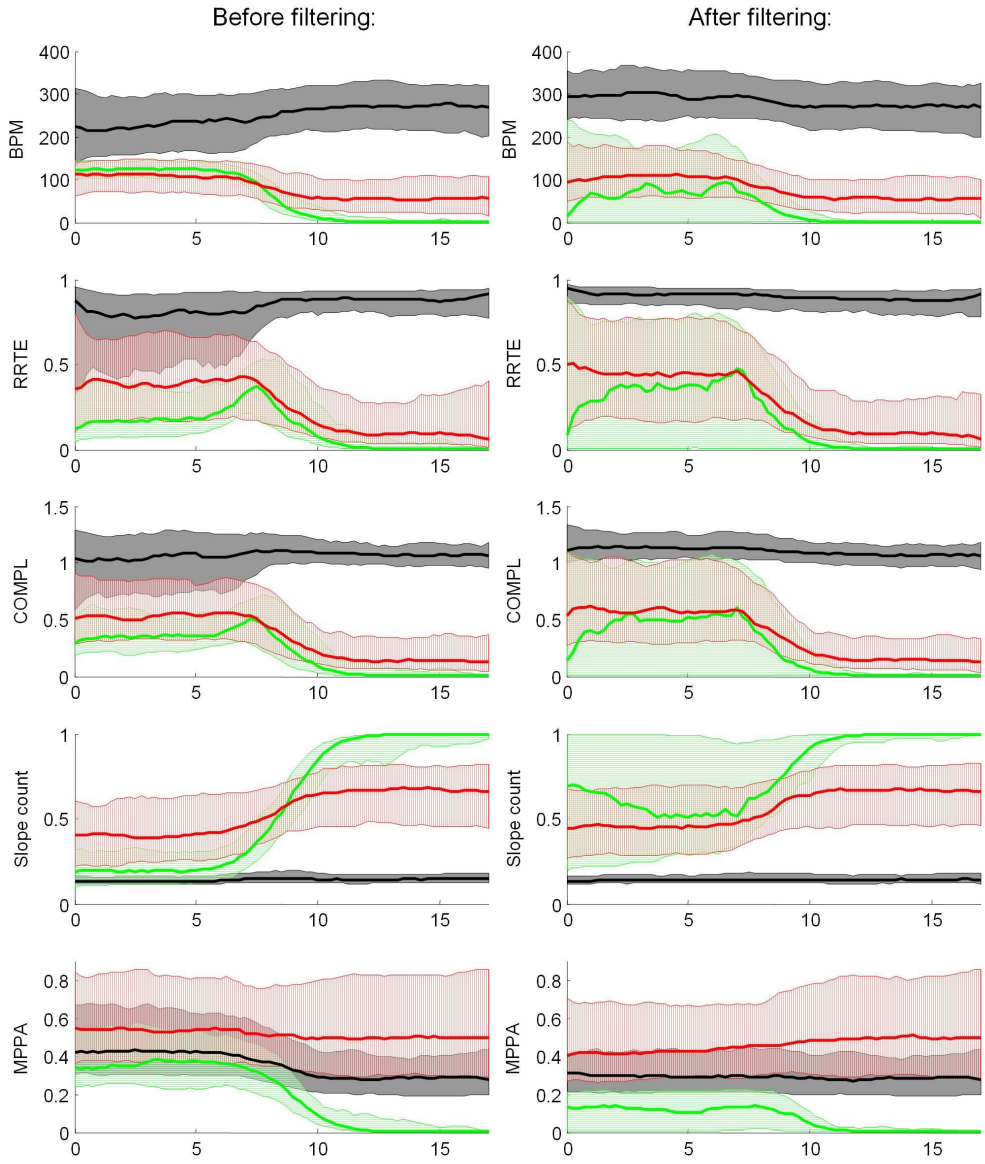

Figure 9.5: For the features BPM, RRTE, COMPL, slope count and MPPA: Ensemble median and quartile feature values for different rhythm classes in ECG segments with first half having CPR artifacts. Layout, symbols and shadings as in Figure 9.2.

Table 9.1: Feature values in VF. URS = Unfiltered right side (calc. start 11–17 s, no artifacts). FRS = Filtered right side. ULS = Unfiltered left side (calc. start 1–6 s, CPR artifacts). FLS = Filtered left side. Each cell includes the averaged (over the given range) ensemble median feature value, and average lower and upper quartiles in parenthesis. The percentage value in square brackets is relative deviation from URS median value.

Feature name	URS	FRS	ULS	FLS
Leakage	0.57 (0.50, 0.65)	0.57 [+0%] (0.50, 0.65)	0.59 [+2%] (0.50, 0.65)	0.59 [+3%] (0.52, 0.65)
T	35.9 (29.6, 43.3)	35.5 [-1%] (29.3, 43.1)	45.9 [+28%] (38.6, 55.8)	35.4 [-1%] (29.5, 41.1)
FSMN	1.69 (1.40, 2.20)	1.69 [-0%] (1.40, 2.18)	1.83 [+8%] (1.49, 2.35)	1.71 [+1%] (1.40, 2.25)
A1	0.08 (0.05, 0.10)	0.08 [+1%] (0.05, 0.10)	0.04 [-47%] (0.02, 0.08)	0.09 [+15%] (0.06, 0.12)
A2	0.39 (0.32, 0.46)	0.39 [+0%] (0.32, 0.46)	0.39 [+2%] (0.32, 0.48)	0.36 [-6%] (0.30, 0.43)
A3	0.25 (0.20, 0.30)	0.25 [-0%] (0.20, 0.30)	0.30 [+23%] (0.23, 0.37)	0.26 [+3%] (0.20, 0.31)
PF	3.75 (2.85, 4.62)	3.78 [+1%] (2.87, 4.64)	2.41 [-36%] (2.01, 3.39)	3.73 [-1%] (2.95, 4.70)
Lempel-Ziv	0.33 (0.24, 0.39)	0.33 [+0%] (0.24, 0.39)	0.32 [-3%] (0.27, 0.37)	0.35 [+7%] (0.28, 0.40)
IRM	0.37 (0.31, 0.44)	0.37 [-0%] (0.31, 0.44)	0.36 [-2%] (0.31, 0.43)	0.38 [+3%] (0.32, 0.46)
Count20	0.42 (0.38, 0.48)	0.42 [-0%] (0.38, 0.48)	0.39 [-7%] (0.34, 0.45)	0.43 [+1%] (0.39, 0.48)
CF	4.46 (3.73, 5.29)	4.51 [+1%] (3.75, 5.33)	3.50 [-21%] (3.00, 4.28)	4.59 [+3%] (3.94, 5.46)
PPF	3.66 (2.82, 4.52)	3.69 [+1%] (2.84, 4.54)	2.61 [-29%] (2.15, 3.52)	3.65 [-0%] (2.91, 4.54)
ENRG	2.96 (1.13, 6.69)	2.90 [-2%] (1.07, 6.50)	7.51 [+154%] (3.47, 20.94)	3.35 [+13%] (1.46, 7.95)
SFM	0.20 (0.12, 0.27)	0.20 [+2%] (0.12, 0.27)	0.12 [-39%] (0.07, 0.18)	0.21 [+5%] (0.14, 0.29)
AMSA	4.13 (2.64, 5.82)	4.13 [+0%] (2.63, 5.81)	5.24 [+27%] (3.62, 7.27)	4.50 [+9%] (3.26, 6.48)
BPM	272 (213, 324)	271 [-0%] (213, 324)	227 [-16%] (159, 298)	296 [+9%] (242, 356)
RRTE	0.89 (0.79, 0.94)	0.88 [-0%] (0.80, 0.94)	0.80 [-9%] (0.46, 0.92)	0.92 [+4%] (0.85, 0.95)
COMPL	1.07 (0.98, 1.17)	1.07 [-0%] (0.97, 1.16)	1.05 [-2%] (0.72, 1.26)	1.13 [+6%] (1.03, 1.27)
Slope count	0.14 (0.12, 0.17)	0.14 [-2%] (0.12, 0.17)	0.13 [-7%] (0.12, 0.16)	0.14 [-4%] (0.12, 0.17)
MPPA	0.28 (0.19, 0.41)	0.28 [-0%] (0.19, 0.41)	0.42 [+49%] (0.30, 0.65)	0.30 [+5%] (0.21, 0.43)
Median abs. dev.:		0.4%	16.5%	3.3%

Table 9.2: Feature values in asystole. Same notation as Table 9.1.

Feature name	URS	FRS	ULS	FLS
Leakage	0.82 (0.76, 0.88)	0.83 [+1%] (0.76, 0.88)	0.54 [-34%] (0.35, 0.67)	0.70 [-15%] (0.65, 0.75)
T	25.4 (18.4, 37.3)	23.4 [-8%] (16.7, 32.3)	60.5 [+138%] (51.0, 71.4)	30.6 [+20%] (24.2, 38.5)
FSMN	5.25 (3.28, 9.03)	5.77 [+10%] (3.38, 9.73)	1.66 [-68%] (1.33, 2.19)	2.76 [-47%] (1.87, 4.43)
A1	0.04 (0.02, 0.07)	0.04 [-5%] (0.02, 0.07)	0.03 [-21%] (0.01, 0.06)	0.08 [+121%] (0.05, 0.12)
A2	0.22 (0.17, 0.28)	0.21 [-5%] (0.16, 0.27)	0.48 [+117%] (0.36, 0.66)	0.26 [+16%] (0.20, 0.32)
A3	0.31 (0.27, 0.34)	0.30 [-2%] (0.26, 0.33)	0.28 [-8%] (0.19, 0.37)	0.30 [-2%] (0.25, 0.34)
PF	1.73 (1.17, 2.50)	1.86 [+7%] (1.21, 2.70)	2.14 [+24%] (1.95, 2.46)	3.10 [+79%] (2.12, 4.42)
Lempel-Ziv	0.03 (0.02, 0.06)	0.03 [-12%] (0.02, 0.05)	0.21 [+614%] (0.17, 0.26)	0.09 [+199%] (0.03, 0.22)
IRM	0.47 (0.33, 0.65)	0.46 [-1%] (0.32, 0.62)	0.31 [-34%] (0.18, 0.44)	0.43 [-8%] (0.35, 0.53)
Count20	0.98 (0.85, 1.00)	0.99 [+1%] (0.89, 1.00)	0.40 [-60%] (0.25, 0.56)	0.72 [-26%] (0.56, 0.98)
CF	3.57 (2.64, 4.91)	4.00 [+12%] (2.87, 5.37)	2.78 [-22%] (2.43, 3.25)	4.76 [+33%] (3.80, 5.85)
PPF	1.45 (0.79, 2.39)	1.59 [+10%] (0.85, 2.59)	2.20 [+52%] (1.94, 2.53)	2.82 [+94%] (1.90, 4.07)
ENRG	0.12 (0.05, 0.31)	0.09 [-32%] (0.03, 0.20)	3.46 [+2672%] (1.40, 8.43)	0.44 [+255%] (0.13, 1.67)
SFM	0.23 (0.12, 0.36)	0.27 [+18%] (0.15, 0.41)	0.06 [-74%] (0.03, 0.11)	0.27 [+18%] (0.15, 0.39)
AMSA	0.91 (0.53, 1.48)	0.86 [-5%] (0.52, 1.43)	2.49 [+175%] (1.54, 4.15)	1.93 [+113%] (1.12, 3.28)
BPM	1 (0, 7)	0 [-41%] (0, 2)	124 [+21397%] (104, 144)	65 [+11160%] (0, 193)
RRTE	0.00 (0.00, 0.06)	0.00 [-40%] (0.00, 0.02)	0.17 [+3830%] (0.08, 0.37)	0.33 [+7439%] (0.00, 0.78)
COMPL	0.01 (0.00, 0.07)	0.00 [-30%] (0.00, 0.02)	0.35 [+6445%] (0.22, 0.56)	0.45 [+8397%] (0.00, 1.01)
Slope count	0.99 (0.89, 1.00)	1.00 [+0%] (0.96, 1.00)	0.19 [-80%] (0.12, 0.31)	0.58 [-41%] (0.25, 0.99)
MPPA	0.00 (0.00, 0.06)	0.00 [-53%] (0.00, 0.02)	0.36 [+7349%] (0.24, 0.54)	0.12 [+2431%] (0.00, 0.22)
Median abs. dev.:		12.1%	116.6%	121.0%

Table 9.3: Feature values in PEA. Same notation as Table 9.1.

Feature name	URS	FRS	ULS	FLS
Leakage	0.74 (0.67, 0.80)	0.74 [+0%] (0.67, 0.80)	0.67 [-9%] (0.61, 0.73)	0.69 [-6%] (0.64, 0.75)
T	39.7 (32.9, 49.3)	39.2 [-1%] (32.6, 48.8)	47.4 [+19%] (37.6, 57.4)	39.1 [-1%] (31.7, 48.8)
FSMN	3.00 (2.13, 4.37)	2.99 [-0%] (2.11, 4.44)	2.43 [-19%] (1.91, 3.24)	2.53 [-16%] (1.91, 3.53)
A1	0.04 (0.02, 0.08)	0.04 [-0%] (0.02, 0.08)	0.05 [+7%] (0.02, 0.08)	0.07 [+65%] (0.04, 0.11)
A2	0.24 (0.19, 0.30)	0.24 [-1%] (0.18, 0.30)	0.29 [+20%] (0.23, 0.37)	0.26 [+6%] (0.21, 0.31)
A3	0.33 (0.29, 0.38)	0.33 [-0%] (0.29, 0.38)	0.34 [+2%] (0.28, 0.39)	0.32 [-3%] (0.27, 0.37)
PF	2.35 (1.63, 3.31)	2.36 [+0%] (1.65, 3.35)	2.28 [-3%] (1.88, 3.03)	2.95 [+25%] (2.10, 3.96)
Lempel-Ziv	0.18 (0.13, 0.24)	0.18 [+1%] (0.13, 0.25)	0.26 [+45%] (0.21, 0.31)	0.28 [+56%] (0.20, 0.33)
IRM	0.49 (0.24, 0.78)	0.50 [+1%] (0.25, 0.78)	0.48 [-2%] (0.35, 0.69)	0.49 [+1%] (0.36, 0.67)
Count20	0.74 (0.58, 0.85)	0.74 [+0%] (0.58, 0.85)	0.57 [-22%] (0.44, 0.72)	0.63 [-14%] (0.52, 0.79)
CF	4.49 (3.43, 5.79)	4.58 [+2%] (3.45, 5.85)	3.81 [-15%] (3.05, 5.11)	4.63 [+3%] (3.66, 5.91)
PPF	2.57 (1.65, 3.52)	2.61 [+2%] (1.72, 3.56)	2.43 [-5%] (1.93, 3.22)	2.96 [+15%] (2.05, 4.00)
ENRG	5.38 (2.22, 18.51)	5.25 [-2%] (2.15, 18.09)	11.17 [+108%] (4.61, 29.05)	7.08 [+32%] (2.50, 19.28)
SFM	0.24 (0.12, 0.39)	0.25 [+2%] (0.12, 0.39)	0.17 [-30%] (0.10, 0.31)	0.25 [+4%] (0.13, 0.39)
AMSA	6.28 (3.83, 10.53)	6.28 [-0%] (3.82, 10.53)	7.73 [+23%] (5.05, 11.99)	7.49 [+19%] (4.77, 11.62)
BPM	55 (22, 104)	55 [-0%] (21, 104)	110 [+100%] (69, 145)	106 [+93%] (58, 174)
RRTE	0.09 (0.03, 0.31)	0.09 [+2%] (0.03, 0.30)	0.39 [+333%] (0.17, 0.68)	0.45 [+405%] (0.17, 0.78)
COMPL	0.14 (0.06, 0.35)	0.14 [+4%] (0.06, 0.35)	0.53 [+291%] (0.32, 0.85)	0.58 [+325%] (0.30, 1.03)
Slope count	0.67 (0.46, 0.81)	0.67 [-0%] (0.46, 0.81)	0.40 [-40%] (0.24, 0.62)	0.45 [-33%] (0.29, 0.69)
MPPA	0.50 (0.30, 0.83)	0.49 [-0%] (0.29, 0.82)	0.54 [+8%] (0.37, 0.83)	0.42 [-16%] (0.28, 0.68)
Median abs. dev.:		0.7%	23.0%	22.6%

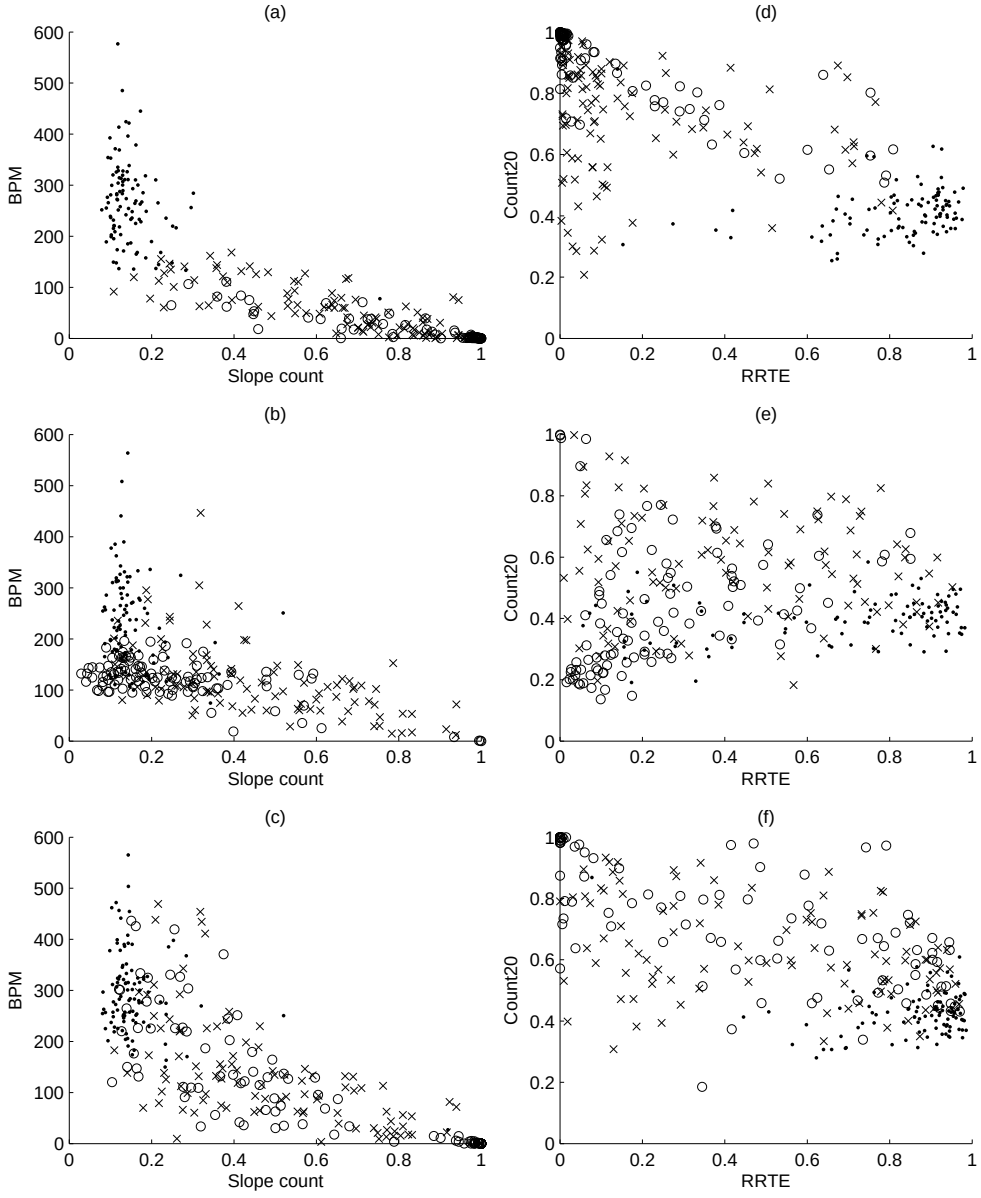

Figure 9.6: Examples of 2D feature space plots for two sets of features calculated from 100 segments each of VF (dots), asystole (circles), and PEA rhythms (x-marks). (a) Features BPM and slope count calculated 12 s into each segment. No artifacts nor filtering. (b) Features BPM and slope count calculated 7 s into each segment. CPR artifacts present, before artifact filtration. (c) Features BPM and slope count calculated 7 s into each segment. After artifact filtration. (d)–(f) same as (a)–(c), but with features count20 and RRTE.

Using 50 VF segments, we investigate the robustness of two features used in VF analysis, CF [29] and AMSA [84]. Figure 9.7 shows the 2D feature space spanned by CF and AMSA populated by the 50 VF segments and individually marked. Figure 9.7(c) shows the situation in ECG with no artifacts and serves as a reference. Figures 9.7(a) and 9.7(b) shows the situation 5.5 s earlier during the CPR, before and after artifact filtering, respectively. Figures 9.7(d) shows the situation in clean ECG 5.5 s after the reference situation.

As can be seen in the feature spaces of Figure 9.7, CPR artifacts perturb the features, but the situation is somewhat remedied by the artifact filtering. Still, most of the individual VFs in Figure 9.7(b) are more or less relocated compared to the reference situation in Figure 9.7(c). However, note that 5.5 s after the reference situation, and also in clean ECG, most VFs are also more or less relocated in the feature space as shown in Figure 9.7(d).

9.2.4 Defibrillation outcome prediction in a mix of animal and human ECG

To further evaluate the feasibility of VF analysis during CPR, this section describes an experiment performed to see the influence of CPR artifacts on a previously published defibrillation outcome predictor by Eftestøl et al. [29]. This experiment uses different material and methods than described in Section 9.1, but which will be described below. A mix of animal and human ECG is used similar to the experiments in Chapter 6.

The prediction is based on a classifier with two main classes, ROSC and No-ROSC, corresponding to a preshock ECG segment where the consecutive shock will cause ROSC or no ROSC, respectively. Four features are extracted from the ECG: CF, PPF, SFM, and ENRG [29] (see Section 5.2.6). An alternate decorrelated feature set is generated by principal component analysis [75]. Using the highest performing classifier from [29] corresponding to two principal components, the effect of adding animal CPR artifacts to human ECG is evaluated. The effect on the defibrillation outcome prediction is evaluated both with and without using MC-RAMP for CPR artifact filtering. The human ECG data set is the same as in [29], but with a few changes:

- The complete data set in [29] is used, except for one ECG segment in the ROSC class being too short for our purpose. See Section 3.1.2 for description of the data set.
- The 4 seconds preshock ECG presented to the classifier for each shock in the data set is taken 1.5 seconds earlier than in [29], i.e. the last 1.5

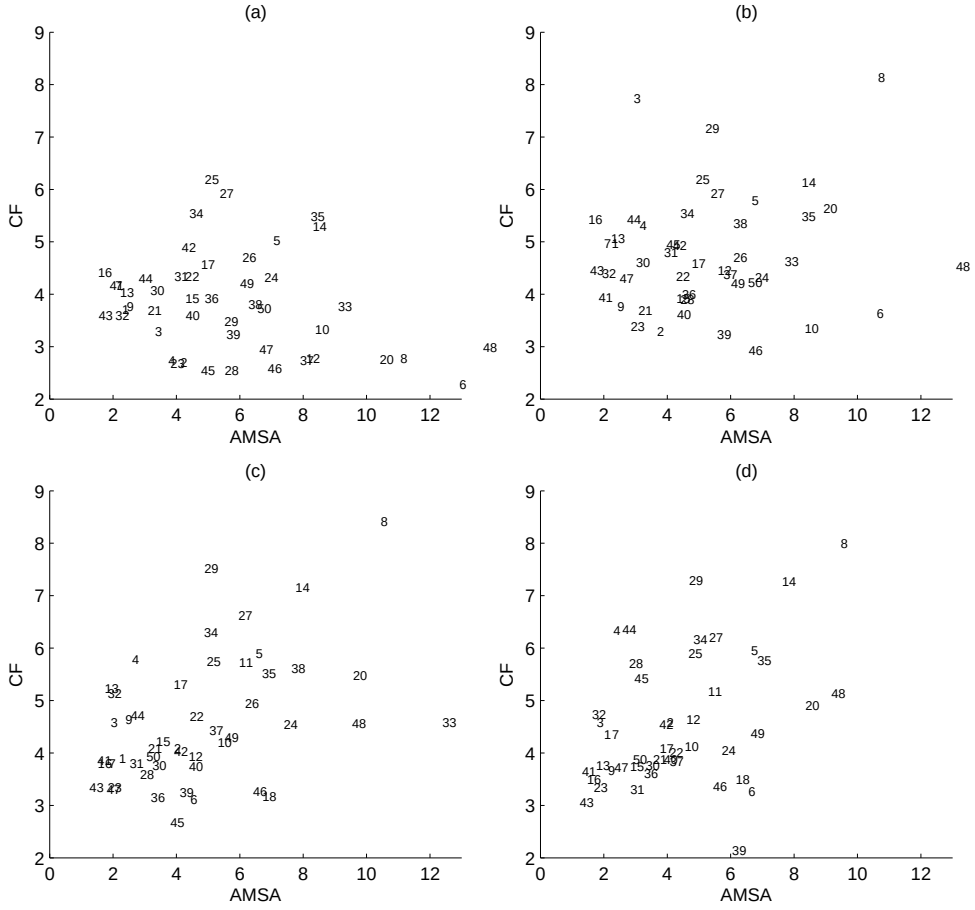

Figure 9.7: 2D feature space for VF analysis using the AMSA and CF features. The numbers represent each of the 50 VF segments of length 20 s used. (a) Features calculated 6 s into each segment. CPR artifacts present. Artifacts not filtered. (b) 6 s into segment, after CPR artifact filtering. (c) 11.5 s into segment. No CPR artifacts. (d) 17 s into segment. No CPR artifacts.

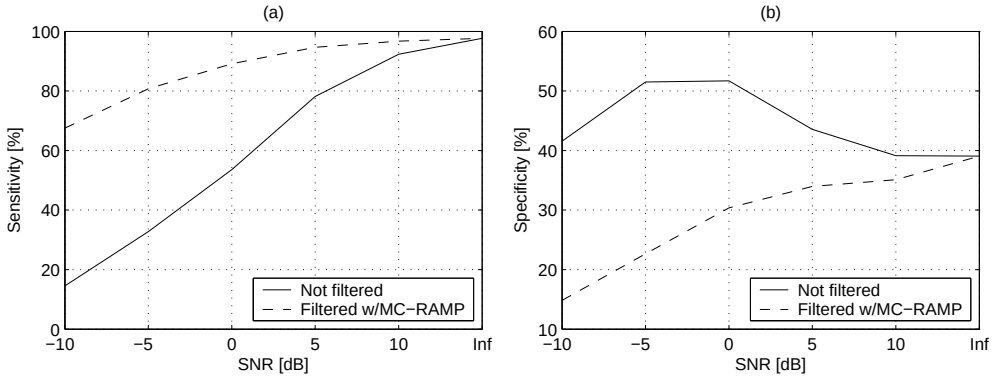

Figure 9.8: Overall sensitivity (the portion of ROSC segments correctly classified, in (a)) and specificity (the portion of No-ROSC segments correctly classified, in (b)) in prediction of defibrillation outcome in noisy ECG, with and without MC-RAMP filtering. SNR=inf corresponds to no artifacts added.

seconds before the shock is not used by the classifier. This is done to avoid MC-RAMP filtering edge effects.

The 867 out-of-hospital ECG segments described in Section 3.1.2 are mixed with the 24 artifact ECGs used in the SNR evaluation of the MC-RAMP filter in Section 6.2.3 giving a total of 20808 ECG segments evaluated in the classifier. For filtering of CPR artifacts, the 3 channel MC-RAMP algorithm with parameters as in Section 6.2.3 is used. Note that the modifications in Section 4.2.3 are not used in this experiment, only MC-RAMP in its basic form. The results are evaluated in terms of sensitivity and specificity, i.e. the portion of ROSC and No-ROSC segments correctly classified, respectively. Figure 9.8 shows the sensitivity and specificity averaged over all artifact mixes. The sensitivity decreases rapidly towards zero for decreasing SNRs. This trend is reduced when the ECG segments are filtered with MC-RAMP. The specificity is actually increased when adding CPR artifacts to the ECG. This is probably due to the general relocation and clustering of the ECG segments in the feature space when adding CPR artifacts (see Figure 9.9(c)) pushing more No-ROSC ECG segments out of the ROSC region. When the ECG segments are filtered however, the specificity is unfortunately reduced.

The decorrelated feature set classifier from [29] has 2 dimensions. This enables us to show the feature space and the classifier decision regions in a 2D plot. Figure 9.9 shows the feature coordinates corresponding to the ROSC and No-ROSC segments (for one artifact mix) populated in the feature space for three different scenarios. As can be seen from Figure 9.9(a) and (b) the added

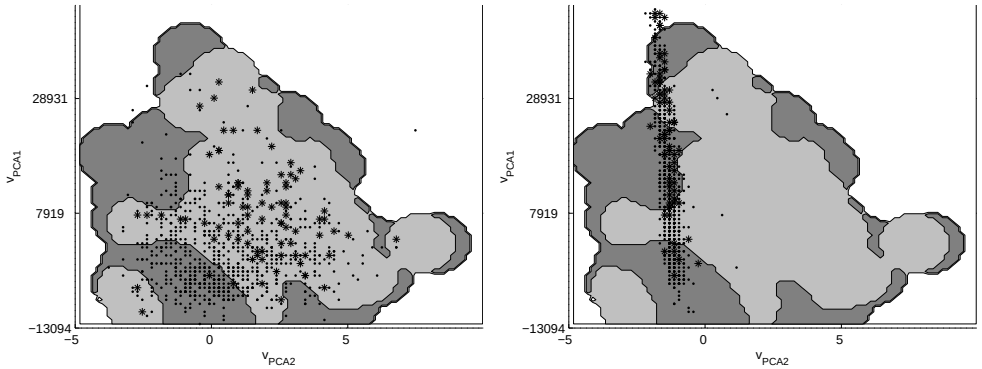

(a) No noise added,
SENS=97.67%, SPEC=39.05%

(b) SNR = -5 dB, unfiltered,
SENS = 24.42%, SPEC = 60.95%

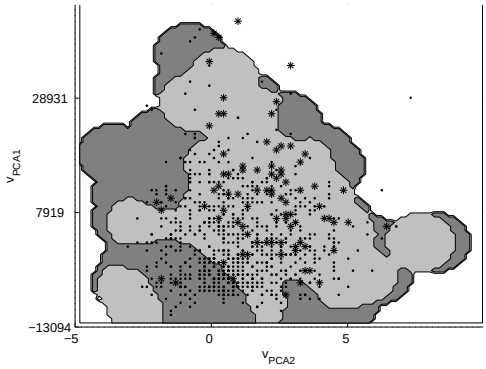

(c) SNR = -5 dB, filtered with MC-RAMP,
SENS = 86.05%, SPEC = 27.27%

Figure 9.9: Feature space plots of the shock outcome predictor from [29] with the classifier decision regions drawn; light shade of gray is ROSC, dark shade of gray is No-ROSC. The feature space plots show ROSC segments (stars) and No-ROSC segments (dots) under various noise and filter conditions.

artifact noise significantly relocates the segments in the feature space. A closer look on the original features reveals that it is the energy and PPF features that changes relatively the most. Also, the PPF is significantly influenced by the CPR artifacts. Since all the segments are mixed with the same artifact, the PPF is actually equal for every segment in our example. This is probably reflected in the second principal component, v_{PCA_2}, being almost constant in Figure 9.9(b). Although filtering of CPR artifacts remedies the situation somewhat, a certain degree of perturbation is still present as can be seen in Figure 9.9(c). This might be due to the filter not removing all of the CPR artifacts or there was some remaining spontaneous electric activity in the heart of the animal, i.e. the animal ECG used in the mix did not consist purely of CPR artifacts. In addition, the sensitivity and noise robustness of the features (or actually the lack thereof) will also account for the reduction in classifier performance.

9.3 Discussion

In order to further investigate the feasibility of rhythm and VF analysis during CPR, we have calculated feature values for ECG segments of VF, asystole, and PEA rhythms, using 20 features described in Chapter 5.

As expected, we have seen that CPR artifacts influences the feature values. Moreover, PEA, and especially asystole seem to be, on average, more influenced than VF. This does not necessarily mean that a larger portion of PEA and asystole segments have large artifacts, only that the prominent ones in these rhythms do more harm to the feature values than for VF. Since CPR artifacts generally look and appear more like VF than the other rhythms considered here, we expected and found the feature values to be less displaced for VFs. An exception is dominant frequency-related features, for instance PPF, since the chest compressions dominating the CPR artifacts have lower frequency than most VFs.

The variability of the feature values, in terms of the upper and lower quartiles, is also increased during CPR for many features. This is an indication of the highly varying presence of CPR artifacts in the ECG. We also note the generally larger variability in asystole and PEA rhythms than for VF. This is to be expected since PEA is a broad rhythm group with many morphological variants, and the low amplitudes of asystole, often mixed with baseline noise, will contribute to larger variability.

Even under artifact free conditions, the class separating abilities of the features highly differ. Features such as BPM, RRTE, slope count, COMPL, and

count20 appear to be good for class separation, whereas IRM, CF, SFM, and A3 are examples of the opposite. However, the features with poor class separating abilities may be suitable for classification within one rhythm class, e.g. VF analysis. Such properties were not measured in this study. The best features for class separation in clean ECG were also the best after filtering in ECG with CPR artifacts.

After filtering in ECG segments with CPR artifacts, the influence of the artifacts on the feature values is lessened. At least, this is the case for VF. Both the trend and variability of the feature values are improved for most features. After filtering, the feature median absolute deviation from the reference clean ECG feature value is 3.3%. Before filtering, the deviation was 16.5%. For PEA and asystole the situation is not that good. The median deviation in PEA segments only went down from 23.0% to 22.6% after filtering. For asystole, the median deviation actually increased, from 116.6% to 121.0%. However, the CPR artifacts in asystole are very large and prominent relative to the underlying heart rhythm. So even if the artifact filter removes large part of the artifacts, a relatively large residual may be present corrupting the features. We have often seen spiky artifacts not linearly correlated with the reference channels for asystole making filtering difficult. Also, for asystole patients, it can not be excluded that CPR may actually induce a small VF-like activity in the heart which disappears immediately with the cessation of compressions.

The problem when filtering CPR artifacts in PEA is to reconstruct the organized PEA components that are disturbed or hidden under the artifact components. This disturbance of the PEA makes it more complex or disorganized, which is reflected in features such as RTTE, COMPL, and the Lempel-Ziv complexity measure. Unfortunately, as the results show, the artifact filtering is not able to cancel this effect properly for these features. We speculate it may reduce the size of the artifacts, but leave small residual adding a disorganized component to the organized PEA. Another problem encountered in PEA is when we have incidental similarities between the reference channels and the PEA rhythm, causing the artifact filter to remove or disturb true PEA components.

Although the artifact filter will not always cancel the influence of CPR artifacts on the individual features, analyses may still be feasible. As earlier artifact filtering results from Chapters 7 and 8 show, as well as indications in the feature space plot in Figure 9.6, rhythm analysis and shock advice during CPR should be possible. However, with the current results, we might expect a slight degradation of performance. This might change with new features, shock advice algorithms or filter improvements. Nevertheless, as will be investigated

in Chapter 10, the potential reduction of NFT using the artifact filter should justify a slight performance degradation.

For VF analysis, the feature space plot in Figure 9.7 gives ambiguous indications. Assuming that no change in the heart's condition occurs over the 11 s time period considered, the feature vectors[2] should ideally be positioned the same in all the feature space plots. Comparing the situation after artifact filtering in corrupted ECG in Figure 9.7(b) to the reference situation of Figure 9.7(c) in clean ECG, this is clearly not the case. This indicates insufficient filtering. However, 5.5 s after the reference situation and also in clean ECG, most feature vectors are also more or less relocated in the feature space as shown in Figure 9.7(d). This is perhaps somewhat unexpected and makes it more difficult to determine if the feature vector relocations are due to insufficient filtering, natural measurement variations for the features used, or that the heart's condition has changed and this is reflected in the features. It has been shown that VF analysis features can change rapidly after cessation of CPR [32], and with 5.5 s between each of the calculations of Figure 9.7(b), (c), and (d), we can perhaps not expect typical VF analysis features to remain constant over the time period considered here. This is a potential source of error for all the feature analyses of this study.

Using a mix of animal and human ECG, we tested the shock outcome predictor presented in [29] for different levels of CPR artifacts. The feature space plots in Figure 9.9 show the displacement of the feature vectors caused by CPR artifacts, and the improved situation after artifact filtering. Despite of artifact filtering, the performance of the shock outcome predictor was decreased for increasing levels of CPR artifacts. However, the animal CPR artifacts may possible have had small amounts of animal heart activity left adding an unknown component to the mix disturbing the shock outcome predictor. We also note the possibility of overtraining in the creation of the shock outcome predictor presented in [29] (very detailed decision regions in Figure 9.9). Nevertheless, we are somewhat skeptical of the feasibility of VF analysis / shock outcome prediction during CPR, and further studies should be carried out on VF analysis during CPR, as well as features for VF analysis in general.

9.4 Summary

In this chapter we have examined the influence of CPR artifacts on 20 different rhythm or VF analysis features. As expected, we have seen that CPR artifacts

[2] A feature vector is a vector combining the individual features to a point in the feature space.

influence the feature values. When prominent, the artifacts alter the features more for asystole and PEA, than for VF rhythms. The MC-RAMP artifact filter generally reduces the influence of the CPR artifacts. The amount varies for different features and ECG rhythms, with VF segments on average being best cleaned. For PEA and asystole the performance often varies more over the segments. However, the results of previous chapters and the current study indicates that rhythm analysis should be feasible during CPR. The robustness of features for VF analysis on the other hand seems more unclear and further studies are needed to determine the feasibility of VF analysis during CPR.

Chapter 10

Reducing no flow times during automated external defibrillation

There has recently been an increased attention to the importance of reducing time without blood flow from chest compressions (NFT) during CPR. Cardiac output up to 25–35% of normal can be achieved with external chest compressions [11] and maintain or even improve the probability of ROSC [34] while even short pauses in CPR reduce the probability of ROSC in a human study [32] and chance for survival and good neurological outcome in animal studies [16, 17, 88, 108].

The chest compressions and ventilations during CPR introduce artifacts in the ECG. For AEDs to perform reliable ECG signal analysis and make a shock/no-shock decision, CPR must be discontinued, introducing NFT. Other factors such as capacitor charging, the delivery of shocks, checking for pulse, pauses for ventilations in unintubated patients etc. also contribute to the total NFT. In a recent study of 176 patients with out-of-hospital cardiac arrest attended to by paramedics and nurse anaesthetists, CPR was not given 48% of the time without spontaneous circulation; 38% when subtracting the time necessary for ECG analysis and defibrillation [104].

This chapter will present a detailed analysis of the NFT time in 105 patients with out-of-hospital cardiac arrest and propose possible solutions to reduce this time by incorporating new technology in the AED such as rhythm analysis during CPR. This is feasible through adaptive filtering as described in the previous chapters.

This chapter is adapted from [38].

10.1 Material and methods

10.1.1 Data collection

The data were collected as part of a prospective study of out-of-hospital cardiac arrest patients, the Sister project described in Section 3.1.3. Data for this study includes patients from Stockholm, Sweden (52 patients) and London, UK (53 patients) recorded between April 2002 and October 2003 using the Laerdal HeartStart 4000SP (HS4000) in semi-automatic mode.

10.1.2 Data summary

In our material of 105 patients, there were 365 AED rhythm analyses indicating shock and 574 indicating no shock as identified from the AED log data. The underlying heart rhythms were annotated into five classes; VF, VT, asystole, pulseless electric activity (PEA) and pulse rhythm (PR). Table 10.1 shows the distribution of the rhythms during the analyses. This gives the AED algorithm used in HS4000 90.51% sensitivity and 96.01% specificity for shock/no-shock classification.

There were a total of 239 shock series, of which 163 (68%) were one shock, 35 (15%) were two shock series, and 41 (17%) were three shock series. Table 10.2 shows the rhythm transition array for the shocks. For initial rhythms VF/VT, the first shock efficiency[1] was 84%, and the overall shock efficiency[2] for shocks on VF/VT was 60%. This is possibly somewhat low for a biphasic defibrillator [44, 74]. A contributing factor to this may have been misplaced defibrillator pads.

10.1.3 Proposed solution for reducing NFT in connection with analyses and shocks

The details of our proposed solution for reducing NFT in connection with analyses and shocks in AEDs are presented and illustrated in Section 10.2, but the key factors are listed below:

- Rhythm analysis during ongoing CPR, followed by a short verification analysis if shock is indicated.

[1] Defined as the portion of *first shocks* given to the patients with initial VF/VT that terminated the VF/VT (giving a non-shockable postshock rhythm).

[2] Defined as the portion of *all* shocks given to the patients that terminated the VF/VT (giving a non-shockable postshock rhythm).

Table 10.1: Underlying rhythm distribution of analyses indicating shock and no-shock.

Num. analyses indicating shock:		
VF	323	(90.73%)
VT	11	(3.09%)
Asystole	6	(1.69%)
PEA	15	(4.21%)
PR	1	(0.28%)
Num. analyses not indicating shock:		
VF	36	(5.83%)
VT	1	(0.17%)
Asystole	275	(46.48%)
PEA	230	(37.91%)
PR	41	(6.35%)

Table 10.2: Rhythm transition array. One cell shows number of shocks from a preshock rhythm (row) to a postshock rhythm (column). Percentage numbers are relative to the total number of one type of preshock rhythm.

		Postshock rhythm				
		VF	VT	Asystole	PEA	PR
Preshock rhythm	VF	124 (38%)	1 (0.3%)	121 (37%)	61 (19%)	16 (5%)
	VT	1 (9%)	6 (55%)	3 (27%)	1 (9%)	0
	Asystole	1 (17%)	0	4 (67%)	1 (17%)	0
	PEA	0	0	0	15 (100%)	0
	PR	0	0	0	0	1 (100%)

- Capacitor charging during analysis, not as a separate event following the rhythm analysis.
- One minute of CPR immediately following all shocks; postponing postshock evaluation of rhythm and possible circulation. This omits the double evaluation (immediately and after one minute) required in the guidelines [9] for postshock non-VF/VT without a pulse. This also enables the rhythm evaluation at the end of the CPR period reducing the NFT as well as the CPR being clinically valuable by itself.
- Distinguishing between asystole and organized rhythm in analyses not indicating shock. Enables the defibrillator to not advice for pulse checking if asystole, avoiding futile pauses checking for pulse.

The key requisite for reducing the NFT in connection with analyses and shocks is to do the rhythm analysis during ongoing CPR (chest compressions). However, the artifact components in the ECG introduced by CPR, impair regular rhythm analyses. As introduced and tested in previous chapters, we propose to use the MC-RAMP filter to remove the CPR artifacts in the ECG and then perform the rhythm analysis.

10.1.4 Analyses

For our analyses we define NFT as the duration of all non-compression intervals where the annotated rhythm is non-perfusing, where a new NFT interval is defined for a larger than one second time gap between compressions.

Seven situations involving rhythm analysis in AEDs were identified and the NFTs accompanied with these were found in the HS4000 data:

1. After end of compressions, shockable rhythm (155 incidences).
2. After a shock (1st or 2nd in a series), shockable rhythm (85 incidences).
3. After a shock (1st or 2nd in a series), non-shockable rhythm (159 incidences).
4. After end of compressions, non-shockable rhythm (282 incidences).
5. After pads on, initial shockable rhythm (32 incidences)
6. After pads on, initial non-shockable rhythm (50 incidences)
7. After change to a shockable rhythm (27 incidences)

The different causes for NFT around these situations were analyzed and NFT numbers compared with the proposed solution. We present seven figures showing the situations graphically with NFTs as found in the HS4000 data as well as what is proposed for a new system. Numbers for HS4000 are median times over all patients found for each interval. Total NFT in the figures is median time from the first to the last event depicted. "Machine caused" NFT numbers (i.e. NFT due to the AED manner of operation such as analysis time and charge time) for the proposed solution are theoretical, whilst the numbers from HS4000 is used for human caused NFT times. We also propose a strategy for what do to when the ECG is so noisy during CPR that the result of the artifact filter can not be trusted.

We wanted to find the NFT for the 105 patients in the study, and how much we could save using the proposed solution. Total NFT for each patient was found, and the situations where we can reduce the NFT were identified and replaced with NFTs according to the proposed solution.

10.2 Results

10.2.1 NFT analyses of some common AED situations

Seven AED situations were identified and NFTs accompanied with these were found in the HS4000 data and compared to the proposed solution.

Figure 10.1 shows situation 1 (after end of compressions, shockable rhythm). The human causes for NFT are waiting for the user to press the "Analyze" button (4.4 s), and waiting for the user to press the "Shock" button (3.4 s). The machine NFT is due to analysis (7.3 s) and charging (2.3 s). The machine also waits 3 s after analysis before charging for an unknown reason. The reduction in NFT in the proposed system is firstly due to having the main rhythm analysis during CPR at the end of a CPR period. Secondly, by starting analysis verification automatically after end of compressions, the human NFT prior to analysis is eliminated. Also, by including charging during verification, another few seconds of NFT are saved. If shock is advised also during verification, the system still has to wait for the user to press the shock button.

Figure 10.2 shows situation 2 (after a shock (1st or 2nd in a series), shockable rhythm). Before automatically starting the analysis, the machine will wait 7.0 s for the ECG to settle after the shock and a rhythm to appear. We propose to start chest compressions immediately after a shock and keep going

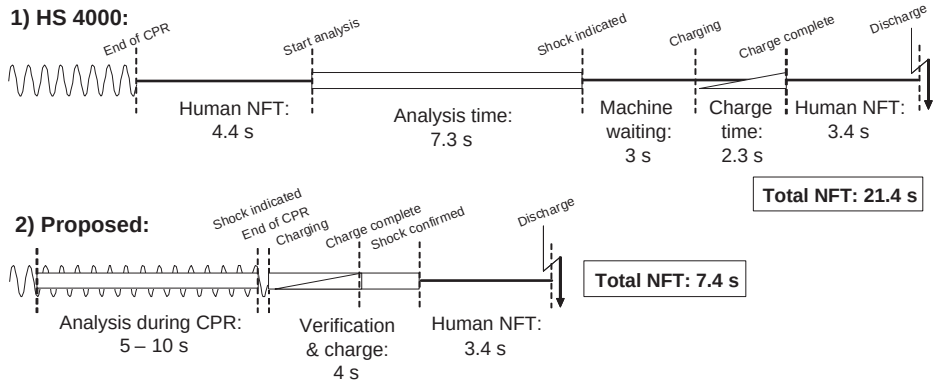

Figure 10.1: NFT analysis, situation 1: After end of compressions, shockable rhythm. Analysis of NFT causes in HS4000 and the proposed solution in one typical AED usage situation. Numbers for HS4000 are median times found for each interval. Numbers for the proposed solution are either theoretical (machine caused NFT) or the same as for HS4000 (human caused NFT). Total NFT for HS4000 is the median time found from the first to last event. Total NFT for the proposed solution is accumulated interval times.

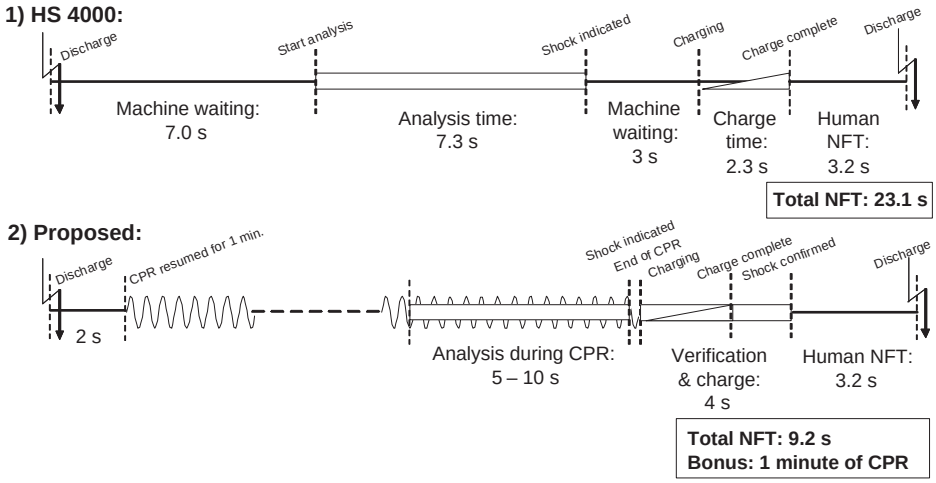

Figure 10.2: NFT analysis, situation 2: After a shock (1st or 2nd in a series), shockable rhythm. Layout and meaning as in Figure 10.1.

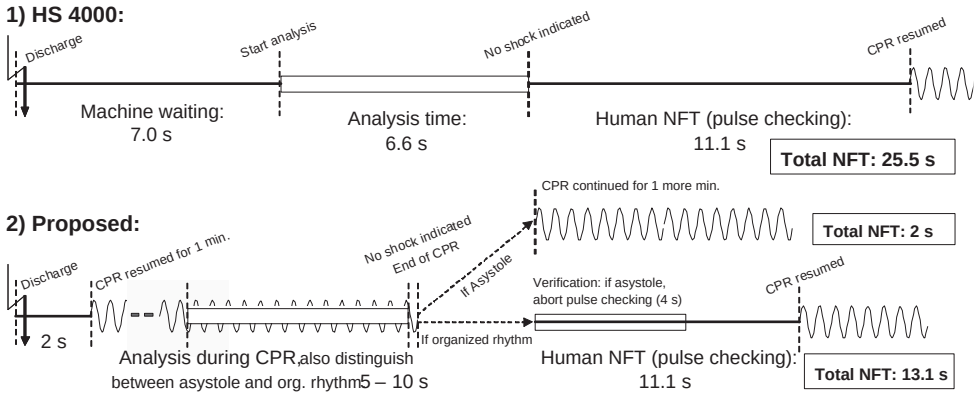

Figure 10.3: NFT analysis, situation 3: After a shock (1st or 2nd in a series), non-shockable rhythm. Layout and meaning as in Figure 10.1.

for one minute before evaluating the rhythm and potentially giving another shock. Such preshock chest compressions will reduce the NFT significantly by enabling the rhythm analysis at the end of the one minute period as in situation 1, and should also be clinically valuable [18, 41]. Note, however, that this is in conflict with the current guidelines [9].

Figure 10.3 shows situation 3 (after a shock (1st or 2nd in a series), non-shockable rhythm), a situation starting out similar to situation 2. However, after the analysis (which is slightly shorter than for shockable rhythms, 6.6 s median) has concluded with no shock indicated there is 11.1 s human NFT for pulse checking. As for situation 2, we propose to immediately start chest compressions for one minute after shock prior to a rhythm analysis. This analysis should also be able to distinguish asystole from an organized rhythm. If an asystole is detected, the machine should tell the user to continue CPR for another minute, not stopping for a futile pulse check. Otherwise, if an organized ECG rhythm is detected, the machine should tell the user to check for pulse. However, an automatically started verification analysis will be run during the pulse checking. If we in spite of the initial analysis have an asystole, the user should be instructed to start CPR again, saving some seconds of NFT otherwise spent on futile pulse checking.

Figure 10.4 shows situation 4 (after end of compressions, non-shockable rhythm). This is situation starting out similar to situation 1, but for the proposed system the analysis will distinguish between asystole and organized rhythm, and call for different actions as in situation 3.

Note that the postshock NFT of situation 1 is covered in situations 2 or 3, unless it is the third shock in a series. The median postshock NFT after

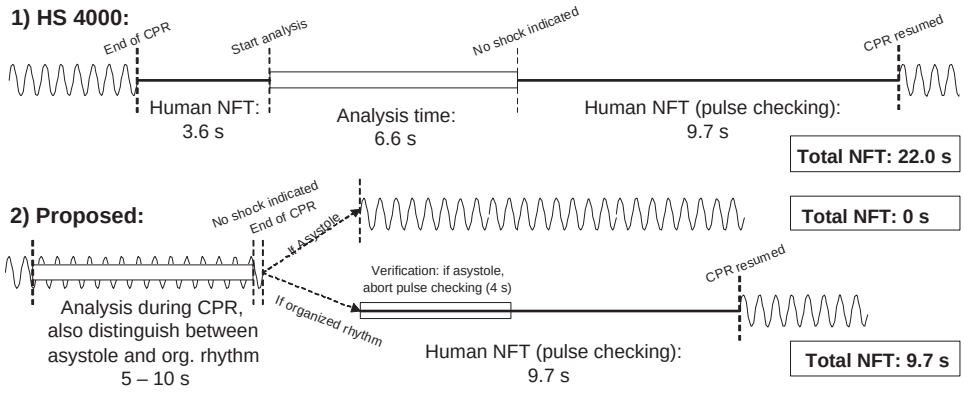

Figure 10.4: NFT analysis, situation 4: After end of compressions, non-shockable rhythm. Layout and meaning as in Figure 10.1.

the third shock in a series was 13.0 s (based on 39 measures of discharge to compressions resumed, non PR rhythm). Note that after the third shock in a series, the HS4000 will not automatically start a rhythm analysis.

There are also some more uncommon situations involving rhythm analyses where we can reduce the NFT. Figure 10.5 shows the situation after pads on with initial shockable rhythm. From pads on, when there are no compressions before the initial analysis, we can only save time by doing the capacitor charging during the analysis. Still, this would reduce the median NFT from 19.3 s in the HS4000 data to 11.4 s.

Figure 10.6 shows the situation after pads on with initial non-shockable rhythm. If no shock is indicated and asystole is found, there is no reason to do pulse checking and we could start CPR earlier and avoid NFT.

Figure 10.7 shows the situation after change from a non-shockable rhythm to a shockable rhythm. Time can be saved by doing the capacitor charging during the analysis and also by having an algorithm that detects rhythm changes and automatically starts a rhythm analysis. The median time today from rhythm change to start of analysis is 11.1 s. It should be possible to reduce this interval to, say, 4 s. These changes would reduce the NFT from 28.2 s to 14.5 s.

The total median NFTs for the situations above are shown in Table 3 and we note that the proposed system have significantly lower NFT for all situations.

Very noisy ECG

Figure 10.8 shows what we can do with very noisy ECG. Sometimes we have very large and spiky CPR artifacts which are difficult to filter properly. In

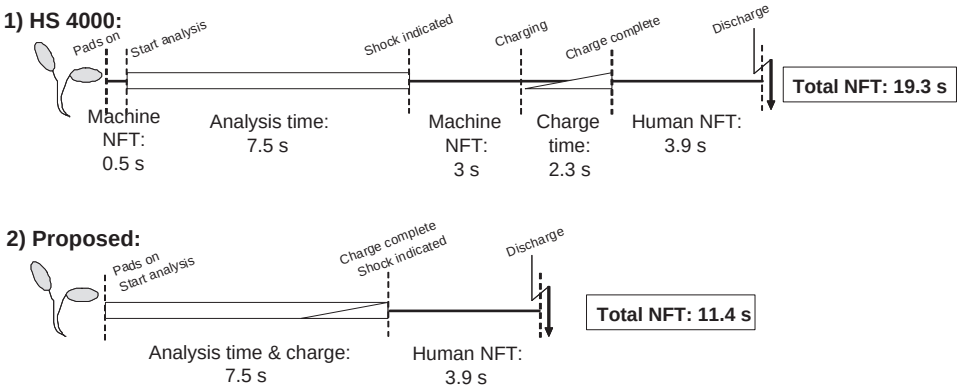

Figure 10.5: NFT analysis, situation 5: After pads on, initial shockable rhythm. Layout and meaning as in Figure 10.1.

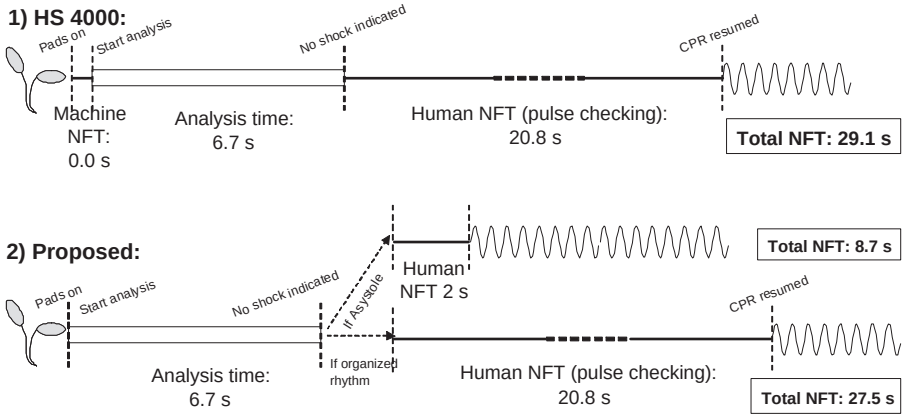

Figure 10.6: NFT analysis, situation 6: After pads on, initial non-shockable rhythm. Layout and meaning as in Figure 10.1.

Table 10.3: Summary of the NFT analyses for HS4000 and the proposed solution. NFT times are median times in seconds with quartile values in parenthesis.

NFT analysis	HS4000	Proposal
1) After end of compressions, shockable rhythm. Time = CPR end to discharge.	21.4 (18.9, 27.2)	7.4
2) After a discharge (1st or 2nd in a series), shockable rhythm. Time = Discharge to next discharge.	23.1 (22.4, 24.3)	9.2 (2 s before 1 min of CPR, 7.2 s after)
3) After a discharge (1st or 2nd in a series), non-shockable rhythm. Time = Discharge to CPR start.	25.5 (18.8, 36.1)	2 / 13.1 s (Asystole / Org.rhythm)
4) After end of compressions, non-shockable rhythm. Time = CPR end to CPR start again.	22.0 (15.6, 30.2)	0 / 9.7 s (Asystole / Org.rhythm)
5) After pads on, shockable rhythm. Time = pads on to discharge.	19.3 (16.3, 21.0)	11.4
6) After pads on, non-shockable rhythm. Time = Pads on to CPR start.	29.1 (17.7, 38.6)	8.7 / 27.5 s (Asystole / Org.rhythm)
7) After change to shockable rhythm. Time = change to discharge.	28.2 (19.9, 51.6)	14.5

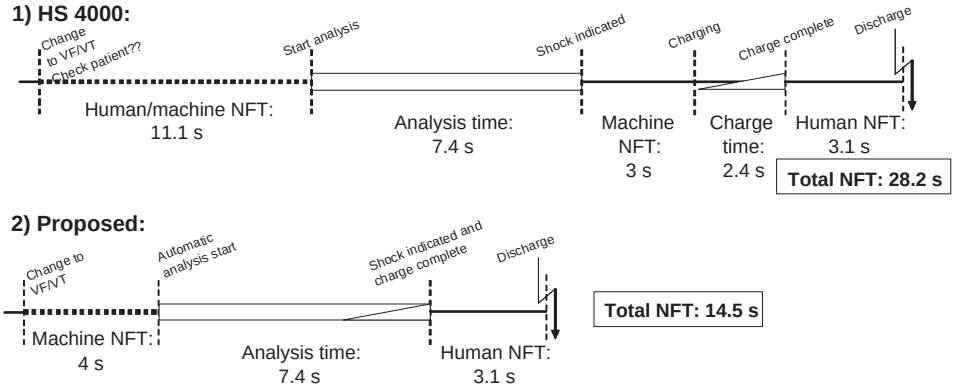

Figure 10.7: NFT analysis, situation 7: After change to a shockable rhythm. Layout and meaning as in Figure 10.1.

Chapter 8 we developed an algorithm to detect this which we could use, and in extreme noise tell the user to pause for analysis as is done today. However, the analysis should be started automatically at the end of the compressions which saves the "pressing the analyze button" human caused NFT. Also, the capacitor should be charged during the analysis. For no shock indicated rhythms, pulse checking should be skipped if asystole is found.

10.2.2 Total NFT per patient

We also wanted to investigate the total NFT for the 105 patients in the study, and how much could be saved by the proposed solution. Patients receiving/not receiving shocks have different NFT reduction potentials and were analyzed separately.

Patients with at least one shock

Of the 58 patients having at least one shock, the mean number of analyze periods per patient was 12.5 and the mean number of shocks was 6.1. The median episode time was 23:30 (minutes:seconds) with a median 11:20 of NFT, i.e. about 48% of the time there was no blood flow to the brain (median NFT ratio). Of the 11:20 NFT, 4:33 (40%) was in connection with analyses and shocks, and 1:18 (11%) was due to ventilations outside compressions, analyses or pulse rhythm. That leaves 49% of the NFT due to other unknown factors.

Figure 10.9 shows the NFT due to analyses and shocks found for each of the 58 patients in the HS4000 data. The figure also shows what could have

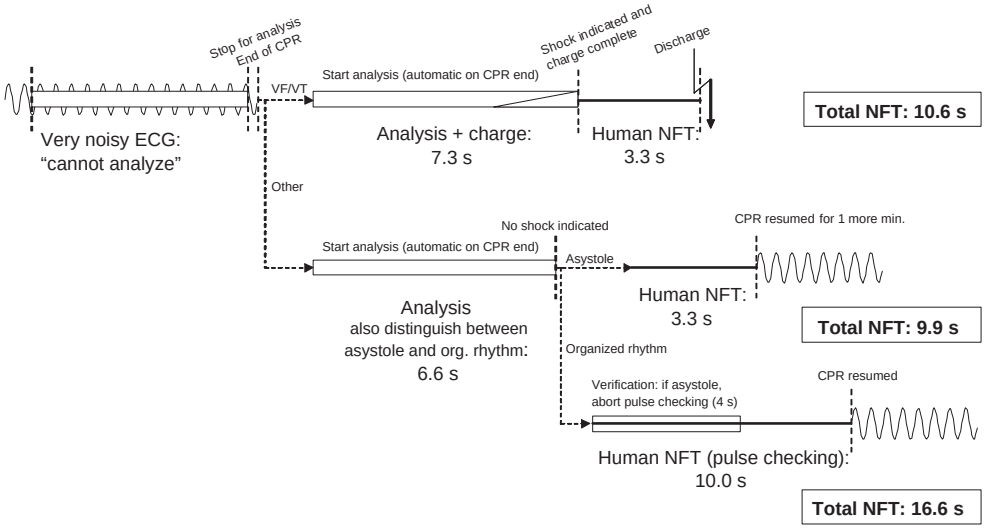

Figure 10.8: NFT analysis: Proposed solution for what to do when experiencing very noisy ECG. Layout and meaning as in Figure 10.1.

been achieved for each patient if the proposed solution had been used. This was done by identifying each incidence of rhythm analysis and shock, and replacing or removing the NFT intervals according to the proposals in the above sections. The lengths of each single human NFT interval (rescuer/not AED dependent) was kept unchanged from the recorded HS4000 data to the alternative proposed solution. We see improvement in NFT for every patient and the median NFT in connection with analyses and shocks is reduced from 4:33 to 1:34.

In Figure 10.10 we look at the total NFT for each patient with HS4000 and the proposed system, i.e. we also include the NFT we can not improve on. The median total NFT is reduced from 11:20 to 6:51. The median NFT ratio, defined as the median of the individual NFT ratios (NFT time divided by total incident time for each patient), is reduced from 51% to 34%.

Patients with no shocks

Of the 47 patients having no shocks, the mean number of analyze periods per patient was 4.3. The median episode time was 21:50 with a median 9:02 of NFT, i.e. about 41% of the time there was no blood flow to the brain. Of the 9:02 NFT, 1:48 (20%) was in connection with analyses, and 1:20 (15%)

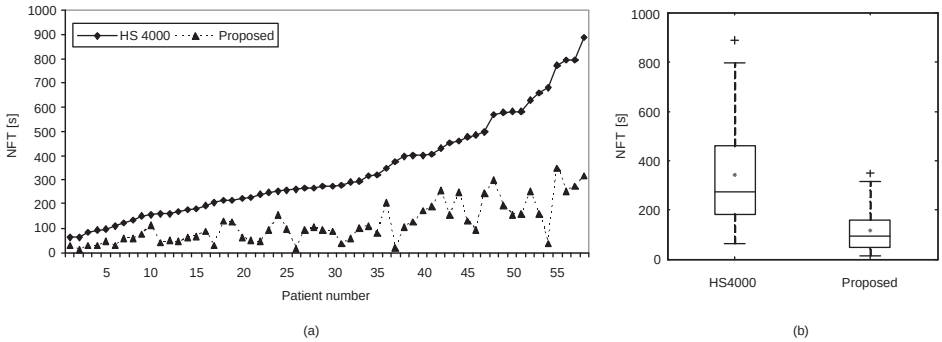

Figure 10.9: NFT in connection with analyses and shocks for patients having at least one shock (sorted on increasing NFT): (a) NFT for each patient for HeartStart 4000 (solid line) and the proposed system (dotted line). (b) Boxplot analysis of the NFT. The box has lines at the lower quartile, median, and upper quartile values. The whiskers are lines extending from each end of the box to show the extent of the rest of the data. Outliers are data with values beyond the ends of the whiskers. The solid dot is the mean value.

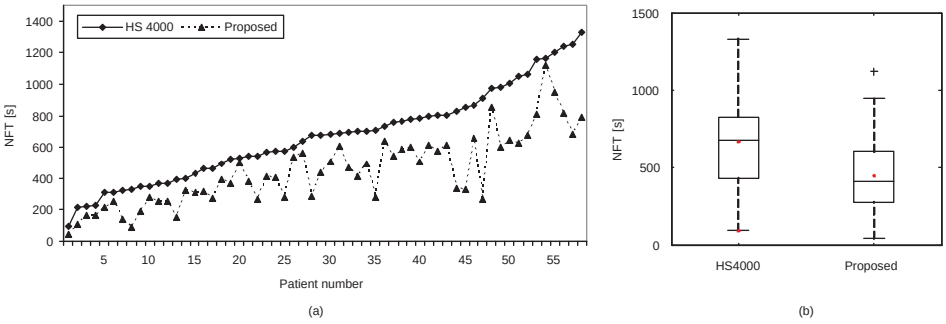

Figure 10.10: 6 Total NFT (i.e. including all causes of NFT) for patients having at least one shock (sorted on increasing NFT): (a) Total NFT for each patient for HeartStart 4000 (solid line) and the proposed system (dotted line). (b) Boxplot analysis of the total NFT.

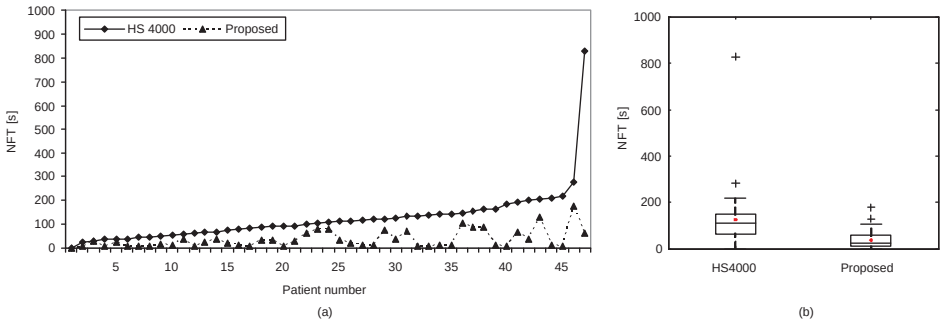

Figure 10.11: NFT due to analyses for patients having no shocks (sorted on increasing NFT): (a) NFT for each patient for HeartStart 4000 (solid line) and the proposed system (dotted line). (b) Boxplot analysis of the NFT due to analyses.

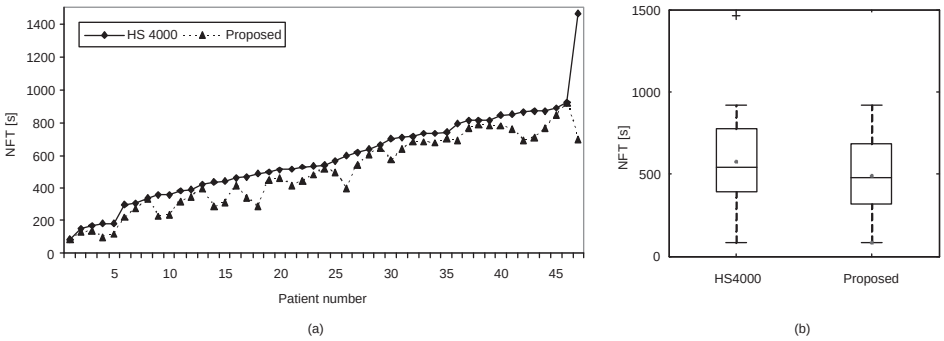

Figure 10.12: Total NFT (i.e. including all causes of NFT) for patients having no shocks (sorted on increasing NFT): (a) Total NFT for each patient for HeartStart 4000 (solid line) and the proposed system (dotted line). (b) Boxplot analysis of the total NFT.

was due to ventilations outside compressions, analyses or pulse rhythm. That leaves about 65% of the NFT due to other unknown factors.

Figure 10.11 shows the NFT in connection with analyses found for each of the 47 patients with no shocks. The figure also shows what could have been achieved for each patient if the proposed solution had been used. As the NFT due to analyses is less here compared to the patients receiving shocks, the reduction potential is less. Still, NFT could be reduced for every patient and the median NFT due to analyses is reduced from 1:48 to 0:23. When looking at the total NFT in Figure 10.12, the median total NFT is reduced from 9:02 to 7:56. The median NFT ratio is reduced from 49% to 39%.

The results of the total NFT analysis for the two groups of patients are summarized in Table 10.4.

Table 10.4: Summary of the total NFT analysis results for the two groups of patients. HS4000 = Actual results from data using HeartStart 4000 SP defibrillators. Prop. = Theoretical results using the proposed methods. All times are (minutes:seconds).

Patient group	Median incident time	Median NFT				Median NFT ratio	
		Total		Analyses & shocks			
		HS4000	Prop.	HS4000	Prop.	HS4000	Prop.
with shocks	23:30	11:20	6:51	4:33	1:34	51%	34%
no shocks	21:50	9:02	7:56	1:48	0:23	49%	39%

10.3 Discussion

When ALS was attempted performed according to the international guidelines for CPR and ECC [9] by paramedics and nurse anaesthetists, approximately half the time was spent without any blood flow generating chest compressions. This is identical to a study by Wik et al. also using data from the Sister project [104], and similar to what van Alem et al. [7] reported for BLS with AEDs by first responders before the ALS team arrived.

We propose a way to reduce this no flow time from median 51% to 34% of the total incident time in patients receiving shocks, and from median 49% to 39% in patients without a shockable rhythm, without dramatic changes in the guidelines [9] or the way the ALS team functions. This reduction potential could therefore come in addition to effects of suggested changes such as chest compressions without ventilation in unintubated patients [66,67], longer periods of uninterrupted CPR before defibrillation attempts [103], focus on reducing unnecessary breaks in chest compressions in CPR training, and eliminating shocks that are unlikely to cause ROSC as evaluated from VF analyses [8,29,48,84].

The proposed method for reducing no flow times is based on factors of which most depend on changing the function of the AED, in addition to one non-AED dependent guideline change: One minute of CPR immediately following all shocks before the first postshock ECG analysis. The latter is probably the most radical suggestion. In most situations this should be of clear benefit. Few shocks given to a patient result in ROSC, in the present study only 17 of 356 (4.8%) shocks resulted in a pulse-giving rhythm. Thus many patients receive chest compressions after a shock regardless, in the present situation often after a long no flow time. When a shock results in ROSC, it is not always achieved within the time allowed for immediate analysis and pulse check in the present

guidelines [9] and therefore the patient receives one minute of CPR before ROSC is recognized even today. For patients who have VF again after the shock, there is new information that the chance of defibrillation success (i.e. ROSC) can increase with CPR before the defibrillation attempt [23, 34, 103]. The only patients where this one minute of CPR could be potentially dangerous are those where ROSC could have been recognized in a first postshock pulse check according to the guidelines. To our knowledge, there is little or no scientific evidence suggesting that chest compressions can induce VF in a patient with spontaneous circulation, and it is well established (and therefore recommended in the guidelines [9]) that chest compressions on top of spontaneous circulation are of benefit in newly born with a pulse rate < 60 per minute. It can be speculated that this also can be the case in adults after successful cardioversion (i.e. ROSC). It has recently been pointed out [42] that ROSC with return of a normal cardiac rhythm depends on emptying the right ventricle to enable left ventricular filling, and shown that this occurs with chest compressions [90]. Chest compressions after successful cardioversion could potentially function as a manual cardiac assist device. We believe that it is at least warranted to do a randomized study of this versus the present guidelines.

The other factors are more AED and less guidelines dependent. Rhythm analysis during ongoing chest compressions has previously been impossible due to the inability of the AED algorithms to accurately analyze the ECG for shockable versus non-shockable rhythms if influenced by artifacts created by CPR. If these artifacts could be filtered out, rhythm analysis could take place during ongoing chest compressions. We have in the previous chapters proposed and tested this using the MC-RAMP multichannel adaptive filter. The filtering technique is not 100% reliable, however, and it is unlikely that the medical community and the medical device approving agencies will accept a significant reduction in the accuracy of the AED algorithm. We therefore propose that the final verification of the rhythm is done during a four-seconds hands-off period. In addition we propose that the AED capacitors are charged during this four-seconds period if the initial ECG analysis indicates a probable shockable rhythm. This would save time and not endanger the rescuers as they already have their hands off the patient. If the AED algorithm also could include the recognition of asystole, it could recommend pulse checks only for non-VF/asystole situations, thereby removing unnecessary no-flow situations. Recognition of asystole should be accomplishable with close to 100% accuracy. Another proposed change, that the AED automatically starts analysis during CPR without requiring the rescuer to actively push the analysis button, removes additional no flow time.

During this study we have seen a great potential for improved CPR and thus reducing unnecessary NFT due to unexplained pauses in CPR. We note that some of these unexplained CPR pauses are probably manual rhythm evaluation by the paramedics, even though AEDs were used. By introducing CPR feedback in the defibrillator [49], telling the user what to do to improve the CPR, the users could produce better and more continuous CPR which would also reduce the overall NFT.

10.4 Summary

In this chapter we have analyzed and quantified the no flow times (NFTs) during external automatic defibrillation in 105 cardiac arrest patients. We found that around half of the time (around 10 minutes), these patients were not perfused. We have proposed methods to reduce NFT in connection with analyses and shocks. The key factors were rhythm analysis during ongoing CPR, capacitor charging during analysis, one minute of CPR immediately after a shock (with rhythm analysis during CPR at the end of the one minute), and distinguishing between asystole and organized rhythm in analyses skipping pulse check if asystole.

The potential reduction in NFT using these methods was calculated theoretically and we found a reduction in the total NFT of about 4.5 and 1 minutes, respectively, in the subgroups of patients having at least one shock and patients having received no shocks. In the present study, the median NFT ratio could theoretically be reduced from 51% to 34% or 49% to 39% depending on if the patient would have a shockable rhythm or not.

By introducing the proposed methods into an AED, the NFT would be significantly reduced, hopefully increasing the survival.

Chapter 11

Conclusions

The ultimate aim of this thesis was to investigate methods for improving the survival rate of out-of-hospital cardiac arrest patients. More specifically, we have focused on removal of CPR artifacts in ECG using a multichannel adaptive filter, the novel MC-RAMP filter. By removing these artifacts, we have shown that reliable ECG signal analysis during CPR is feasible. Using the MC-RAMP filter we have proposed methods to reduce the detrimental NFT (with no myocardial and cerebral blood flow) during treatment of cardiac arrest patients using an AED. We have shown a great potential in reduction of NFT compared to an existing AED. Implementing this scheme in an AED should contribute to improved survival rate of out-of-hospital cardiac arrest.

The major contributions and conclusions of this work are:

- In Chapter 4 we developed a new multichannel adaptive filter, the MultiChannel Recursive Adaptive Matching Pursuit (MC-RAMP) filter. It is a general purpose multichannel adaptive filter which is computationally efficient and numerically robust. In this thesis we have used MC-RAMP for removal of CPR artifacts in ECG. We have used four reference channels reflecting the CPR artifacts: compression depth, compression acceleration, thorax impedance, and ECG common mode voltage.
- Comparison of the performance of the theoretically optimal time-varying Wiener filter versus MC-RAMP in the setting of CPR artifact removal in a mix of human and animal ECG was done in Chapter 6. The results of the study showed that MC-RAMP performed (in terms of SNR improvement) about the same as the theoretically optimal time-varying Wiener filter, but having the advantages of being more numerically robust and computationally efficient.

- The MC-RAMP filter was further tested in Chapter 7 comparing the performance of a proprietary AED shock advice algorithm in human ECG segments with and without CPR artifacts, before and after artifact filtering. After MC-RAMP filtering in CPR artifact corrupted ECG, the test set gave a sensitivity of 96.7% and specificity of 79.9%, an increase of approximately 15% and 13% respectively, compared to no filtering. Although good sensitivity on par with the performance without CPR artifacts, the specificity is probably too low for clinical use. That is, we found artifacts in non-shockable rhythms to be more difficult to filter. Several factors are speculated to have contributed to the relatively low specificity, such as missing artifact components in the reference channels, inadequate shock advice algorithm, and spontaneous underlying heart activity. Methods to increase the specificity were introduced in Chapter 8, although at the expense of some additional time needed and slightly reduced sensitivity. Using a short verification analysis in clean ECG and/or postponing decision when too difficult noise is present, the performance in the test set was 92.4% sensitivity and 96.0% specificity – a satisfactory result. From these results we deem rhythm analysis / shock advice during CPR feasible.

- In Chapter 9, rhythm analysis during CPR was further indicated feasible through investigations of the influence of CPR artifacts on common individual features used in ECG analyses. The features used were a collection of existing ones found in the literature and new ones developed for this dissertation. CPR artifacts were found to influence the individual features, but artifact filtering reduced this influence. However, we were not convinced of the possibility of VF analysis during CPR, and further testing is required.

- In Chapter 10 we analyzed and quantified the no flow times (NFTs) during external automatic defibrillation in 105 cardiac arrest patients. We found that around half of the time (around 10 minutes), these patients were not perfused. We proposed methods to reduce NFT in connection with analyses and shocks. The key factors were rhythm analysis during ongoing CPR, charging of the capacitor during analysis, one minute of CPR immediately after a shock (with rhythm analysis during CPR at the end of the one minute), and distinguishing between asystole and organized rhythm in analyses skipping pulse check if asystole. The potential reduction in NFT using these methods was calculated theoretically and we found a reduction in NFT of almost 4.5 and 1 minutes, respectively, in the subgroups of patients having at least one shock and patients hav-

ing received no shocks. By introducing the proposed methods into an AED, the NFT would be significantly reduced, hopefully increasing the survival.

To sum it up:

- ECG corrupted with CPR artifacts can be filtered using the MC-RAMP filter.
- Artifacts in non-shockable rhythms are more difficult to filter than artifacts in shockable rhythms.
- We believe rhythm analysis during CPR is feasible.
- We are more skeptical about the feasibility of VF analysis during CPR.
- Using CPR artifact filtering to enable rhythm analysis during CPR should significantly contribute to reduced NFT in AEDs, and hopefully, increased survival of cardiac arrest patients.

11.1 Directions for future research

Based on the experience gained during this work, we give some possible directions for future research:

- Clinical studies should be done investigating the nature of CPR artifacts. Is it reasonable, as we assume today, that filtering of CPR artifacts will reveal the same heart rhythm as if we ended the CPR and looked at the same clean ECG? Or may CPR alter the true underlying heart rhythm momentarily and temporarily, not just contributing to long term changes?
- It may be possible to find other sources of reference channels in CPR artifact filtering. Our tests have indicated artifact components in the ECG not found in, or not linearly correlated with, any of the reference channels. The preprocessing of the ECG and reference channels could be further investigated to ensure maximum artifact correlation and zero delay between channels, possibly compensating for currently unknown physiological effects.

- The AED shock advice rhythm we used may not be the best choice for rhythm analysis during CPR after artifact filtering. Possibly, a new shock advice algorithm should be developed. One that takes into consideration the types of residuals left after artifact filtering and based upon pattern recognition principles and possibly trained also on ECG with filtered CPR artifacts.

- Work may be done to improve the MC-RAMP filter, or try out completely different types of filter solutions. However, we do not expect much improvement in just changing the core filter solution. Adding ad hoc elements for the current application is more likely to improve the results.

- In Chapter 10 we introduced the concept of an algorithm for distinction of asystole and organized rhythm to avoid advising for pulse check when we have asystole. Such an algorithm need to be developed, possible using features from Chapter 5.

- Further studies on the possibility of VF analysis during CPR should be carried out. We remain unconcluded, although somewhat doubtful, on the issue.

- Finally, the concepts and methods of this thesis need to be implemented in an AED and used in real clinical tests to evaluate the potential benefits of this work in treatment of out-of-hospital cardiac arrest.

Appendix A

Efficient MC-RAMP algorithm implementation

In this appendix we develop the elements of the algorithm structure presented in Section 4.2.2 further, we present a quantitative complexity analysis, and comment on algorithm initialization. This appendix is adapted from [55] and applies primarily to MC-RAMP without the modifications in Section 4.2.3.

The adaptive filter algorithm described in Section 4.2.2 corresponds to applying the computational steps of the BMP algorithm [25] to a dictionary of vectors given by the columns of $\mathbf{X}(n)$ for the purpose of building an approximation to $\underline{d}(n)$. The only difference is that we do this for each new time instant n while keeping the results of the BMP computations from the previous time instant $n-1$. In this way we are also able to maintain the approximation in a non-stationary environment. It is interesting to note [54] that a slightly different, but equivalent, procedure to the one described above would result if we tried to find the least squares solution to the overdetermined set of equations (remember $L > M$):

$$\mathbf{X}(n)\underline{h}(n) = \underline{d}(n) \tag{A.1}$$

subject to the constraint that, given an initial solution, say $\underline{h}_o(n)$, we are allowed to adjust only one element of this vector.

From the above, it is evident that the key computations of our adaptive filter algorithm are those of Eqs. 4.13 and 4.15. Making use of Eqs. 4.11 and 4.9, we find

$$j_0(n) = \arg\max_j \frac{1}{\|\underline{x}_j(n)\|} \; |< \underline{d}(n), \underline{x}_j(n) > - \sum_{k=0}^{M-1} h_k(n-1) < \underline{x}_k(n), \underline{x}_j(n) >|, \tag{A.2}$$

and

$$h_{j_0(n)}^{update}(n) = \frac{1}{\|\underline{x}_{j_0(n)}(n)\|^2}\{< \underline{d}(n), \underline{x}_{j_0(n)}(n) > - \sum_{k=0}^{M-1} h_k(n-1) < \underline{x}_k(n), \underline{x}_{j_0(n)}(n) >\}. \quad \text{(A.3)}$$

These are the pertinent equations if one coefficient update, i.e. one MP-iteration is performed for each new signal sample. Note that having computed the terms of Eq A.2, very little additional work is involved in finding the update of Equation A.3.

The inner products $< \underline{d}(n), \underline{x}_j(n) >$ and $< \underline{x}_k(n), \underline{x}_j(n) >$ evidently play prominent roles in the computations involved in the algorithm. Having identified the key computations involved, we proceed by presenting an efficient implementation of the algorithm. In doing this, we first present the algorithm implementation, along with its computational complexity when doing only one MP-iteration for each new signal sample. Following this, we present the implementation for possible subsequent iterations along with the attendant computational costs. We close this appendix by some comments on algorithm initialization.

A.1 Efficient algorithm implementation

The key to a computationally efficient algorithm lies in the time-shift relationship of the input data in each of the K channels. This leads, we will show below, to efficient recursions for all the key computations of our adaptive algorithm. In counting the number of arithmetic operations, we focus on the number of multiplications and divisions needed. *In the following four subsections we assume that only one MP-iteration is performed for every new signal sample (in each channel), i.e. every MP-iteration will uniquely be associated with a time index. In Subsection A.5 of this appendix we explain the added steps and computational complexity associated with more MP-iterations for a given time instant.*

Finding $\|\underline{x}_j(n)\|^2$ and $< \underline{x}_k(n), \underline{x}_j(n) >$

The term $\|\underline{x}_j(n)\|^2$ is directly involved in both Eqs. A.3 and A.2 and consequently need to be updated from one time sample to the next . We will also need to update $< \underline{x}_k(n), \underline{x}_j(n) >$ for each new time instant. Observing that this latter expression corresponds to the squared norm of $x_j(n)$ when $k = j$, we need only consider the update of the inner products.

$< \underline{x}_k(n), \underline{x}_j(n) >$ for $k = 0, 1, \ldots, M-1$ and $j = 0, 1, \ldots, M-1$ are the elements of the matrix $\mathbf{X}^T(n)\mathbf{X}(n)$. Using Equation 4.6, this matrix is seen to possess the structure:

$$\begin{bmatrix} \mathbf{X}^{(0)^T}(n)\mathbf{X}^{(0)}(n) & \cdots & \mathbf{X}^{(0)^T}(n)\mathbf{X}^{(K-1)}(n) \\ \vdots & \ddots & \vdots \\ \mathbf{X}^{(K-1)^T}(n)\mathbf{X}^{(0)}(n) & \cdots & \mathbf{X}^{(K-1)^T}(n)\mathbf{X}^{(K-1)}(n) \end{bmatrix}. \tag{A.4}$$

Recalling the definition of the columns of $\mathbf{X}^{(k)}(n)$ given in Equation 4.5 we observe that $\underline{x}_{j-1}^{(k)}(n-1) = \underline{x}_j^{(k)}(n)$ for $j = 1, 2 \ldots, M_k - 1$. This means that in finding $\mathbf{X}^{(k)^T}(n)\mathbf{X}^{(k)}(n)$ given the knowledge of $\mathbf{X}^{(k)^T}(n-1)\mathbf{X}^{(k)}(n-1)$, we need only find the upper row and leftmost column of $\mathbf{X}^{(k)^T}(n)\mathbf{X}^{(k)}(n)$ as all other elements of this matrix are given by $\mathbf{X}^{(k)^T}(n-1)\mathbf{X}^{(k)}(n-1)$. Also noting that $\mathbf{X}^{(k)^T}(n)\mathbf{X}^{(k)}(n)$ is symmetric, we realize that only the upper row (*or* the leftmost column) need be computed for complete determination of $\mathbf{X}^{(k)^T}(n)\mathbf{X}^{(k)}(n)$. This entails finding $< \underline{x}_0^{(k)}(n), \underline{x}_j^{(k)}(n) >$ for $j = 0, 1, \ldots, M_k - 1$. The recursion for this is:

$$\begin{aligned} < \underline{x}_0^{(k)}(n), \underline{x}_j^{(k)}(n) > =& < \underline{x}_0^{(k)}(n-1), \underline{x}_j^{(k)}(n-1) > \\ &+ x^{(k)}(n)x^{(k)}(n-j) - x^{(k)}(n-L)x^{(k)}(n-j-L). \end{aligned} \tag{A.5}$$

If the result of the multiplication $x^{(k)}(n-L)x^{(k)}(n-j-L)$, which has been computed in a previous iteration has been stored, the updates needed to find the inner products of the columns of $\mathbf{X}^{(k)}(n)$ require only one multiplication for each value of j, i.e. we need a total of M_k multiplications.

Continuing with an argument along the lines of that given above for the non diagonal block sub matrices of $\mathbf{X}^T(n)\mathbf{X}(n)$, i.e. the matrices $\mathbf{X}^{(k)^T}(n)\mathbf{X}^{(j)}(n)$ for $j \neq k$, we finally find that the number of multiplications needed in the update is given by

$$K\{M - \frac{K-1}{2}\}. \tag{A.6}$$

Finding $< \underline{d}(n), \underline{x}_j(n) >$

Interpreting the index j as indicated in Equation 4.10, and assuming that it corresponds to column no. ν_q in the data matrix for channel no. q, the recursion for this term is given by

$$\begin{aligned} < \underline{d}(n), \underline{x}_j(n) > =& < \underline{d}(n-1), \underline{x}_j(n-1) > + \\ & d(n)x^{(q)}(n-\nu_q) - d(n-L)x^{(q)}(n-\nu_q-L). \end{aligned} \tag{A.7}$$

The term $d(n-L)x^{(q)}(n-\nu_q-L)$ will have been computed at an earlier stage and need not be recomputed if we have stored the result. For each $j=0,1,\ldots,M-1$ we need to compute $d(n)x^{(q)}(n-\nu_q)$. This obviously requires M multiplications.

Finding $\sum_{k=0}^{M-1} h_k(n-1) < \underline{x}_k(n), \underline{x}_j(n) >$

The key observation in finding an efficient recursion for this term, is that from one iteration to the next, only one single filter coefficient is updated. Thus, suppose that at time $n-1$, the *single* filter coefficient updated is coefficient no. $j_0(n-1)$. A consequence of this is that we can express the filter coefficients at time $n-1$ (after the update) in terms of the filter coefficients at $n-2$ and the update at time $n-1$ as follows:

$$h_j(n-1) = h_j(n-2) + \delta(j-j_0(n-1))h^{update}_{j_0(n-1)}(n-1), \tag{A.8}$$

where $\delta(n)$ is the unit pulse. Interpreting the indices j as corresponding to column no. ν_q in the data matrix for channel no. q, and k as column no. ρ_p in the data matrix for channel no. p, we have the recursion for $< \underline{x}_k(n), \underline{x}_j(n) >$ as

$$\begin{aligned} < \underline{x}_k(n), \underline{x}_j(n) > =& < \underline{x}_k(n-1), \underline{x}_j(n-1) > \\ &+x^{(p)}(n-\rho_p)x^{(q)}(n-\nu_q) - x^{(p)}(n-\rho_p-L)x^{(q)}(n-\nu_q-L). \end{aligned} \tag{A.9}$$

Using this we get the relation below. In the terms of form $x'(n-m)$ and $x'(n-m-L)$ the index m is to be interpreted as in Equation 4.10, i.e. as an index to the appropriate element of the appropriate column of one of the channel sub matrices comprising $\mathbf{X}(n)$.

$$\begin{aligned} &\sum_{k=0}^{M-1} h_k(n-1) < \underline{x}_k(n), \underline{x}_j(n) > = \\ &\quad \sum_{k=0}^{M-1} h_k(n-2) < \underline{x}_k(n-1), \underline{x}_j(n-1) > + \\ &\quad h^{update}_{j_0(n-1)}(n-1) < \underline{x}_{j_0(n-1)}(n-1), \underline{x}_j(n-1) > + \\ &\quad x'(n-j) \sum_{k=0}^{M-1} h_k(n-1)x'(n-k) - \\ &\quad x'(n-j-L) \sum_{k=0}^{M-1} h_k(n-1)x'(n-k-L). \end{aligned} \tag{A.10}$$

Note that the first term on the right hand side of the equality sign is the same as the left hand side expression *of the previous iteration*. Given the availability of the column inner products $< \underline{x}_k(n-1), \underline{x}_j(n-1) >$ of the previous iteration, the term $h^{update}_{j_0(n-1)}(n-1) < \underline{x}_{j_0(n-1)}(n-1), \underline{x}_j(n-1) >$ requires M multiplications (one for each value of j). The last two terms require a total of $4M$ multiplications.

A.1.1 Putting it all together

The complete algorithm, *when doing one MP-iteration at time* n, can now be summarized as follows:

For each time instant n do:

1. Update $< \underline{x}_k(n), \underline{x}_j(n) >$ and consequently also $\|\underline{x}_j(n)\|^2$. ($K\{M - \frac{K-1}{2}\}$ multiplications)
2. Update $< \underline{d}(n), \underline{x}_j(n) >$. ($M$ multiplications)
3. Update $\sum_{k=0}^{M-1} h_k(n-1) < \underline{x}_k(n), \underline{x}_j(n) >$. ($5M$ multiplications)
4. $| < \underline{d}(n), \underline{x}_j(n) > - \sum_{k=0}^{M-1} h_k(n-1) < \underline{x}_k(n), \underline{x}_j(n) > |$ for $j = 0, 1, \ldots, M-1$ is computed. For each j divide this by $\|\underline{x}_j(n)\|^2$ and find the index j giving the largest result. (M multiplications and divisions (as well as $M-1$ comparisons))
5. Update filter coefficient according to Equation A.3. (One division)

Thus, for each iteration we need $(7+K)M - \frac{K(K-1)}{2}$ multiplications, $M+1$ divisions and $M-1$ comparisons.

A.1.2 Additional MP-iterations

Allowing for more than one MP-iteration at time n, the pertinent update expressions are given by slightly modified versions of Eqs. A.2 and A.3: $h_k(n-1)$, which denote the previous filter vector element k computed at time $n-1$, must be substituted by the value of $h_k(n)$ *resulting from the previous MP-iteration at (current) time* n. We denote by $h_k^{(i)}(n)$, element no. k of the filter vector after MP-iteration no. i at the n-th time instant[1]. With this, the

[1]Since we are not explicitly dealing with channel numbers here, we reuse the superscript-notation used earlier for explicit channel identification, for our present purpose.

difference between the zero'th MP-iteration and subsequent such iterations is in the second term of Equation A.2. This part of that equation for the MP-iteration indexed i is

$$\sum_{k=0}^{M-1} h_k^{(i-1)}(n) < \underline{x}_k(n), \underline{x}_j(n) > . \tag{A.11}$$

With the filter update for MP-iteration no. $i > 0$ given by

$$h_{j_i(n)}^{(i)}(n) = h_{j_i(n)}^{(i-1)}(n) + h_{j_i(n)}^{update}(n), \tag{A.12}$$

where $j_i(n)$ denote the index of the filter vector element to be updated, we see that Equation A.11 can be written as[2]

$$\sum_{k=0}^{M-1} h_k^{(i-2)}(n) < \underline{x}_k(n), \underline{x}_j(n) > + h_{j_{(i-1)}(n)}^{update}(n) < \underline{x}_{j_{(i-1)}(n)}(n), \underline{x}_j(n) > . \tag{A.13}$$

Since the first term is known from previous iteration no. $(i-1)$ all we need is computing the last term which requires M multiplications and M additions. Computation of the filter update requires in addition one addition and division per MP-iteration. Putting the above into the modified Equation A.2 we see that another M additions are needed. Summarizing, each additional MP-iteration requires M multiplications, 1 division, $2M+1$ additions and $M-1$ comparisons. From this we can conclude that, relative to the zero'th MP-iteration at time n, the subsequent MP-iterations are cheap.

A.1.3 Algorithm initialization

There are several ways to initialize our adaptive filtering algorithm. Whatever reasonable initialization strategy is selected, the matrices and vectors will be filled with signals within a short period of time, whereupon the algorithm will quickly adjust the filter coefficients to remove the CPR artifacts. One good initialization strategy is as follows: Initialize $\mathbf{X}(-1)$, $\underline{h}(-1)$ and $\underline{h}(-1)$ to be all zero. As signal samples arrive for $n \geq 0$ we fill the matrices and vectors with incoming signal samples. While this is being done, the quantities of item 1 and item 2 in the algorithm implementation in Subsection A.4 of this

[2]This is not strictly correct for $i = 1$, but the same observations to be made are easily shown to be valid also in this case if we treat this situation separately.

appendix are updated. Only when the matrices and vectors are filled with a reasonable number of real signal samples, for example $20 - 50$ samples, not just zeros as a consequence of the initialization, the filter coefficient updates are computed in each iteration.

Appendix B

Available patient episodes from the Sister data

In this appendix we list the available patient episodes from the Sister project and for what studies they were used (Table B.1). The table also lists patient data such as incident length, initial heart rhythm, number of shocks given, if ROSC was achieved, and if the patient was admitted to the hospital alive. More about the patient demographics in the Sister data can be found in [104]. Note that not all of the patient episodes, which would otherwise have been included, were available at the time the different studies were conducted.

Table B.1: Available patient episodes and for what studies they were used. Patient filenames reveal origin (a = Akershus, l = London, s = Stockholm) and date and time of incident (yymmdd-hhmm).

Patient data						Used in study	
Filename	Incident length	Initial rhythm	Num. shocks	ROSC achieved	Admitted alive	Chapters 7–9	Chapter 10
a020317-2307	40:07	VF	5	✓		✓	
a020404-1103	42:07	VF	21	✓		✓	
a020408-1950	43:57	VF	12	✓		✓	
a020418-2130	38:02	PR	0			✓	
a020501-1706	06:47	VF	0			✓	

continued on next page

continued from previous page

Patient data						Used in study	
Filename	Incident length	Initial rhythm	Num. shocks	ROSC achieved	Admitted alive	Chapters 7–9	Chapter 10
a020512-0553	31:32	PR	1	✓	✓	✓	
a020514-1217	55:02	VT?	0	✓	✓	✓	
a020528-0802	44:42	PEA	3			✓	
a020619-1707	49:31	PEA	3	✓		✓	
a020720-0852	50:51	PEA	14	✓		✓	
a020724-1851	07:02	VF	0				
a020725-1844	32:07	PEA?	0			✓	
a020726-1033	20:12	VF	1	✓	✓	✓	
a020726-2019	39:57	PEA	2			✓	
a020728-2053	08:37	Asystole	0			✓	
a020804-0156	28:17	VF	5	✓	✓	✓	
a020809-1250	32:22	Asystole	2			✓	
a020812-1312	50:27	VF	7	✓	✓	✓	
a020814-0727	46:37	VF	28			✓	
a020827-0903	46:37	VF	24			✓	
a020830-1028	21:07	VF	3	✓	✓	✓	
a020901-1628	30:02	Asystole	0			✓	
a020910-1248	32:37	VF	15			✓	
a020913-1357	35:37	PEA	0	✓		✓	
a020925-1218	27:47	PEA	2			✓	
a021002-1838	27:47	VF	12			✓	
a021007-1202	52:12	VF	15	✓		✓	
a021021-1703	32:46	PEA	0	✓	✓		
a021025-1925	30:07	VF	4			✓	
a021117-2015	58:17	VF	5	✓	✓	✓	
a021125-0610	38:27	PEA	0			✓	
a021205-0814	51:17	VF	7	✓	✓	✓	
a021206-1518	27:47	VF	6	✓		✓	
a021209-0910	21:27	Asystole	0			✓	
a021212-1626	05:02	VF	1			✓	
a021218-1543	51:31	VF	0				

continued on next page

continued from previous page

Patient data						Used in study	
Filename	Incident length	Initial rhythm	Num. shocks	ROSC achieved	Admitted alive	Chapters 7–9	Chapter 10
a021225-1430	29:42	VF	5			✓	
a021229-1034	23:07	VF	6			✓	
a030113-2045	21:37	Asystole	0			✓	
a030119-1249	43:37	VF	3			✓	
a030120-1117	22:26	VF	0			✓	
a030120-2146	32:16	Asystole	0			✓	
a030203-1133	36:02	VF	19	✓		✓	
a030204-1210	59:21	PEA	0	✓	✓	✓	
a030213-1129	14:52	VF	8			✓	
a030218-1416	40:47	VF	20			✓	
a030225-1916	32:22	Asystole	15	✓		✓	
a030304-1509	13:02	VF	5			✓	
a030314-1702	37:17	VF	1	✓		✓	
a030321-0413	16:51	Asystole	0				
a030323-1143	27:17	PR	0			✓	
a030407-1254	08:27	Asystole	3				
a030407-1641	1:01:32	VF	7	✓	✓		
a030419-1621	43:37	VF	2	✓	✓		
a030502-1657	22:17	VF	2	✓	✓		
a030502-1928	24:07	VF	2				
a030518-1114	44:07	Asystole	19	✓			
a030527-1137	53:46	VF	30				
a030529-1310	17:21	Asystole	1				
a030531-1331	32:52	Asystole	0	✓			
a030531-1851	30:07	Asystole	3				
a030626-0901	25:37	Asystole	0				
a030630-1522	1:01:17	Asystole	0	✓	✓		
a030701-1105	26:57	VF	8	✓	✓		
a030722-1111	24:12	Asystole	0				
a030728-0324	28:57	Asystole	7				
a030805-1740	24:27	Asystole	0				

continued on next page

continued from previous page

Patient data						Used in study	
Filename	Incident length	Initial rhythm	Num. shocks	ROSC achieved	Admitted alive	Chapters 7–9	Chapter 10
a030820-2100	19:08	Asystole	9	✓			
a030826-1903	45:22	VF	1	✓	✓		
a030907-2303	25:02	PEA	0	✓	✓		
l020920-1932	26:07	Asystole	0	✓		✓	✓
l020922-0351	28:22	Asystole	8			✓	✓
l020922-2042	26:07	VF	22			✓	✓
l020930-1453	22:27	VF	9			✓	✓
l021010-2040	11:47	PR/PEA	0			✓	✓
l021014-2142	32:57	PEA	0				✓
l021020-1844	11:57	VF	3			✓	✓
l021201-0948	10:42	VF	2	✓	✓		✓
l021203-1953	06:07	VF	11	?	?	✓	✓
l021216-1556	23:32	Asystole	0				✓
l021219-1736	15:31	PEA	6			✓	✓
l021223-1253	33:17	Asystole	0			✓	✓
l021223-1600	28:42	Asystole	1			✓	✓
l021228-0410	26:47	PR	0				✓
l021229-2355	15:32	PEA	0	✓	✓	✓	✓
l030108-1321	36:47	VF	1			✓	✓
l030110-1714	16:47	VF	2			✓	✓
l030114-2142	32:57	PEA	0			✓	✓
l030122-0254	54:22	Asystole	0			✓	✓
l030122-2333	12:52	VF	6			✓	✓
l030124-0924	28:02	Asystole	0				✓
l030125-1951	21:17	Asystole	0				
l030131-2232	20:37	Asystole	1			✓	✓
l030218-1247	28:52	PEA	0			✓	✓
l030223-0525	22:23	VF	5			✓	✓
l030227-1217	31:02	Asystole	1			✓	✓
l030330-0033	33:52	Asystole	0				✓
l030420-1128	23:17	VF	1				✓

continued on next page

continued from previous page

Patient data						Used in study	
Filename	Incident length	Initial rhythm	Num. shocks	ROSC achieved	Admitted alive	Chapters 7–9	Chapter 10
l030427-2131	26:17	PR	2				✓
l030504-0819	17:12	VF	9				✓
l030513-1657	10:22	Asystole	0		?		✓
l030521-0419	24:22	PEA	0	✓			✓
l030524-1247	24:22	PEA	0				✓
l030610-1848	20:42	Asystole	0	✓	✓		✓
l030611-0541	12:22	VF	13	?			✓
l030620-0220	20:02	Asystole	0				✓
l030701-1635	31:12	VF	3				✓
l030715-1124	30:57	Asystole	0				✓
l030727-1017	20:47	VF	17				✓
l030807-1123	12:17	VF	10	?	?		✓
l030809-0911	21:42	PEA	0	✓	?		✓
l030824-0338	26:17	PEA	0	✓	✓		✓
l030920-0223	43:57	PEA	8				✓
l030920-2004	32:37	VF	24				✓
l030924-2245	24:52	PEA	1				✓
l030926-2053	10:52	Asystole	0				✓
l030927-2100	25:02	Asystole	0				✓
l030930-1359	25:07	VF	3	✓	✓		✓
l031001-0515	50:12	VF	13	✓			✓
l031009-0942	41:57	Asystole	20				✓
l031010-0948	13:47	Asystole	0				✓
l031010-2117	10:22	Asystole	0				✓
l031013-1004	24:22	Asystole	0				✓
l031016-1658	24:22	VF	10				✓
s020409-1241	27:47	VF	1	✓	✓		✓
s020415-1928	23:27	VF	2	✓	✓	✓	✓
s020617-0240	09:32	Asystole	0			✓	✓
s020617-2159	21:07	Asystole	0			✓	✓
s020627-1614	34:47	VF	1			✓	✓

continued on next page

continued from previous page

Patient data						Used in study	
Filename	Incident length	Initial rhythm	Num. shocks	ROSC achieved	Admitted alive	Chapters 7–9	Chapter 10
s020710-1615	32:27	PEA	0	✓		✓	✓
s020716-2059	27:08	PEA	14	✓		✓	✓
s020722-0920	28:07	VF	11	✓		✓	✓
s020726-0940	15:33	VF	9			✓	✓
s020730-0325	19:47	Asystole	0	✓	✓		✓
s020805-0147	31:02	PEA	0			✓	✓
s020808-0550	31:32	PEA	0			✓	✓
s020821-1350	32:27	Asystole	0			✓	✓
s020903-1258	40:37	PR	4			✓	✓
s020916-0823	35:12	Asystole	3	✓	✓	✓	✓
s020920-1430	57:57	PEA	0	✓	✓		✓
s020921-0844	39:12	VF	12	✓		✓	✓
s020924-1839	25:17	Asystole	0			✓	✓
s021008-1841	29:57	Asystole	0			✓	✓
s021019-0855	53:47	VF	13	✓	✓	✓	✓
s021022-1152	36:37	PEA	7			✓	✓
s021031-0909	24:17	VF	6	✓	✓	✓	✓
s021111-1618	30:32	Asystole	11			✓	✓
s021119-1850	31:47	VF	6	✓	✓	✓	✓
s021120-1433	20:37	PEA	0	✓	✓		✓
s021212-1816	10:17	Asystole	0	✓	✓	✓	✓
s021218-0304	32:02	VF	2	✓		✓	✓
s021228-0823	20:57	Asystole	0			✓	✓
s030103-2017	17:52	VF	6			✓	✓
s030107-1428	41:47	VF	8			✓	✓
s030203-1059	34:07	Asystole	1			✓	✓
s030205-2100	20:37	Asystole	0			✓	✓
s030209-1321	1:01:32	VF	10	✓	✓	✓	✓
s030215-1112	29:37	VF	2				✓
s030215-1704	17:32	VF	2			✓	✓
s030222-1759	39:27	VF	11			✓	✓

continued on next page

continued from previous page

Patient data						Used in study	
Filename	Incident length	Initial rhythm	Num. shocks	ROSC achieved	Admitted alive	Chapters 7–9	Chapter 10
s030228-2310	30:32	VF	2	✓		✓	✓
s030301-2016	39:27	VF	2	✓		✓	✓
s030305-1418	12:42	VF	4				✓
s030310-2111	28:22	Asystole	0			✓	✓
s030312-1236	29:37	VF	1				
s030318-1623	44:47	Asystole	2			✓	✓
s030417-1154	12:37	VF	8			✓	✓
s030430-1221	15:32	PEA	3			✓	✓
s030501-1712	47:22	PEA	0			✓	✓
s030513-0921	15:37	Asystole	0				✓
s030626-0914	22:47	Asystole	0	✓	✓		✓
s030802-1553	23:12	Asystole	0				✓
s030809-1337	22:02	VF	9				✓
s030909-2317	16:27	Asystole	0				✓
s030919-0922	35:17	PEA	0				✓
s031004-1358	20:57	VF	2				✓
s031005-1638	33:57	Asystole	0	✓	✓		✓
Sum:			761	60	35	105	105

Bibliography

[1] S. O. Aase, T. Eftestøl, J. H. Husøy, K. Sunde, and P. A. Steen. CPR artifact removal from human ECG using optimal multichannel filtering. *IEEE Trans. Biomedical Engineering*, 47(11):1440–1449, Nov. 2000.

[2] S. O. Aase and H. Myklebust. Compression depth estimation for CPR quality assessment using DSP on accelerometer signals. *IEEE Trans. Biomedical Engineering*, 49(3):263–268, Mar. 2002.

[3] U. Achleitner, V. Wenzel, H.-U. Strohmenger, K. H. Lindner, M. A. Baubin, A. C. Krismer, V. D. Mayr, and A. Amann. The beneficial effect of basic life support on ventricular fibrillation mean frequency and coronary perfusion pressure. *Resuscitation*, 51(2):151–158, Nov. 2001.

[4] B. Aehlert. *ACLS Quick Review Study Guide.* Mosby, St. Louis, Missouri, 2nd edition, 2002.

[5] B. Aehlert. *ECGs Made Easy.* Mosby, St. Louis, Missouri, 2nd edition, 2002.

[6] M. Akay, editor. *Nonlinear Biomedical Signal Processing – Volume II, Dynamic Analysis and Modeling.* IEEE Press, New York, NY, 2001.

[7] A. P. V. Alem, B. T. Sanou, and R. W. Koster. Interruption of cardiopulmonary resuscitation with the use of the automated external defibrillator in out-of-hospital cardiac arrest. *Annals of Emergency Medicine*, 42(4):449–457, Oct. 2003.

[8] A. Amann, K. Rheinberger, and U. Achleitner. Algorithms to analyze ventricular fibrillation signals. *Current Opinion in Critical Care*, 7:152–156, 2001.

[9] American Heart Association. Guidelines 2000 for cardiopulmonary resuscitation and emergency cardiovascular care – an international consensus on science. *Circulation*, 102(8):I–1–I–384, Aug. 2000.

[10] American Heart Association. *Heart Disease and Stroke Statistics – 2004 Update.* American Heart Association, Dallas, TX, 2003. www.americanheart.org.

[11] K. N. Anderson, L. E. Anderson, and W. D. Glanze, editors. *Mosby's Medical, Nursing, & Allied Health Dictionary.* Mosby, St. Louis, Missouri, 5th edition, 1998.

[12] T. P. Aufderheide and D. J. DeBehnke. Therapy of pulseless electrical activity. In N. Paradis, H. Halperin, and R. Nowak, editors, *Cardiac arrest: The science and practice of resuscitation medicine*, chapter 32, pages 607–620. Williams & Wilkins, Baltimore, 1996.

[13] S. Barro, R. Ruiz, D. Cabello, and J. Mira. Algorithmic sequential decision-making in the frequency domain for life threatening ventricular arrhythmias and imitative artefacts: A diagnostic system. *J. Biomed Eng.*, 11(4):320–328, July 1989.

[14] L. B. Becker. The epidemiology of sudden death. In N. A. Paradis, H. R. Halperin, and R. M. Nowak, editors, *Cardiac arrest: The science and practice of resuscitation medicine*, chapter 2, pages 28–47. Williams & Wilkins, Baltimore, 1996.

[15] M. D. Berg, T. D. Valenzuela, L. L. Clark, and R. A. Berg. Post-countershock chest compression delays with automated external defibrillator usage. *Circulation*, 108(17):IV–582 (Suppl), Oct. 2003.

[16] R. A. Berg, A. B. Sanders, K. B. Kern, R. W. Hilwig, J. W. Heidenreich, M. E. Porter, and G. A. Ewy. Adverse hemodynamic effects of interrupting chest compressions for rescue breathing during cardiopulmonary resuscitation for ventricular fibrillation cardiac arrest. *Circulation*, 104:2465–2470, Nov. 2001.

[17] R. A. Berg, R. W. Hilwig, K. B. Kern, A. B. Sanders, L. C. Xavier, and G. A. Ewy. Automated external defibrillation versus manual defibrillation for prolonged ventricular fibrillation: Lethal delays of chest compressions before and after countershocks. *Annals of Emergency Medicine*, 42(4):458–467, Oct. 2003.

[18] R. A. Berg, M. Berg, R. Hilwig, K. Kern, and M. Hayes. One minute or three minutes of prompt uninterrupted post-shock chest compressions are similarly effective for prolonged VF. *Critical Care Medicine*, 31(12):A34 Part 2 (Suppl), Dec. 2003.

[19] R. Broomfield. A quasi-experimental research to investigate the retention of basic cardiopulmonary resuscitation skills and knowledge by qualified nurses following a course in professional development. *Journal of Advanced Nursing*, 23(5):1016–1023, May 1996.

[20] R. H. Clayton, A. Murray, and R. W. F. Campbell. Comparison of four techniques for recognition of ventricular fibrillation from the surface ECG. *Medical & Biological Engineering & Computers*, 31:111–117, Mar. 1993.

[21] R. H. Clayton and A. Murray. Linear and non-linear analysis of the surface electrocardiogram during human ventricular fibrillation shows evidence of order in the underlying mechanism. *Medical & Biological Engineering & Computing*, 37(3):354–358, May 1999.

[22] R. H. Clayton, D. J. Yu, M. Small, V. N. Biktashev, R. G. Harrison, and A. V. Holden. Linear and nonlinear characteristics of ECG signals produced by simulations of ventricular tachyarrhythmias. *Proc. Computers in Cardiology*, 26:479–482, 1999.

[23] L. A. Cobb, C. E. Fahrenbruch, T. R. Walsh, M. K. Copass, M. Olsufka, M. Breskin, and A. P. Hallstrom. Influence of cardiopulmonary resuscitation prior to defibrillation in patients with out-of-hospital ventricular fibrillation. *Journal of American Medical Assosciation*, 281:1182–1188, 1999.

[24] L. A. Cobb, C. E. Fahrenbruch, M. Olsufka, and M. K. Copass. Changing incidence of out-of-hospital ventricular fibrillation, 1980-2000. *Journal of American Medical Assosciation*, 288(23):3008–3013, Dec. 2002.

[25] S. F. Cotter, R. Adler, B. Rao, and K. Kreutz-Delgado. Forward sequential algorithms for best basis selection. *IEE Proceedings – Vision, Image and Signal Processing*, 146(5):235–244, Oct. 1999.

[26] R. O. Cummins, M. S. Eisenberg, A. P. Hallstrom, and P. E. Litwin. Survival of out-of-hospital cardiac arrest with early initiation of cardiopulmonary resuscitation. *American Journal of Emergency Medicine*, 3(2):114–119, Mar. 1985.

[27] R. O. Cummins, D. A. Chamberlain, N. S. Abramson, et al. Recommended guidelines for uniform reporting of data from out-of-hospital cardiac arrest: The Utstein Style. A statement for health professionals

from a task force of the american heart assosciation, the european resuscitation council, the heart and stroke foundation of Canada, and the Australian resuscitation council. *Circulation*, 84(2):960–975, Aug. 1991.

[28] R. O. Duda, P. E. Hart, and D. G. Stork. *Pattern Classification*. Wiley, New York, NY, 2nd edition, 2001.

[29] T. Eftestøl, K. Sunde, S. O. Aase, J. H. Husøy, and P. A. Steen. Predicting outcome of defibrillation by spectral characterization and nonparametric classification of ventricular fibrillation in patients with out-of-hospital cardiac arrest. *Circulation*, 102:1523–1529, Sept. 2000.

[30] T. Eftestøl. *Signal analysis of out-of-hospital cardiac arrest electrocardiograms for decision support during cardiopulmonary resuscitation*. PhD thesis, Stavanger University College, Stavanger, Norway, Sept. 2000.

[31] T. Eftestøl, K. Sunde, S. O. Aase, J. H. Husøy, and P. A. Steen. 'Probability of successful defibrillation' as a monitor during CPR in out-of-hospital cardiac arrested patients. *Resuscitation*, 48(3):245 – 254, Mar. 2001.

[32] T. Eftestøl, K. Sunde, and P. A. Steen. Effects of interrupting precordial compressions on the calculated probability of defibrillation success during out-of-hospital cardiac arrest. *Circulation*, 105:2270–2273, May 2002.

[33] T. Eftestøl, J. Eilevstjønn, and P. A. Steen. Advanced life support therapy on out-of-hospital cardiac arrest patients: An engineering perspective (review). *Expert Review of Cardiovascular Therapy*, 1(2):203–213, July 2003.

[34] T. Eftestøl, L. Wik, K. Sunde, and P. A. Steen. Effects of CPR on predictors of VF defibrillation success during out-of-hospital cardiac arrest. *Circulation*, 110:10–15, July 2004.

[35] J. Eilevstjønn, J. H. Husøy, T. Eftestøl, S. O. Aase, and P. A. Steen. Multichannel adaptive filtering using an efficient matching pursuit-like algorithm for removal of CPR artifacts in ECG signals. In *Proc. IEEE Int. Conf. Acoust. Speech, Signal Proc.*, volume 4, pages IV–3864 – IV–3867, Orlando, Florida, May 2002.

[36] J. Eilevstjønn, T. Eftestøl, and P. A. Steen. Reducing the hands-off interval by filtering CPR artefacts in ECG. *Scand J Trauma Emerg Med*

(Akuttjournalen), 11(4):212, 2003. Abstract from HLR 2003 conference presentation (Stavanger, Norway, Sep. 2003).

[37] J. Eilevstjønn, T. Eftestøl, S. O. Aase, H. Myklebust, J. H. Husøy, and P. A. Steen. Feasibility of shock advice analysis during CPR through removal of CPR artefacts from human ECG. *Resuscitation*, 61(2):131–141, May 2004.

[38] J. Eilevstjønn, J. Kramer-Johansen, T. Eftestøl, M. Stavland, H. Myklebust, and P. A. Steen. Reducing no flow times during automated external defibrillation. 2004. To be submitted to *Resuscitation*.

[39] J. Eilevstjønn, T. Eftestøl, J. Kramer-Johansen, and P. A. Steen. Reducing the no flow time in automated external defibrillation. *Resuscitation*, 2004. Abstract, from ERC 2004 conference presentation (Budapest, Hungary, Sep. 2004).

[40] M. S. Eisenberg, B. T. Horwood, R. O. Cummins, R. Reynolds-Haertle, and T. R. Hearne. Cardiac arrest and resuscitation: A tale of 29 cities. *Annals of Emergency Medicine*, 19(2):179–186, Feb. 1990.

[41] G. A. Ewy. A new approach for out-of-hospital CPR: A bold step forward. *Resuscitation*, 58(3):271–272, Sept. 2003.

[42] M. Frenneaux. Cardiopulmonary resuscitation – some physiological considerations. *Resuscitation*, 58(3):259–265, Sept. 2003.

[43] W. J. Germann and C. L. Stanfield. *Principles of Human Physiology*. Pearson Education, San Francisco, CA, 2002.

[44] B. E. Gliner, D. B. Jorgensen, J. E. Poole, R. D. White, K. G. Kanz, T. D. Lyster, K. W. Leyde, D. J. Powers, C. B. Morgan, R. A. Kronmal, and G. H. Bardy. Treatment of out-of-hospital cardiac arrest with a low-energy impedance-compensating biphasic waveform automatic external defibrillator. *Biomedical Instrumentation & Technology*, 32:631–644, 1998.

[45] B. E. Gliner and R. D. White. Electrocardiographic evaluation of defibrillation shocks delivered to out-of-hospital sudden cardiac arrest patients. *Resuscitation*, 41(2):133–144, July 1999.

[46] R. A. Gray and J. Jalife. Spiral waves and the heart. *Int. J. Bifurcation and Chaos*, 6(3):415–435, 1996.

[47] R. A. Gray, A. M. Pertsov, and J. Jalife. Spatial and temporal organization during cardiac fibrillation. *Nature*, 392(6671):75–78, Mar. 1998.

[48] F. A. Hamprecht, U. Achleitner, A. C. Krismer, K. H. Lindner, V. Wenzel, H.-U. Strohmenger, W. Thiel, W. F. V. Gunsteren, and A. Amann. Fibrillation power, an alternative method of ECG spectral analysis for prediction of countershock success in a porcine model of ventricular fibrillation. *Resuscitation*, 50(3):287–296, Sept. 2001.

[49] A. J. Handley and S. A. J. Handley. Improving CPR performance using an audible feedback system suitable for incorporation into an automated external defibrillator. *Resuscitation*, 57(1):57–62, Apr. 2003.

[50] K. M. Hargarten, H. A. Stueven, E. M. Waite, D. V. Olson, J. R. Mateer, T. P. Aufderheide, and J. C. Darin. Prehospital experience with defibrillation of coarse ventricular fibrillation: A ten-year review. *Annals of Emergency Medicine*, 19:157–162, 1990.

[51] S. S. Haykin. *Adaptive Filter Theory*. Prentice Hall PTR, Englewood Cliffs, New Jersey, 4th edition, 2002.

[52] J. Herlitz, J. Bahr, M. Fischer, M. Kuisma, K. Lexow, and G. Thorgeirsson. Resuscitation in Europe: A tale of five European regions. *Resuscitation*, 41(2):121–131, July 1999.

[53] M. Holmberg, S. Holmberg, and J. Herlitz. Incidence, duration and survival of ventricular fibrillation in out-of-hospital cardiac arrest patients in Sweden. *Resuscitation*, 44(1):7–17, Mar. 2000.

[54] J. H. Husøy and J. Ommundsen. A novel algorithm for adaptive filters based on optimum selective update of coefficients. In *Proc. Applied Electronics*, pages 114 – 121, Plzen, Czech Republic, Sept. 2001.

[55] J. H. Husøy, J. Eilevstjønn, T. Eftestøl, S. O. Aase, H. Myklebust, and P. A. Steen. Removal of cardiopulmonary resuscitation artifacts from human ECG using an efficient matching pursuit-like algorithm. *IEEE Trans. Biomedical Engineering*, 49(11):1287–1298, Nov. 2002.

[56] J. Jalife. Ventricular fibrillation: Mechanisms of initiation and maintenance. *Annual Review of Physiology*, 62:25–50, 2000.

[57] N. S. Jayant and P. Noll. *Digital Coding of Waveforms*. Prentice-Hall, Englewood Cliffs, 1984.

[58] I. Jekova. Comparison of five algorithms for the detection of ventricular fibrillation from the surface ECG. *Physiol. Meas.*, 21(4):429–439, Nov. 2000.

[59] I. Jekova, A. Cansell, and I. Dotsinsky. Noise sensitivity of three surface ECG fibrillation detection algorithms. *Physiol. Meas.*, 22(2):287–297, May 2001.

[60] I. Jekova and P. Mitev. Detection of ventricular fibrillation and tachycardia from the surface ECG by a set of parameters acquired from four methods. *Physiol. Meas.*, 23(4):629–634, Nov. 2002.

[61] H. Kantz and T. Schreiber. *Nonlinear Time Series Analysis*. Cambridge Nonlinear Science Series. Cambridge University Press, Cambridge, UK, 1997.

[62] F. Kaspar and H. G. Schuster. Easily calculable measure for the complexity of spatiotemporal patterns. *Physical Review A*, 36(2):842–848, July 1987.

[63] W. Kaye, S. F. Rallis, M. E. Mancini, K. C. Linhares, M. L. Angell, D. S. Donovan, N. C. Zajano, and J. A. Finger. The problem of poor retention of cardiopulmonary resuscitation skills may lie with the instructor, not the learner or the curriculum. *Resuscitation*, 21:67–87, 1991.

[64] R. E. Kerber and C. E. Robertson. Transthoracic defibrillation. In N. A. Paradis, H. R. Halperin, and R. M. Nowak, editors, *Cardiac arrest: The science and practice of resuscitation medicine*, chapter 20, pages 370–381. Williams & Wilkins, Baltimore, 1996.

[65] R. E. Kerber, L. B. Becker, J. D. Bourland, R. O. Cummins, A. P. Hallstrom, M. B. Michos, G. Nichol, J. P. Ornato, W. H. Thies, R. D. White, and B. D. Zuckerman. Automatic external defibrillators for public access defibrillation: Recommendations for specifying and reporting arrhythmia analysis algorithm performance, incorporating new waveforms, and enhancing safety: A statement for health professionals from the american heart association task force on automatic external defibrillation, subcommittee on AED safety and efficacy. *Circulation*, 95:1677–1682, Mar. 1997.

[66] K. B. Kern, R. W. Hilwig, R. A. Berg, A. B. Sanders, and G. A. Ewy. Importance of continuous chest compressions during cardiopulmonary resuscitation: Improved outcome during a simulated single lay-rescuer scenario. *Circulation*, 105:645–649, Feb. 2002.

[67] K. B. Kern. Limiting interruptions of chest compressions during cardiopulmonary resuscitation. *Resuscitation*, 58(3):272–274, Sept. 2003.

[68] S. Kuo and R. Dillman. Computer detection of ventricular fibrillation. In *Proc. Computers in Cardiology*, pages 347–349, Long Beach, CA, 1978. IEEE Computer Society Press.

[69] A. Langhelle, T. Eftestøl, H. Myklebust, M. Eriksen, B. T. Holten, and P. A. Steen. Reducing CPR artefacts in ventricular fibrillation in vitro. *Resuscitation*, 48:279–291, 2001.

[70] M. P. Larsen, M. S. Eisenberg, R. O. Cummins, and A. P. Hallstrom. Predicting survival from out-of-hospital cardiac arrest: a graphic model. *Annals of Emergency Medicine*, 22(11):1652–1658, Nov. 1993.

[71] S. G. Mallat and Z. Zhang. Matching pursuits with time-frequency dictionaries. *IEEE Trans. Signal Processing*, 41:3397–3415, Dec. 1993.

[72] J. P. Marenco, O. J. Wang, M. S. Link, M. K. Homud, and N. A. M. Estes. Improving survival from sudden cardiac arrest: The role of the automated defibrillator. *Journal of American Medical Assosciation*, 9:1193–1200, 2001.

[73] A. Marn-Pernat, M. H. Weil, W. Tang, A. Pernat, and J. Bisera. Optimizing timing of ventricular defibrillation. *Critical Care Medicine*, 29(12):2360–2365, Dec. 2001.

[74] P. R. Martens, J. K. Russell, B. Wolcke, H. Paschen, M. Kuisma, B. E. Gliner, W. D. Weaver, L. Bossaert, D. Chamberlain, and T. Schneider. Optimal response to cardiac arrest study: Defibrillation waveform effects. *Resuscitation*, 49(3):233–243, June 2001.

[75] T. K. Moon and W. C. Stirling. *Mathematical Methods and Applications for Signal Processing*. Prentice Hall, Upper Saddle River, NJ, 2000.

[76] A. Murray, R. H. Clayton, and R. W. F. Campbell. Comparative assessment of the ventricular fibrillation detection algorithms in five semi-automatic or advisory defibrillators. *Resuscitation*, 26(2):163–172, Oct. 1993.

[77] A. Murray, R. H. Clayton, and R. W. F. Campbell. Assessment of the ventricular fibrillation detection algorithm in the semi-automatic Cardio-Aid defibrillator. *Resuscitation*, 29(2):113–117, Apr. 1995.

[78] M. Noc, M. H. Weil, W. Tang, S. Sun, A. Pernat, and J. Bisera. Electrocardiographic prediction of the success of cardiac resuscitation. *Critical Care Medicine*, 27(4):708–714, Apr. 1999.

[79] Norges Offentlige Utredninger. *NOU 1998: 9 Hvis Det Haster.....: Faglige Krav Til Akuttmedisinsk Beredskap*. Norges Offentlige Utredninger, Juni 1998.

[80] A. V. Panfilov. Three-dimensional organization of electrical turbulence in the heart. *Physical Review E*, 59(6):R6251–R6254, June 1999.

[81] N. A. Paradis, H. R. Halperin, and R. M. Nowak, editors. *Cardiac Arrest: The Science and Practice of Resuscitation Medicine*. William & Wilkins, Baltimore, 1996.

[82] T. Pellis, J. Bisera, W. Tang, and M. H. Weil. Expanding automatic external defibrillators to include automated detection of cardiac, respiratory, and cardiorespiratory arrest. *Critical Care Medicine*, 30(4):176–178, Apr. 2002.

[83] Philips Medical Systems. AED algorithm application note. Technical report, Philips Medical Systems, Andover, MA, 2003. (www.medical.philips.com/main/products/resuscitation/assets/docs/M3500-91040ED3.pdf).

[84] H. P. Povoas, M. H. Weil, W. Tang, J. Bisera, K. Klouche, and A. Barbatsis. Predicting the success of defibrillation by electrocardiographic analysis. *Resuscitation*, 53(1):77–82, Apr. 2002.

[85] J. G. Proakis and D. M. Manolakis. *Digital Signal Processing: Principles, Algorithms and Applications*. Prentice-Hall, Upper Saddle River, NJ, 3rd edition, 1996.

[86] F. Ravelli and R. Antolini. Complex dynamics underlying the human electrocardiogram. *Biological Cybernetics*, 67(1):57–65, May 1992.

[87] K. L. Ripley, T. E. Bump, and R. C. Arzbaecher. Evaluation of techniques for recognition of ventricular arrhythmias by implanted devices. *IEEE Trans. Biomedical Engineering*, 36(6):618–624, June 1989.

[88] Y. Sato, M. H. Weil, S. Sun, W. Tang, J. Xie, M. Noc, and J. Bisera. Adverse effects of interrupting precordial compression during cardiopulmonary resuscitation. *Critical Care Medicine*, 25:733–736, 1997.

[89] M. Small, D. Yu, R. G. Harrison, R. Clayton, T. Eftestøl, K. Sunde, and P. A. Steen. Temporal evolution of nonlinear dynamics in ventricular arrhythmia. *Int. J. Bifurcation and Chaos*, 11(10):2531–2548, 2001.

[90] S. Steen, Q. Liao, L. Pierre, A. Paskevicius, and T. Sjöberg. The critical importance of minimal delay between chest compressions and subsequent defibrillation: A haemodynamic explanation. *Resuscitation*, 58(3):249–258, Sept. 2003.

[91] H.-U. Strohmenger, K. H. Lindner, A. Keller, I. M. Lindner, and E. G. Pfenninger. Spectral analysis of ventricular fibrillation and closed-chest cardiopulmonary resuscitation. *Resuscitation*, 33(2):155–161, Dec. 1996.

[92] H.-U. Strohmenger, K. H. Lindner, and C. G. Brown. Analysis of the ventricular fibrillation ECG signal amplitude and frequency parameters as predictors of countershock success in humans. *Chest*, 111(3):584–589, Mar. 1997.

[93] H.-U. Strohmenger, T. Eftestøl, K. Sunde, W. Wenzel, M. Mair, K. H. Lindner, and P. A. Steen. Predictive value of ventricular fibrillation ECG signal frequency and amplitude parameters in patients with out-of-hospital cardiac arrest. *Anasthesia and Analgia*, 93:1428–1433, 2001.

[94] K. Sunde, T. Eftestøl, C. Askenberg, and P. A. Steen. Quality assessment of defibrillation and advanced life support using data from the medical control module of the defibrillator. *Resuscitation*, 41:237–247, 1999.

[95] N. V. Thakor. Chaos in the heart: Signals and models. In *Proceedings of the 1998 2nd International Biomedical Engineering Days*, pages 11–18. IEEE, 20–22 May 1998.

[96] S. Theodoridis and K. Koutroumbas. *Pattern Recognition*. Academic Press, London, UK, 1999.

[97] G. F. Tomaselli. Etiology, electrophysiology and mechanics of ventricular fibrillation. In N. Paradis, H. Halperin, and R. Nowak, editors, *Cardiac arrest: The science and practice of resuscitation medicine*, chapter 16, pages 301–319. Williams & Wilkins, Baltimore, 1996.

[98] R. J. Van Hoeywegen, L. L. Bossaert, and A. M. et al. Quality and efficiency of bystander CPR. *Resuscitation*, 26(1):47–52, Aug. 1993.

[99] J. G. Webster, editor. *Medical Instrumentation – Application and Design*. John Wiley & Sons, New York City, NY, 3rd edition, 1998.

[100] L. Wik, R. T. Brennan, and A. Braslow. A peer-training model for instruction of basic cardiac life support. *Resuscitation*, 29:119–128, 1995.

[101] L. Wik, J. Thowsen, and P. A. Steen. An automated voice advisory manikin system for training in basic life support without an instructor. A novel approach to CPR training. *Resuscitation*, 50(2):167–172, Aug. 2001.

[102] L. Wik, H. Myklebust, B. H. Auestad, and P. A. Steen. Retention of basic life support skills 6 months after training with an automated voice advisory manikin system without instructor involvement. *Resuscitation*, 52(3):273–279, Mar. 2002.

[103] L. Wik, T. B. Hansen, F. Fylling, T. Steen, P. Vaagenes, B. H. Auestad, and P. A. Steen. Delaying defibrillation to give basic cardiopulmonary resuscitation to patients with out-of-hospital ventricular fibrillation: A randomized trial. *Journal of American Medical Assosciation*, 289(11):1389–1395, Mar. 2003.

[104] L. Wik, J. Kramer-Johansen, H. Myklebust, H. Sørebø, L. Svensson, B. Fellows, and P. A. Steen. Quality of advanced cardiopulmonary resuscitation (CPR) performance by ambulance personnel. A novel approach to monitor real cardiac arrests and CPR performances. *Journal of American Medical Assosciation*, Submitted 2004.

[105] F. X. Witkowski, L. J. Leon, P. A. Penkoske, W. R. Giles, M. L. Spano, W. L. Ditto, and A. T. Winfree. Spatiotemporal evolution of ventricular fibrillation. *Nature*, 392(6671):78–82, Mar. 1998.

[106] M. Woollard, R. Whitfield, A. Smith, M. Colquhoun, R. G. Newcombe, N. Vetter, and D. Chamberlain. Skill acquisition and retention in automated external defibrillator (AED) use and CPR by lay responders: A prospective study. *Resuscitation*, 60(1):17–28, Jan. 2004.

[107] J. Xie, M. H. Weil, S. Sun, W. Tang, Y. Sato, X. Jin, and J. Bisera. High-energy defibrillation increases the severity of postresuscitation myocardial dysfunction. *Circulation*, 96:683–688, July 1997.

[108] T. Yu, M. H. Weil, W. Tang, S. Sun, K. Klouche, H. Povoas, and J. Bisera. Adverse outcomes of interrupted precordial compression during automated defibrillation. *Circulation*, 106:368–372, July 2002.

[109] X.-S. Zhang, Y.-S. Zhu, N. V. Thakor, and Z.-Z. Wang. Detecting ventricular tachycardia and fibrillation by complexity measure. *IEEE Trans. Biomedical Engineering*, 46(5):548–555, May 1999.

[110] Z.-J. Zheng, J. B. Croft, W. H. Giles, and G. A. Mensah. Sudden cardiac death in the united states, 1989 to 1998. *Circulation*, 104:2158–2163, Oct. 2001.

[111] D. P. Zipes and H. J. J. Wellens. Sudden cardiac death. *Circulation*, 98:2334–2351, Nov. 1998.

[112] ZOLL Medical Corporation. Automated external defibrillator with CPR feedback. Technical report, ZOLL Medical Corporation, Burlington, MA, 2002. Technical Application Note (www.zoll.com/AEDtechnote.pdf).